US Army Corps of Engineers

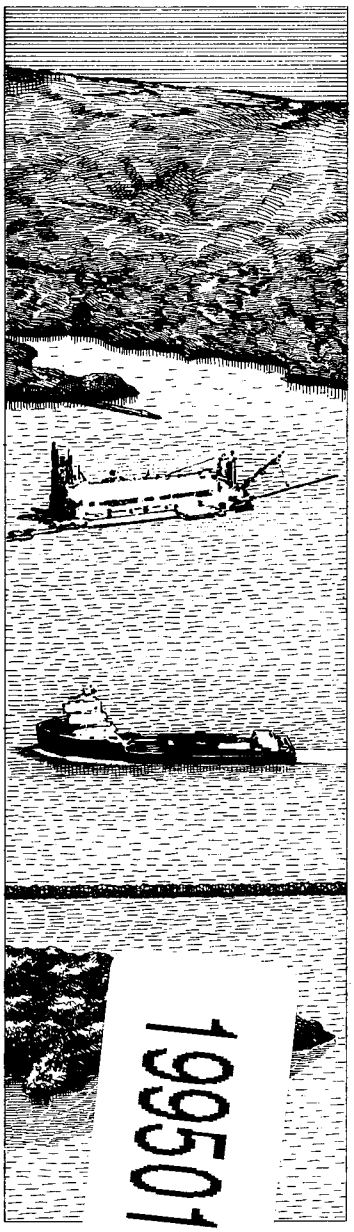

DREDGING RESEARCH PROGRAM

CONTRACT REPORT DRP-94-6

COHESIVE SEDIMENT EROSION

by

S.-C. Lee, A. J. Mehta

Coastal and Oceanographic Engineering Department
University of Florida
Gainesville, Florida 32611

November 1994
Final Report

Prepared for DEPARTMENT OF THE ARMY
U.S. Army Corps of Engineers
Washington, DC 20314-1000

Under Work Unit 32590

Monitored by U.S. Army Engineer Waterways Experiment Station
3909 Halls Ferry Road, Vicksburg, Mississippi 39180-6199

The Dredging Research Program (DRP) is a seven-year program of the U.S. Army Corps of Engineers. DRP research is managed in these five technical areas:

Area 1 - Analysis of Dredged Material Placed in Open Water
Area 2 - Material Properties Related to Navigation and Dredging
Area 3 - Dredge Plant Equipment and Systems Processes
Area 4 - Vessel Positioning, Survey Controls, and Dredge Monitoring Systems
Area 5 - Management of Dredging Projects

Dredging Research Program Report Summary

US Army Corps of Engineers
Waterways Experiment Station

Cohesive Sediment Erosion (CR DRP-94-6)

ISSUE: Evaluation of the long-term dispersion of cohesive dredged material depends on estimates of sediment erodibility. This is a difficult problem since only a small number of sediments have been tested and the erodibility of those varied widely. If direct erosion testing is to be performed, a number of different laboratory and field apparatus might be applied. If direct testing cannot be performed, it is essential that some sediment characterization be used to estimate erodibility parameters.

RESEARCH: The Dredging Research Program (DRP) has developed and refined computer models to predict short- and long-term fate of disposed dredged material (STFATE and LTFATE models, respectively). The LTFATE model has a cohesive module which uses sediment-specific coefficients to calculate sediment movement. A PC-computer utility program has been developed which contains a database of laboratory erosion test results. The DRP includes a continuing effort to improve process descriptors and test methods for cohesive sediment erosion assessment.

SUMMARY: Characteristics of erosion test devices and field instrument assemblies were compiled, categorized, and reviewed. Erosion test data were compiled and analyzed to develop a functional link between the characteristic erosion rate constant and shear strength of the cohesive bed. A succession of curves were developed based on variations in the state of the sediment bed and the total salt content in the pore fluid. A nomograph is presented.

AVAILABILITY OF REPORT: The report is available through the Interlibrary Loan Service from the U.S. Army Engineer Waterways Experiment Station (WES) Library, telephone number (601) 634-2355. National Technical Information Service (NTIS) report numbers may be requested from WES Librarians.

To purchase a copy of the report, call NTIS at (703) 487-4780.

About the Authors: Dr. Ashish J. Mehta is a major professor and Say-Chong Lee is a graduate student in the Coastal and Oceanographic Engineering Department of the University of Florida, Gainesville, FL. Mr. Allen M. Teeter, Hydraulics Laboratory, WES, was Principal Investigator for this work unit. For further information about the DRP, contact Mr. E. Clark McNair, Jr., Manager, DRP, at (601) 634-2070.

November 1994

Dredging Research Program

Contract Report DRP-94-6
November 1994

Cohesive Sediment Erosion

by S.-C. Lee, A. J. Mehta

Coastal and Oceanographic Engineering Department
University of Florida
Gainesville, FL 32611

Final report

Approved for public release; distribution is unlimited

Prepared for U.S. Army Corps of Engineers
Washington, DC 20314-1000

Under Work Unit 32590

Monitored by U.S. Army Engineer Waterways Experiment Station
3909 Halls Ferry Road, Vicksburg, MS 39180-6199

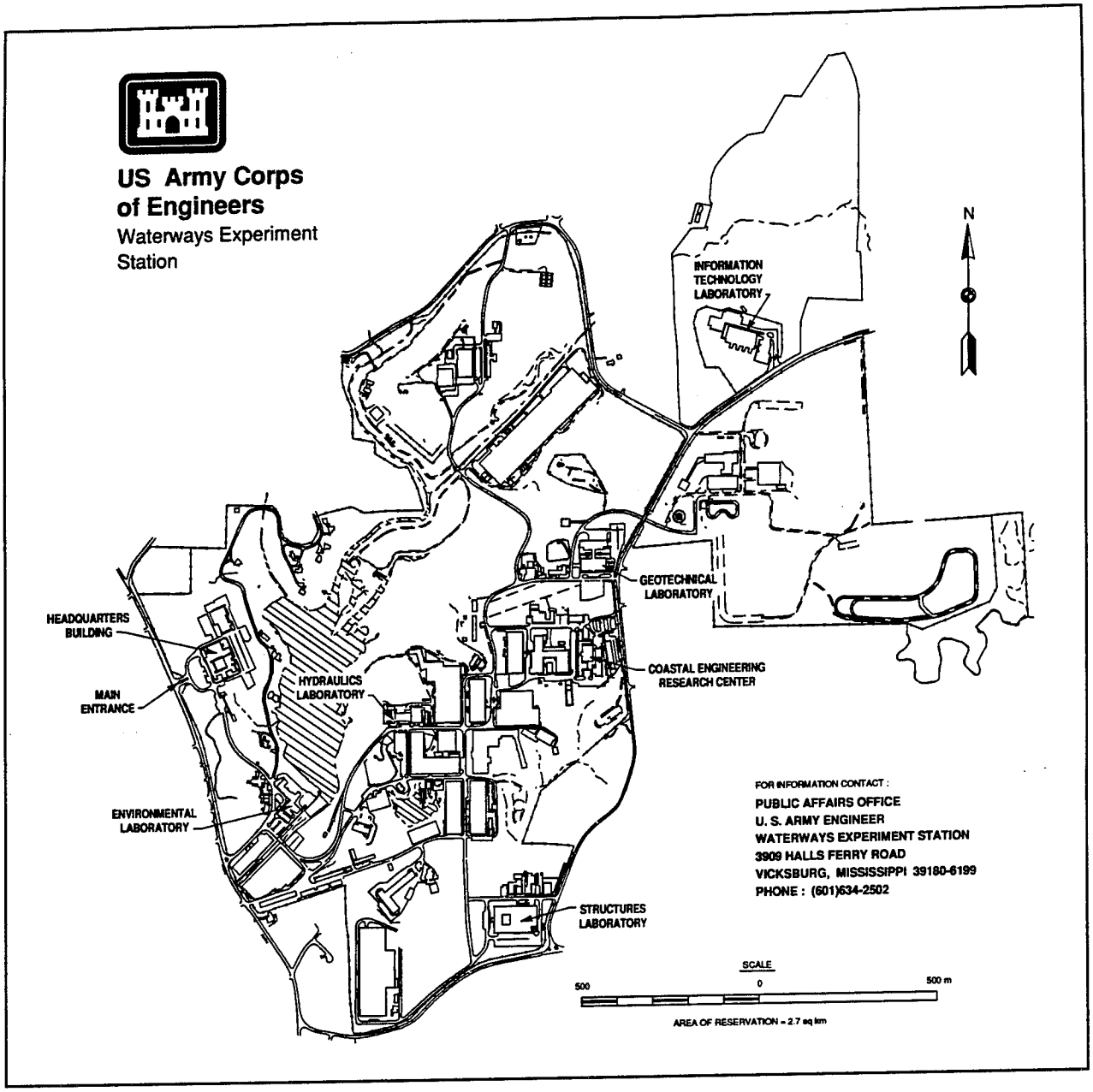

Waterways Experiment Station Cataloging-in-Publication Data

Lee, Say-Chong.
Cohesive sediment erosion / by S.-C. Lee, A.J. Mehta ; prepared for U.S. Army Corps of Engineers ; monitored by U.S. Army Engineer Waterways Experiment Station.
83 p. : ill. ; 28 cm. -- (Contract report ; DRP-94-6)
Includes bibliographical references.
1. Marine sediments -- Testing. 2. Sediment transport -- Measurements -- Instruments. 3. Sedimentation and deposition -- Measurement. 4. Soil consolidation -- Testing. I. Mehta, A. J. (Ashish Jayant), 1944- II. United States. Army. Corps of Engineers. III. U.S. Army Engineer Waterways Experiment Station. IV. Dredging Research Program. V. Title. VI. Series: Contract report (U.S. Army Engineer Waterways Experiment Station) ; DRP-94-6.
TA7 W34c no.DRP-94-6

Contents

List of Tables

List of Figures

Preface

The cohesive sediment study reported herein was the third and final phase of contract research performed by the University of Florida, Dr. Ashish Mehta, Principal Investigator, for the Dredging Research Program (DRP) sponsored by Headquarters, U.S. Army Corps of Engineers. This work was conducted from January to May 1994. The other phases dealt with characterization and water wave-cohesive sediment interactions. Mr. Barry W. Holliday is the DRP Technical Monitor, Mr. E. Clark McNair, Jr., is the Program Manager (PM) for the DRP, Dr. Lyndell Z. Hales is Assistant PM, and Dr. Billy Johnson is Technical Area Manager.

Contract monitoring and report editing were performed by Mr. Allen M. Teeter, Hydraulics Laboratory (HL), U.S. Army Engineer Waterways Experiment Station (WES), under DRP Work Unit 32590. Work was conducted under the general supervision of Mr. F. A. Herrmann, Jr., Director, HL; Mr. R. A. Sager, Assistant Director, HL; Mr. W. H. McAnally, Chief, Estuaries Division (ED), HL; and Mr. T. Fagerburg, Acting Chief, Estuarine Processes Branch, ED.

At the time of publication of this report, Director of WES was Dr. Robert W. Whalin. Commander was COL Bruce K. Howard, EN.

Further information on this report can be obtained by contacting Mr. E. Clark McNair, Program Manager, at (601) 634-2070.

Summary

This report consists of three chapters: Chapters 1 and 2 deal with erosion test devices and field instrument assemblies, while Chapter 3 is an analysis of published erosion rate ($\dot{\epsilon}$)-bed shear strength (τ_s) data in an attempt to establish a functional link between the characteristic erosion rate constant (defined as the slope of the erosion rate-bed shear stress plot), s, and τ_s. A wide range of erosion test devices has been used both in the laboratory and in the field in the effort to further elucidate the phenomena of cohesive sediment erosion. They differ in configuration and flow geometry, size, mechanisms of generating flow, operation protocol, and measurement methodology. These devices are further complemented by various custom-designed field instrument assemblies, which provide valuable prototype data for model validation. The report reviews six categories of laboratory erosion test devices and eight categories of field devices/measuring assemblies. For each category, a representative device from the literature is described with a view to illustrating its salient features and typical test results. Similarly, the field instrument assemblies are individually described, including a brief discussion on typical field results. The description is confined to a documentation of the suite of equipment with incidental comments on their merits without an effort to compare them on a relative basis.

In Chapters 1 and 2, 152 pairs of measured erosion rate constant-bed shear strength values have been gleaned from the literature for analysis. The data are limited to those that exhibit a linear relationship linking the rate of erosion to the bed shear strength. A family of curves of the functional form $s = 200\exp(-a\tau_s^b)$ where a and b are empirical constants and the relevant units are g/N-s and Pa for s and τ_s, respectively, is apparent from the data spread. Further examination of the trend of several important erosion resistance characterizing factors reveals that the succession of curves behaves consistently with respect to the variation in the state of sediment bed (undisturbed or remolded) and the total salt concentration in the pore fluid. Based on these observations, a nomograph has been suggested for estimating the erosion rate constant, given the bed shear strength, subject to the caveat that the nomograph be used only as a last resort to provide general guidance, and is not intended to supplant erosion experiments, which should always remain the first choice. It may be noted that the nomograph is applicable only for placed beds, undisturbed beds, or remolded beds having a uniform shear strength with depth.

1 Test Devices

Preamble

A wide array of erosion devices has been employed in the study of cohesive sediment erosion both to elucidate the associated phenomena under controlled conditions, and to provide the values of the relevant input parameters that appear in the erosion flux functions used in analytical and numerical modeling. In order to obviate scale effects inherent in laboratory investigations, some of the devices have also been applied to field situations. Earlier reviews of laboratory equipment can be found in the Task Committee on Erosion of Cohesive Material (1968) and Partheniades and Paaswell (1970). Later reviews appear to be more selective in coverage (e.g., Berlamont et al., 1993), and do not include field equipment (e.g., van Leussen and Winterwerp, 1990). In addition, *ad hoc* field instrument assemblies have also been used for similar purposes.

The report reviews selected laboratory and field-based devices/assemblies. They are conveniently categorized according to their primary features of flow geometry as summarized in Table 1. For each category (and sub-category where appropriate) a representative device or assembly is described with respect to the basic features and operation of the equipment. Several field measuring instrument assemblies listed in Table 1 are also included, and brief descriptions of each follow those of the erosion test equipment. Each description is accompanied by typical results. The report is confined to a documentation of erosion test devices and field measuring assemblies with incidental comments on their merits; no effort has been made to compare them on a relative basis.

Straight Flumes

Introduction

This is by far the most common laboratory equipment used in studying erosion of cohesive sediments. Such flumes are too numerous to name individually, and include recirculating, non-recirculating, and tilting types. One of the largest of its kind, the Delft tidal flume, is briefly described herein based on the work of Kuijper et al. (1989).

Table 1
Erosion Test Devices and Field Instrument Assemblies

Category	Sub-category	Investigators
Laboratory Erosion Test Devices		
Flumes	Straight flume	Alishahi and Krone (1964); Dash (1968); Peirce et al. (1970); Lonsdale and Southard (1974); Einsele et al. (1974); Thorn and Parsons (1980); Mehta et al. (1982); Kamphuis and Hall (1983); Maa and Mehta (1987); Shaikh et al. (1988); Kuijper et al. (1989); Talebbeydokhti and Klingeman (1992); Tofts (1993); Mimura (1993)
	Laboratory rotating annular flume	Partheniades and Kennedy (1966); Mehta (1973); Fukuda (1978); Kusuda et al. (1985); Burt and Game (1985); Tsai and Lick (1988); Kuijper et al. (1989); Murakami et al. (1989); Li (1989); Lau and Krishnappan (1991); Krishnappan (1991); Moller-Jensen (1993)
	Race-track flume	Watanabe et al. (1978); Ali et al. (1991); Mehta and Srinivas (1993)
	Rocking flume	Villaret and Paulic (1986)
Closed-conduits		Raudkivi and Hutchison (1974); Kelly and Gularte (1981); Teeter and Pankow (1989)
Rotating cylinders		Moore and Masch (1962); Arulanandan et al. (1975); Croad (1981); Chapuis and Gatien (1986)
Drill-hole apparatus		Christensen and Das (1973); Rohan et al. (1986)
Mechanical agitation	Oscillating grid	Tsai and Lick (1986); Wolanski et al. (1989); Teeter (1994)
	Propeller-based	Holland et al. (1970); Paulic et al. (1986); Schunemann and Kuhl (1993)
Others	Rotating disk	Liou (1970)
	Submerged jet	Dunn (1959); Moore and Masch (1962); Dash (1970)
Field Erosion Test Devices and Measuring Assemblies		
Field inverted channel		Young (1977); Nowell et al. (1985); Gust and Morris (1989)
Field rotating annular flume		Peirce et al. (1970); Maa (1991); Amos et al. (1992)
ISIS - instrument for shear strength in situ		Hydraulics Research Limited (1994)
Sediment-water interface probe		Nichols et al. (1978); Nichols (1989)
DAISY tower		Bohlen (1982)
OSU instrumentation		Bedford et al. (1982, 1987)
COE field tower		Mehta and Jiang (1990)
Instrumented bed frame		Diserens et al. (1993), Teisson et al. (1993)

Description

The Delft tidal flume, schematically shown in Figure 1, consists of a 130-m straight open channel with a cross section of 1 m x 1 m. The flume terminates in a sea basin where the water level, salinity, and sediment concentration can be controlled. A glass bottom and glass sidewalls enable visual observations to be made from all sides. Tides with a maximum period of 1,800 s and flow rates up to 0.3 m^3/s can be realized. At the upstream side, tap water with a selected sediment content can be injected to simulate river inflow. Two return pipes allow the flume to be used as a flow recirculating system.

The flow is generated by a constant-head tidal tank and the ensuing fluid-sediment interaction can be studied from the perspective of erosion and sedimentation fluxes under steady and non-steady, and homogeneous and non-homogeneous conditions, the last including gravity circulation and flocculation.

Operation

The sediment layer in the flume is first formed by deposition in still water after some period of mixing. Subsequently the layer is allowed to consolidate for a longer period of time. The bed is then eroded in various stages during which the fluid-induced bed shear stress is successively increased. The bed shear stress is calculated assuming a logarithmic velocity profile. The sediment concentration is measured with an optical instrument consisting of six probes. From various water depths, water is pumped through the probes and led through small cells and the concentration level determined via light absorption. The dry density of the mud is determined using a conductivity probe. The same probe is also used for detecting the surface of the mud layer.

Sample results

Figure 2 shows a typical suspended sediment concentration-time curve under steady flow testing conditions using China Clay (80 percent kaolinite and 15 percent illite) with a mean diameter of 3 microns. In this particular case, the consolidation period was 8 days. From Figure 2, it is seen that for the first two lower stress applications, i.e., 0.11 Pa and 0.17 Pa, the erosion rate reaches zero about 10 to 15 hr following test initiation, while the erosion rate eventually becomes constant at the application of the third shear stress (0.22 Pa).

Other similar flumes

As mentioned at the outset, the laboratory straight flume is the most common equipment used in the study of cohesive sediment erosion both under steady and oscillatory flow conditions. Table 2 is a non-exhaustive list of flumes in this category. Straight closed-end flumes, equipped with wave makers, are also commonly used in wave-sediment interaction studies (e.g., Maa and Mehta (1987), Mimura (1993)). Typically, the waves are mechanically generated using a plunger or a piston-type wave maker, and the horizontal sediment bed is accommodated in a drop section or trench in the

middle of the false bottom construction. Typical measurement parameters include suspended sediment concentration, wave height envelope, density and pore pressure variation with depth, and mud mass transport. In some flumes, e.g., Alishahi and Krone (1964), waves are wind-generated. Further details on some representative flumes in this category are included in Table 2.

Table 2
Straight Flumes

Investigator(s)	Sub-category	Dimensions (m) (length x width x depth)	Remarks
Alishahi and Krone (1964)	Wave flume, closed end	18.3 x 0.30 x 0.39	Wind-generated waves using centrifugal fan.
Dash (1968)	Recirculating, tilting	9.1 x 0.76 x 0.46	0.32 m x 0.32 m square sample housing unit with a movable base; filter frame covered with wire mesh and filter paper at downstream end.
Peirce et al. (1970)	Non-recirculating, tilting	3.7 x 0.14 x 0.15	Upstream supply via surge chamber and downstream gated control outlet to waste.
Lonsdale and Southard (1974)	Recirculating, tilting	6.0 x 0.17	
Einsele et al. (1974)	Recirculating, tilting	10.0 x 0.57 x 0.25[1]	20.6 cm x 13.4 cm x 5.4 cm sample holder.
Thorn and Parsons (1980)	Recirculating	17.4 x 0.30 x 0.20	Closed rectangular section.
Mehta et al. (1982)	Recirculating	10.0 x 0.6 x 0.9	Underflow gated control at downstream end.
Kamphuis and Hall (1983)		9.1 x 0.15 x 0.30	0.61 m x 0.15 m x 0.15 m drop section to hold sediment.
Maa and Mehta (1987)	Wave flume, closed end	20.0 x 0.46 x 0.45	Plunger-type wave maker.
Shaikh et al. (1988)	Recirculating, tilting	2.5 x 0.16 x 0.11	15.2 cm x 10.5 cm x 2.25 cm sample container for unsaturated compacted soils.
Kuijper et al. (1989)	Recirculating	130.0 x 1 x 1	Steady, non-steady, homogeneous and non-homogeneous (gravity circulation, etc.) testing conditions.
Talebbeydokhti and Klingeman (1992)	Recirculating, tilting	7.9 x 0.46 x 0.61	Sediment layer thickness 4 cm.
Tofts (1993)	Recirculating, tilting	9.0 x 0.4 x 0.4	Sediment layer thickness 8 cm.
Mimura (1993)	Wave flume, closed end	13.0 x 0.3	Bottom-hinged flap-type wave maker.

[1] water depth

Laboratory Rotating Annular Flumes

Introduction

Annular flumes have been used in laboratory investigation by several investigators. Those adapted for field use are noted under a separate heading. The following description pertains to the flume used by Mehta (1973).

Description

The apparatus, shown schematically in Figure 3, consists of a system of an annular channel and ring that rotate in opposite directions. The channel is made of 10-mm-thick fiberglass and the annular space is flanked by two concentric cylinders with a mean diameter of 1.50 m, giving a rectangular cross section 0.20 m wide and 0.46 m deep. The cylinders are mounted on a 13-mm-thick steel turntable 0.61 m in diameter. Four units of 76-mm by 51-mm plexiglass windows are provided every 90° in the lower part of its outer wall for visual observation. An annular false bottom made of 3-mm-thick plexiglass and having the same dimensions as the annular ring is used to facilitate direct measurement of the bed shear stress using temperature-compensated strain gages.

The annular 6-mm-thick plexiglass ring, which has the same mean diameter as the channel, but with a slightly smaller width of 0.19 mm, is positioned within the channel. The ring is suspended from four flexible stainless steel blades that are 0.6 mm thick, 0.08 m wide, and 0.52 m long. The width of the ring is 6 mm less than that of the channel, yielding a radial gap of 3 mm between each edge and the channel wall. The speeds of the ring and the channel are controlled independently through two variable speed driving motors using a concentric shaft assembly.

Theory

The fluid confined within the annular space is driven by the differential motion of the ring in contact with the fluid and the channel. The rotational motion of the channel and the ring sets up a flow field that is mainly in the azimuthal direction, thereby eliminating undesirable end effects associated with a straight flume assembly. The essentially axi-symmetric flow that ensues is then analyzed based on a one-dimensional (azimuthal) flow condition. However, a secondary flow in the radial direction is also induced due to the varying radial pressure gradient across any cylindrical plane, and may violate the assumptions of little variation in both the azimuthal and radial directions inherent in one-dimensional flow analyses.

Partheniades and Kennedy (1966) argued that the desired near-uniform flow field in the radial direction can be achieved by rotating the channel and the ring in opposite directions, the latter at a greater speed. At a sufficiently large differential speed, the larger vertical momentum of the downward flow induced by the faster rotating ring then balances the radial pressure gradient near the channel bottom, and hence reduces the secondary flow there. Their

contention was supported by flow experiments using plastic beads and small threads attached to the channel bottom, which indicated that the secondary current velocities were of the order of 10 to 20 percent of the corresponding azimuthal velocities when the operating curves for the channel and ring speeds were followed.

More recently, Sheng (1988) calculated the strength of secondary flow within rotating annuli using an integral boundary layer model and measured azimuthal velocities. When applied to a rotating-ring-fixed-channel assembly with specified configuration [see Table 3 under Fukuda (1978) for dimensions], it was shown that the average radial velocity would be approximately 20 percent of the mean azimuthal velocity outside the boundary layer, but 50 percent of the azimuthal velocity at 0.1 cm above the bottom.

Using the Reynolds equations in a simplified form in conjunction with the continuity equation in cylindrical coordinates, Maa (1993) showed by numerical experiments that near the channel bottom [see Table 3 under Maa (1993) for dimensions] the maximum radial velocity would be about 10 percent of the nearby azimuthal velocity, which is reasonably constant except close to the two corners for a ring rotating speed of 8 rpm. In addition, the radial bed shear stresses would be about 20 percent of the azimuthal bed shear stresses, and the total stresses would be close to the azimuthal bed shear stresses. These calculations indicate that the effects of secondary flow can be reduced to an insignificant level by a judicious choice of flume dimensions and the rotating protocol.

Operation

Water and sediment are first introduced into the annular space through the open top of the channel with the ring raised. The ring is then positioned in the channel such that it just touches the surface of the water. For each channel speed, the ring is then rotated at a predetermined speed based on operating curves established to accomplish uniform deposition of sediment across the channel width.

Sample results

Two typical results of resuspension experiments using the apparatus (Mehta and Partheniades (1979)) are shown in Figure 4 (density-stratified bed) and Figure 5 (uniform bed). The density-stratified bed was obtained from gradual sediment deposition from suspension while the channel was in slow motion and the bed shear stress was kept slightly less than the shear stress at which the entire sediment deposits. The uniform bed was prepared outside the channel at a mean density close to that of the deposited sediment and subsequently placed and leveled into the channel. The sediment used in both cases was a commercial kaolinite.

In the case of the stratified bed, which emulates a typical situation with respect to the surficial sediment layers found in estuaries, it is seen that the slope of the concentration-versus-time curve, hence the erosion rate, decreases

with time as the strength of the bed increases with depth. In contrast, Figure 5 exhibits a constant slope, i.e., constant rate of erosion, after a relatively short transient period. More results are available in Parchure (1984).

Other rotating annular flumes

Variously dimensioned rotating annular flumes can be found in the literature. They all follow the same general principles described above and differ mainly in instrumentation for measurement. Table 3 lists several such flumes.

Table 3
Laboratory Annular Flumes

Investigator(s)	Dimensions (m)[a]				Operating Mode
	d_i	d_o	w	h	
Partheniades and Kennedy (1966)	0.72	0.91	0.10	0.30	Counter-rotating
Mehta (1973)	1.12	1.52	0.20	0.46	Counter-rotating
Fukuda (1978)	1.02	1.32	0.15	0.30	Rotating ring
Fukuda (1978)	0.92	1.52	0.30	0.30	Rotating ring
Kusuda et al. (1985)	0.80	1.20	0.20	0.20	Counter-rotating
Burt and Game (1985)	5.20	6.00	0.40	0.35	Rotating ring
Tsai and Lick (1988)	1.70	2.00	0.15	0.20	Rotating ring
Kuijper et al. (1989)	1.90	2.30	0.20	0.30	Counter-rotating
Murakami et al. (1989)	1.25	1.55	0.15	0.20	Counter-rotating
Li (1989)	1.08	1.50	0.21	0.41	Counter-rotating
Lau and Krishnappan (1991)	1.60	2.00	0.20		Rotating ring
Krishnappan (1991)	4.70	5.30	0.30	0.30	Counter-rotating
Moller-Jensen (1993)	1.50	1.90	0.20	0.26	Rotating ring

[a] $d_i = 2r_i$ = inner diam; $d_o = 2r_o$ = outer diam; $w = r_o - r_i$ = width; h = height.

Race-track Flumes

Introduction

Several flumes of this type have been used. The following description pertains to that of Mehta and Srinivas (1993). The apparatus is similar in concept to its counterpart in the study of salt-stratified flows (Narimousa and Fernando (1987)).

Description

The flume, shown schematically in Figure 6, consists of a horizontal recirculating open channel with a disk pump system to generate fluid shear in the study of interfacial instability and resultant fluid mud entrainment. The flume is made of variable thickness plexiglass (3.2 mm at the curved portions and 12.7 mm at the thickened linear test section and pump section). The width of the flume narrows linearly from 48 cm at the base of a bi-triangular section containing the pump and flow separators to 10 cm at the junction with the curved portion (a tapering distance of 79 cm) and thereafter. The flume is symmetrical about the above pump section with a 200-cm-long linear section for testing purposes.

The disc pump consists of two vertical, motor-driven shafts, which rotate in opposite directions. Each shaft is stacked with a number of thin discs of sand-blasted plexiglass. These are of two diameters, 4 and 13 cm, and are stacked alternately on each shaft, arranged so that a small disc on one shaft meshes with the larger of the other, thus almost sealing the center of the pump, while the fluid is thrown as a series of horizontal jets around the outside of the smaller discs and between the larger discs. In order to prevent the discs from "sucking up" the density interface, a horizontal "splitter plate," which extends downstream into the curved segment, is placed at a height of 31 cm above the flume floor to effect horizontal partitioning.

The disk pump, which is designed to minimize any intrusive effect of pumping on the interfacial dynamics, drives the initially clear water layer relative to the higher density fluid below. The ovate geometry guides the flow gradually into the linear test segment without undue interference. In addition, the effect of helical secondary flows on the processes occurring within the linear test segment is minimized by the installation of the splitter plate. Hence, the incorporation of the straight test segment allows secondary flows developed in the bends to decay, yielding an experimental environment with a generally unidirectional flow.

When the pump is turned on, the energy of the generated turbulent shear flow leads to the development of substantial instabilities at the density interface. The cumulative effect of the movement of the density interface and the increasing dissipation of turbulent kinetic energy on the entrained sediment aggregates manifests in a change in the mixed (upper) layer mean velocity, which is monitored.

Operation

During a test, the flume is first filled to the requisite pre-selected height of water. Pre-mixed fluid mud is then introduced through the intake at the flume bottom. The initial height of the fluid mud layer is kept at just below the elevation of the splitter plate. With time, as the fluid mud is entrained, movement of the density interface is tracked and velocity variation in the mixed layer is monitored.

Sample results

Figure 7 illustrates typical velocity profiles when kaolinite was used as fluid mud sediment. Time t is the elapsed time during which the characteristic velocity is U, and the shear layer thickness is δ_s. With increasing velocity, an outward "bulge" developed in the velocity profile due to the combined effect of the disk pump, flow inertia below the disks, and the confining effect of the interface. The corresponding variation in density (Figure 8) attests to the fact that above the lutocline (mud-water interface) the sediment was consistently well-mixed. Below the lutocline, hindered settling and self-weight dewatering caused the density to become increasingly non-uniform with depth.

Other similar devices

In mud studies, an apparatus of similar setup has been used by Ali et al. (1992). It differs essentially from the one just described in that the flow is driven by a toothed belt in contact with the water surface in the rear straight section. Further details are summarized in Table 4, which also includes an earlier version used by Watanabe et al. (1978).

Table 4
Race-track Flumes

Investigators	Dimensions	Instrumentation	Use
Watanabe et al. (1978)	Two semicircular bends of internal radius 50 cm joined by two straight sections each 5 m long. The channel is 0.15 m wide and 0.5 m high.	Rotating paddle wheel capable of generating both steady and sinusoidal velocity.	Study of concentration profiles.
Ali et al. (1992)	Two semicircular bends of internal radius 75 cm joined by two straight sections 4 m long each. The channel is 30.5 cm wide and about 1 m high (with a maximum working depth of 57 cm).	Toothed belt in the rear straight section and laser-doppler anemometer for velocity measurement.	Study of fluid mud formation and transport.
Mehta and Srinivas (1993)	Two semicircular bends of internal radius 46 cm joined by a straight section 2 m long. The rear section is bi-triangular in shape to accommodate the disc pump and flow separator assembly. The channel is 10 cm wide and 61 cm high.	Disk pump with a horizontal splitter plate, a vertically adjustable electro-magnetic current meter and a flow-through densimeter.	Study of fluid mud-water interfacial dynamics.

Rocking Flumes

Introduction

Thus far only one such apparatus has been reported in the literature. The following description is based on the work of Villaret and Paulic (1986).

Description

The rocking flume, shown schematically in Figure 9a, is constructed of 12.5-mm-thick plexiglass. It measures 2.4 m in length and 0.36 m in height with an inner width of 0.15 m. A 7-cm-high false bottom is built into the flume within which a deepened section (54 cm long x 5 cm deep) is located to function as the test section, hence yielding an actual depth of 0.29 m. The entire assembly is mounted on a table via a pivot, giving a bottom clearance of 16 cm above the table top, which permits a rocking motion.

The flume is operated by a hydraulic transmission attached to a 0.75-hp motor. A metal shaft (rocking arm) at one end of the flume connects a rotating plate driven by the motor through a motor shaft to the flume via a hub. In operation, the rotating shaft moves the rocking arm up and down, thereby causing the flume to rock back and forth. Both the period and the magnitude of the rocking motion can be adjusted by varying the motor speed and the eccentricity of the rocking arm/rotating plate connection, respectively.

A plexiglass top constriction 19 cm high and 54 cm long (Figure 9b) is placed in the water column over the sediment bed to increase flow velocity. Its ends are sloped to reduce turbulence at the flow entrance and its height above the bed can be varied. Hence, the free surface flow in the flume is transformed into flow in a "tunnel" in the central portion of the flume.

Due to the controlled rocking motion imparted to the flume, the current generated at the sediment surface has a sinusoidal velocity variation. The flume is calibrated to produce a maximum shear stress up to 0.8 Pa. Rocking flume data were compared with those from the annular flume as follows. The maximum velocity was first determined by using direct measurement of the displacement of the water level, by an electromagnetic current meter, and by considering flow continuity. These velocity data were then used to compute the maximum applied shear stress using the relationships established by Jonsson (1966), which was formulated for progressive waves. To adapt to the case of standing waves, the computed maximum shear stress was integrated over one-half a wave period to obtain the mean shear stress, which is one-half the maximum shear stress. This is the shear stress that was used in comparing the results of erosion experiments obtained from an annular flume (steady current) and the rocking flume (oscillatory current). In general, the bed shear strength was lower under oscillatory currents than under steady currents. The discrepancy was attributed to the process of bed softening under oscillatory currents, implying a degradation of bed shear strength due to a breakdown of the structure of the deposited aggregates.

Operation

Two types of bed can be tested: placed bed, wherein a thick pre-mixed slurry is placed in the flume to uniform depth, and deposited bed, wherein a dilute suspension of sediment is allowed to settle out of the water column and consolidate into a bed. The bed is then subjected to selected shear stresses. During the test, samples at various depths in the water column are collected periodically for concentration determination.

Sample results

Figures 10 and 11 show typical concentration-time curves for two deposited beds composed of different sediments. The kaolinite was of a commercial grade while the estuarine mud was collected from a tidal flat near Cedar Key, Florida, which had a principally montmorillonitic content (73 percent). Both curves exhibit a series of steady states (characterized by constant final concentrations). Higher concentrations were observed for the kaolinite bed for the same applied shear stress, due to its greater erodibility than the estuarine mud.

Other similar devices

In mud studies, this device appears to be the only one of its kind. Tilting flumes are generally used to study the effects of gravity-induced instability, and are thus different materially from the rocking flume arrangement (e.g., Ali and Georgiadis (1991)).

Closed-Conduit Sediment-Water Tunnel

Introduction

Closed conduits in which the fluid recirculates in either the vertical or the horizontal plane have been used to study cohesive sediment erosion. The following description pertains to that of Teeter and Pankow (1989).

Description

The device, shown schematically in Figure 12, is a closed-conduit sediment-water tunnel designed to safely test contaminated sediments. Hence, it is open to air only at a small expansion chamber. The water tunnel, which is made of 12.5-mm-thick clear acrylic, has a uniform cross section, which changes from rectangular (38 cm wide x 9 cm deep) in the horizontal deposition/ resuspension sections to circular (20.3-cm internal diameter) in the vertical settling and pumping sections. The volume of the water tunnel is 0.28 m^3, and the available surface area for sediment deposition and resuspension is 1.64 m^2. Flow in the tunnel is driven by a tandem pair of two-bladed, skewed propellers and by a variable-induction motor. Settling tests can be performed in the descending tube while the deposition and resuspension tests are performed in the rectangular conduit sections by sampling.

The water tunnel has been calibrated so that the propeller speed is related to average velocity and bed shear stresses using a tachometer, a flowmeter, and a hot-film shear stress sensor. The effects of secondary flow and other flow irregularities have been examined using flow visualization techniques and judged to be small based on the overall smooth flow pattern and a uniform turbulence structure. The propeller wakes are confined within the ascending tube.

Operation

In a particular test involving composite dredged material from New Bedford Harbor, Massachusetts, reconstituted sea water was used in the tunnel, with the addition of formaldehyde solution to inhibit microbial growth. An initial water tunnel sediment bed was established by injection of sediment during deposition periods. Subsequent tests then alternated between resuspension and deposition episodes accompanied by addition of sediment to the water tunnel without removal of material from previous tests. Hence, sediments resuspended from the bed of the tunnel at the beginning of the each test became incorporated into the test material.

Strict safety procedures such as full length disposable suits, neoprene gloves, respirators, etc., are required of all personnel when the sediment contains hazardous substances.

Sample results

In the above test, no resuspension results in graphical form were presented, but the equilibrium resuspension concentration at each applied shear stress was tabulated. It was observed that erosion was rapid during the first few minutes after the application or increase in bed shear stress. Erosion decreased rapidly as the tests progressed, and the suspended concentration reached an equilibrium value.

Other similar devices

A similar device, but of simpler construction, was used by Raudkivi and Hutchison (1974). The details are given in Table 5, which also includes another device (Kelly and Gularte (1981)) where the fluid recirculates in the horizontal plane.

Rotating Cylinder Apparatus

Introduction

Several devices of this general type have been used. The following description pertains to that of Chapuis and Gatien (1986).

Table 5
Closed-Conduit Devices

Investigators	Dimensions	Instrumentation	Remarks
Raudkivi and Hutchison (1974)	51 mm x 51 mm rectangular cross-section with a sediment holder (51 mm x 38 mm wide) placed flushed with the conduit floor.	Circulating pump, flowmeter, preston tubes and heat exchanger unit.	Made from stainless steel, perspex and rigid PVC for studying the dependence of sediment erodibility on temperature, salinity, zeta potential, and ion exchange capacity.
Kelly and Gularte (1981)	15.2 cm x 15.2 cm rectangular cross-section.	Four-blade ducted propeller; refrigerated water tunnel.	
Teeter and Pankow (1989)	38 cm x 9 cm rectangular cross-section.	Two-bladed skewed propeller, flowmeter, hot-film shear stress probes.	Made from 12.5-mm-thick clear acrylic to test contaminated sediments.

Description

The device, shown schematically in Figure 13, consists of a cylinder of cohesive soil mounted coaxially inside a slightly larger transparent plexiglass cylinder which rotates during the test. The annular space between the cylindrical soil sample and the outer rotating cylinder is filled with the desired eroding fluid to transmit shear from the rotating cylinder to the surface of the soil sample. In this particular configuration, the prepared cylindrical soil sample (75 mm diam x 89 mm long) is placed between two metallic short cylinders (base and head), both guided in rotation by ball bearings. There is no shaft within the sample, which distinguishes it from that of Moore and Masch (1962) in that in the latter device the clay sample was reconstituted around a metallic shaft to which lower and upper plates were connected for support and trimming of the sample. The base rotates freely relative to the bottom of the outer cylinder in order to measure the torque transmitted by the eroding fluid to the soil cylinder by means of an upper shaft connected to the head. The transparent cylinder has an inside diameter of 102 mm and can be rotated at regulated speeds up to 1,750 rpm.

Theory

The apparatus makes use of annular water flow between two concentric cylinders due to the motion of the outer cylinder, while the inner one remains stationary. When the outer cylinder is rotated, rotation is imparted to the fluid, which in turn transmits a shear to the surface of the soil sample. The shear stress at the clay-fluid interface is computed from the torque required to hold the sample stationary, which is directly measured using a pulley and weight system with masses ranging from 0 to 40 g with a 0.1-g precision, as opposed to the use of a calibration curve between the applied shear stress and rpm of the outer cylinder by Moore and Masch (1962).

Moore and Masch (1962) reasoned that because of the stabilizing inertial forces resulting from a velocity distribution that increases in the radial direction, the turbulence level at the soil surface should be relatively low, resulting in a small variation in the instantaneous value of shear stress. Hence, the cylindrical form of soil samples and the action of the end pieces (mounted immediately above and below the soil sample) should result in a uniform value of the shear stress over the entire surface of the sample. However, in analyzing the hydrodynamic conditions in a rotating cylinder setup, Rohan and Lefebvre (1991) showed that the flow between the two cylinders is always turbulent due to the relatively high rotational velocity attainable (1,750 rpm, maximum in the device of Chapius and Gatien (1986). The turbulent flow structure in an annulus departs from that of a rectilinear flow due to the presence of a centrifugal force. The latter flow regime more closely mimics field situations. Hence, Rohen and Lefebvre (1991) caution that the real shear stress may be underestimated by an order of magnitude due to streamline curvature and the fluctuations in the radial component of velocity.

Operation

First the sample is either cut from intact blocks using a template and a steel wire, or reconstituted and reconsolidated in a triaxial cell after physicochemical or mechanical treatment. The clay cylinder is then mounted on a pivoting base and emplaced. After the eroding fluid is added into the annular space, the test commences with several stages, each at a constant rpm. Each stage is held for 10-30 minutes and the shear-stress-induced couple continuously recorded. At the end of each stage, the fluid is removed and the cell cleaned with fresh fluid. All eroded particles thus recovered are oven-dried and weighed to obtain the eroded mass. This procedure obviates repetitive manipulations of the sample, which may contribute to sample remolding.

Sample results

Typical results of tests conducted on undisturbed natural clays from Northern Quebec are shown in Figure 14, which illustrates the influence of the sample preparation method (Chapuis 1986). The consistently lower curve for the minimum registered value of the hydraulic shear stress at a given speed exhibited by the triaxially prepared samples is attributed to their smoother surface compared to the cut samples. The test results indicate that the hydraulic shear stress depends on surface roughness, which in turn is influenced by the erosion process.

Other similar devices

The device described is a modified version of the one originally developed by Moore and Masch (1962); the changes being in the use of intact samples, rotation guidance, alignment and influence of end supports on the annular flow regime. A similar device has also been used by Arulanandan et al. (1975). Further details are summarized in Table 6.

Table 6
Rotating Cylinder Devices

Investigators	Dimensions	Instrumentation	Remarks
Moore and Masch (1962)	Cylindrical clay sample with a 76-mm outer diameter x 76-mm length, with a central metallic shaft as the core in a slightly larger cylinder capable of rotating up to 2,500 rpm.	Torque is derived from a calibration curve obtained using a pulley-weight system.	Only remolded samples can be tested.
Arulanandan et al. (1975)	Cylindrical clay sample with a 76-mm outer diameter x 82-mm length, with a center metallic shaft as the core in an outer cylinder with an inner diameter of 102 mm capable of rotating up to 1,100 rpm.	Torque is obtained from a calibration curve obtained using a pulley-weight system. Wet sample is periodically removed for determination of eroded sediment mass.	Only remolded samples can be tested.
Croad (1981)	Cylindrical sample suspended concentrically in the flow.	Rotating outer drum drives the flow.	
Chapius and Gatien (1986)	A wholly cylindrical clay sample 75 mm in diameter x 89 mm long in plexiglass outer cylinder with an inner diameter of 102 mm capable of rotating up to 1,750 rpm.	Pulley-weight assembly to measure torque; eroding fluid withdrawn for determination of eroded sediment mass.	Both reconstituted and intact samples can be tested.

Drill-hole Test Apparatus

Introduction

The following description pertains to the apparatus of Rohan et al. (1986).

Description

The device, shown schematically in Figure 15, consists of a stainless steel tube serving as the sediment compartment through which the eroding fluid is forced down an axial circular hole created earlier by drilling. The sample tube measures 44.5 mm in outer diameter and 35.4 mm in inner diameter and 100 mm in length. The hydraulic head for the flow is provided by a constant head reservoir capable of generating a flow velocity in the drill hole up to 10 m/s corresponding to an applied shear stress of 450 Pa.

First the relative change of the diameter of the drill hole caused by erosion is calculated based on the dry weight of the eroded sediment collected in the sedimentation basin at the outflow end of the specimen. The flow rate is measured by a flowmeter, and the pressure difference caused by frictional

losses in the specimen is then measured by differential manometer, the various losses being accounted for with the use of the Moody diagram. The evaluation of the applied shear stress is then based on the control-volume momentum equation.

Operation

The device is designed for studying the erodibility of intact undisturbed clays, and hence the specimens are trimmed from block samples to minimize sample disturbance. The specimen is first trimmed to a diameter of about 37 mm and lowered into the tube whose other end is fixed by a circular cutting tool. A mechanical lathe is used to drill the hole in the rotating soil cylinder, giving an initial hole diameter of 6.4 mm and presenting a total surface of 20.0 cm^2 for erosion.

Sample results

Typical results of two Canadian clays are shown in Figure 16. As noted by Rohan et al. (1986), at the end of the test period, the St. Barnabe clay had not reached its critical shear stress at an applied shear stress of 400 Pa, as evidenced by the rather constant amount of eroded material. On the other hand, a critical shear stress of 170 Pa can be defined for the Grande Baleine clay as characterized by the net increase in the rate of erosion.

Other similar devices

A somewhat similar device was used earlier by Christensen and Das (1973), in which the sediment sample is prepared in the annular space between a brass tube and an inner molding tube. Further details are given in Table 7.

Vertical Grid Oscillator

Introduction

This is a portable device designed for rapid erodibility assessment. The following description relates to the device of Tsai and Lick (1986).

Description

The apparatus, shown schematically in Figure 17, consists of a cylindrical chamber inside of which a horizontal grid oscillates vertically. The cylindrical chamber, which is made of cast acrylic tubing, is 27.9 cm high with an outside diameter of 12.7 cm and inside diameter of 11.7 cm. The grid element is a 6-mm-thick plexiglass disc 11 cm in diameter, which is perforated with 12-mm-diameter holes at 15-mm centers, giving a porosity of 42.8 percent. The grid is oscillated by a 1/8-hp permanent magnet DC motor via drive rod and linkage bar connection.

Table 7
Drill-hole Test Devices

Investigators	Dimensions	Instrumentation	Remarks
Christensen and Das (1973)	Molded 3.2-mm-thick smooth clay lining of 1.9 cm inside diameter, 10.2 cm long.	Constant-head tank, flowmeter, and shear stress computed using approximate friction factor.	Made from brass tube to test saturated, compacted samples.
Rohan et al. (1986)	Drilled cylindrical erosion surface with 6.4-mm diameter x 100-mm length.	Constant-head tank, flowmeter, differential manometer, and shear stress computed using approximate friction factor.	Made from stainless steel tube to test undisturbed sediments.

The sediment whose erodibility is to be determined is placed at the bottom and overlain by water. The grid oscillates in the water and creates turbulence which penetrates down to the sediment-water interface and causes resuspension. It is recognized that while the turbulence generated by an oscillating grid is different from that operating in the field, i.e., due to currents and waves, the issue is circumvented by calibrating resuspension results from the grid oscillator to those obtained in a conventional flume experiment. The basic premise is that when the flume (with a given applied bed shear stress) and oscillator (with a given frequency) produce the same concentration of resuspended sediment under the same environmental conditions, the stresses required are considered equivalent.

Operation

The grid oscillating device can be used in both the laboratory or field setting. In field operation, the cylindrical chamber consists of three parts: an open-ended cylindrical tube, a bottom disc, and a top plate. The diver first pushes the tube down into the sediment. The bottom disc is then forced into the sediment from the side of the tube and slid to the location of the tube. By pushing the bottom disc up, the sediment core is firmly confined in the tube. Finally, the top plate is placed on the top of the tube and the whole assembly brought up to the ship. After the thickness of the sediment core is measured, the overlying water is adjusted to the height used in the calibration experiment (12.7 cm) and the test started with periodic suspension concentration measurement by sampling.

Sample results

A typical result from a shallow-water field test carried out in Lake St. Clair near Detroit, Michigan, is shown in Figure 18 based on two different equivalent shear stresses. At each station, the concentration at the higher shear stress is observed to be higher. In all cases, the concentration rises very rapidly initially and then levels off until it reaches a quasi-steady state. The decrease of the concentration noted in most cases thereafter is believed to be

the result of sediment compaction created by the fluctuating grid-generated pressure, which could change the entrainment process. Hence, it is advised that the device not be used for multiple shear tests.

Other similar devices

Other similar devices used in sediment entrainment studies are given in Table 8.

Table 8
Vertical Grid Oscillators

Investigators	Dimensions (cm)[a] d_i	d_d	h	Remarks
Tsai and Lick (1986)	11.7	11.0	27.9	6-mm-thick plexiglass horizontal perforated grid in cast acrylic tube cylinder.
Wolanski et al. (1989)	9.5	8.5	50.0	15 circular flat rings (7 mm wide x 5 mm thick, 2 cm apart vertically) constitute the grids.
Teeter (1994)	11.5	11.0	12.7	6-mm-thick plexiglass horizontal perforated grid in cast acrylic tube cylinder. The height indicated is the depth of fluid.

[a] d_i = inner diam; d_d = disc diam; h = height of cylinder.

Propeller-based Apparatus

Introduction

Several apparatuses in this category have been reported in the literature. The following description pertains to that of Schunemann and Kuhl (1993).

Description

The device, code-named the EROMES System and shown schematically in Figure 19, consists of a tube containing the sample and a large container to store the eroded material during an experiment in a turbulent suspension. It is another experimental approach to investigate the erosion of muddy sediments with possible surface coatings intact and sedimentary textures preserved. Contrary to the more conventional approaches whereby clearly defined parameters from a wide-ranging suite of environmental factors are singled out for examination, the emphasis here is to investigate what happens in a simulated environment. The sample tube is the actual tube used in collecting field samples. The submerged sample is mounted in a vise with a calibrated propeller in water and located 3 cm above the sample surface. The propeller consists of six evenly spaced lamellae as baffles. The sample tube, which is made of perspex with a diameter of 10 cm, is connected by pipes via a dispersing machine and a pump to a large container for storing the eroded

material in a turbulent suspension. The sample as placed has an exposed surface area of 78.5 cm^2 for testing purposes. A calibrated gamma probe measures the density profile of the sediment bed sample based on attenuation of emitted rays, while an attenuation meter continuously monitors the concentration in the container by measuring the attenuation of a beam of transmitted light of constant intensity.

The apparatus uses turbulence artificially induced by the propeller to erode the samples and to keep the eroded material in suspension. The eroded material is stored in the large container with a different and larger set of propellers, which run at a higher speed in order to induce a homogeneous distribution of suspended matter in the container. The suspension in the sample tube is continuously pumped into the storage container and a second connection, the return pipe, carries the suspension back to the sample tube. Thus, there is an exchange of suspension between the storage container and the sample tube to simulate natural conditions in the sample tube. The attenuation meter is calibrated by sampling the concentration of the suspension and using filtering techniques to relate the attenuation factor to the suspension concentration. In this way, the erosion rate can be computed from the calibrated curve that converts the attenuation value to g/l of suspended matter.

Operation

The propeller initially turns at 50 rpm. The revolution is then increased in steps of 20 rpm in 5-min intervals until clearly perceptible erosion starts. Then the propeller revolution is kept constant for 40 min to record the erosional behavior under constant conditions. Finally, the revolution is reduced below the level of the critical bottom shear stress and the suspension sampled for the determination of concentration. After 10 min of stabilization the next increment is initiated.

Sample results

Figure 20 shows the results from a typical erosion experiment. The three subplots are from the same experiment. The top diagram displays the time variation of concentration in the storage container. The center diagram depicts the time series of bottom shear stress applied to the sample. The bottom diagram shows the change in the erosion rate with time. It is seen that during increasing bottom shear stress episodes, the erosion rate generally increases as well, while during the 40 min of constant applied shear stress it decreases, which reflects increasing erosion resistance of the sediment bed with depth.

Other similar devices

Simpler versions of the above concept have been used to study microbially enhanced stability in the laboratory setting. The apparatus essentially consists of a flask containing the cultured bed agitated by a mechanical stirrer. The relative erosion of different sediments and under different biotic control is measured as the dry mass of the sediment in suspension after stirring at a known rpm for 5 min (Holland et al. 1974, Paulic et al. 1986).

Other Erosion Test Devices

Introduction

The devices included here are those that were used in the 1960's through early 1970's and have since seldom been used in studying cohesive sediment dynamics. They are included here for completeness.

Rotating disk device

The rotating disk device of Liou (1970), schematically shown in Figure 21, was used to study the variation of the critical erosion shear stress of clay samples with different chemical additives and subjected to different ambient temperatures. It consists of a rotating disk (0.33-m diam x 1.3-cm thickness) in a steel cylindrical container (0.34-m diam x 0.2-m height), the bottom of which is a circular steel soil sample pan (0.29-m diam x 5-cm height). The disk, rotating in a fluid that is at rest and confined, essentially generates an axi-symmetric boundary layer structure. At sufficiently high disk Reynolds number, separate boundary layers form on the surfaces of the disk and the fixed bottom. The flow condition near the soil sample consists of an inward radial velocity, tangential velocity, and axial upward velocity. By solving the Navier-Stokes equation in cylindrical coordinates with simplifying assumptions, it is shown that the fluid shear stress above the soil sample depends on the rotational speed in the core region; i.e., the fluid region between the top and bottom boundary layers. There is a dynamic equilibrium between the centrifugal forces and the radial pressure gradient. Hence, for a given rotational speed, the shear stress is linearly proportional to the distance from the center, which is calibrated with the disk positioned 2.5 cm above the surface of the sample and covered in 6.4 cm of eroding fluid.

The test commences by turning on the rotating disk at the selected rotational speed. The turbid fluid is periodically drained and replaced with fresh fluid. The point at which the outer edge of the sample begins to erode is found by the use of a point gage.

A typical test result on bentonite samples in terms of the erosion shear stress-time variation with different chemical additives is shown in Figure 22. The constant value reached by the erosion shear stress after a period of time is identified as the critical erosion shear stress. Hence, the critical erosion shear stress is seen to be the highest for the case of 0.1N NaCl as the additive.

Submerged jet

This is essentially a technique used to empirically relate the scour resistance of a cohesive soil sample to a vertically directed water jet to bulk soil properties such as plasticity and clay mineralogy. The description here is based on the work of Dash (1970).

The jet apparatus, schematically shown in Figure 23, consists of a 0.76-m-long plexiglass tube with 2.5-cm internal diam fitted with a 3.2-mm-diam jet

nozzle at the lower end. Water is supplied from a constant-head tank. The cylindrical sample tube measures 7.6 cm in diameter by 32 cm, with the soil sample seating snugly at its bottom.

During the test, the jet tip is placed 2.5 cm above the sediment surface. Erosion losses are determined based on the change in the weight of the sample. Figure 24 shows a typical test result conducted on kaolin samples. In the figure, σ_{cmax} refers to the maximum consolidation pressure the sample has been subjected to prior to testing. Generally it is seen that a lower consolidation pressure and a higher jet head both lead to higher erosion. Table 9 compares the submerged jet devices used by several investigators.

Table 9
Submerged Jet Devices

Investigators	Description	Primary Soil Variables	Primary Hydraulic Variables	Major Dependent Variables
Dunn (1959)	A nozzle produces a submerged vertical jet of water directed perpendicularly at the surface of the soil sample placed at the bottom of a lucite cylinder. No dimensions are available.	Plastic properties, vane shear strength	Head	Critical tractive stress
Moore and Masch (1962)	2.5-cm-diam tube fitted with variable size nozzles; 12.7 cm diam x 10.2 cm cylindrical sample holder in 0.91 m square x 0.46 m lucite tank	Shear strength	Jet elevation	Depth of erosion, location of incipient scour
Dash (1970)	0.76-m-long plexiglass tube with 2.5-cm internal diam fitted with a 3.2-mm-diam nozzle; 7.6-cm-diam x 32-cm cylindrical sample tube	Clay mineralogy, percent clay, tensile strength	Head	Eroded sediment mass

2 Field Devices and Instrument Assemblies

Introduction

Both field erosion test devices and instrument assemblies have been used, the latter specifically to collect erosion data in near-bottom areas composed of cohesive beds. Following the descriptions of the field erosion test devices, several field instrument assemblies as summarized in Table 10 are briefly described.

Field Inverted Channels

Introduction

This is an application of the commonly used straight flumes to field situations for in situ determination of erosion threshold and entrainment rates of undisturbed deep sea bottom sediments. Several investigators have used this device; the following description pertains to that of Gust and Morris (1993).

Description

The apparatus consists of a 2-m x 0.4-m x 0.2-m deep inverted channel, which forms a duct upon contact with the sediment surface. The design is based on the original equipment of Young and Southard (1978) used in the study of the erosion of in situ fine sands, but with modifications to the instrument package and superstructure that permit free-falling deployments and recovery at water depths less than 4,000 m.

The flume is located within a triangular outer tripod with a base length of 3.5 m and height of 3 m, which carries the flotation-anchoring assembly and the hydraulic piston from which the flume is suspended. The flume section is equipped with a pump, discharge control, and sensor and power supply packages. The channel is made from 6-mm-thick aluminum sheet and is fitted with a 40-cm flared entrance to reduce flow disturbance there. The duct outlet is bolted to a gated control box and a DC-driven axial pump that sucks the water through the duct. Speed of flow is determined by the cross section of the duct, the position of the gate, and the power delivered to the pump.

Table 10
Field Instrument Assemblies

Investigator(s)	Assembly/Array	Construction	Instrumentation[a]							
			TU	CM	PT	DP	TE	SA	CA	WS
Nichols et al. (1978); Nichols (1989)	Sediment-water interface probe	Steel tripod frame 3.7 m high with a circular base 1.8 m in diam equipped with lead ballast and steel pads for stability; central hydraulic cylinder with 1.44 m vertical free play	✓	✓	✓	✓				
Bohlen (1982)	DAISY Tower	Aluminum tripod frame 3 m high with a circular base 2 m in diam in-filled with lead and concrete for stability	✓	✓			✓	✓	✓	✓
Bedford et al. (1982; 1987)	OSU instrumentation	Mounted on a host tower (e.g., DAISY Tower)	✓[b]	✓	✓		✓			
Mehta and Jiang (1990)	COE field tower[c]	Aluminum tower 2.45 m high with a rectangular base 1.5 m x 1.0 m with protruding pins from the leg supports for anchoring; a central 4.2-cm-diam aluminum shaft within a concentric pipe with an outer diameter of 5.8 cm serves as sensor holder.		✓	✓					
Diserens et al. (1993); Teisson et al. (1993)	HR instrumented bed frame	Triangular framed open structure with protruding legs for anchoring	✓	✓	✓					

[a] TU = turbidimeter/transmissometer; CM = current meter; PT = pressure transducer; DP = density probe; TE = thermistor; SA = salinity sensor; CA = camera; WS = water sampler.
[b] Includes an acoustic sediment concentration profiler.
[c] Includes a biaxial accelerometer.

The straight flume operates as a flow-through system. The rectilinear flow generated by the sucking action of the axial pump produces an applied bed shear stress to the sediment surface, which is measured by flush-mounted friction velocity sensors. An additional array of hot-film anemometers measures the velocity profile. The suspended sediment load that results is measured by fore and aft optical attenuation meters, and the remolding of the sediment surface is monitored by a camera. Natural flows superimposed on the pump-generated flow do not invalidate the measurements, since the friction velocity probes always measure the resulting wall shear stresses exerted on the sediment surface.

Operation

For deployment, the flume section is first retracted above the tripod base by the bleeding action of the suspending piston, and the entire assembly is lowered into water. Once the superstructure makes contact with the sea bottom, the suspended flume is made to settle onto the sea bottom whereby the sidewalls penetrate to a depth of about 5 cm, resulting in a flow cross section of 630 cm^2. A weight then triggers off a succession of automated operations involving the recorder, probes, camera, discharge control gate and pump motor. Data are stored in a digital multi-channel recorder. The sensors are calibrated in the laboratory for the anticipated ambient temperature range, and checked with a portable calibration device prior to deployment.

At the completion of field operation, a spring-loaded pulley jettisons the anchor stones and the assembly returns to the surface where its retrieval is facilitated by the emission of radio and strobe signals.

Sample results

A typical result from a field deployment in Puget Sound, Washington, where the sediment surface consisted of a layer of consolidated cohesive mud is shown in Figure 25 in terms of the time variation of the optical transmissometer output voltages, which in turn is used to compute the mean concentration of suspended sediment in the flume duct. In the figure, open circles denote voltage from the front (inlet) transmissometer and closed circles, the back (outlet) transmissometer. Time series of entrainment rates are then calculated using these concentration data, leading eventually to the determination of the functional relation between erosion rate and applied shear stress.

Other similar flumes

Two other similar flumes have been reported earlier in the literature. They are the SEAFLUME (Young 1977), and the SEADUCT deployed at the HEBBLE (the High Energy Benthic Boundary Layer Experiment) site (Nowell et al. 1985) to measure in situ erosion rates of sea beds.

Field Rotating Annular Flumes

Introduction

This is an application of laboratory-developed rotating annular flumes to field scale for in situ experiments to study the complex erosion processes of natural seabeds. While the theory of generating hydrodynamic forcing is the same as their laboratory counterparts, these devices differ essentially in that they are necessarily bottomless, and employ a high level of sophistication in deployment requirement and instrumentation packages in order to operate in the field. Several investigators have used this device; the following description pertains to that used by Maa (1991).

Description

The apparatus, shown schematically in Figure 26, is functionally similar to laboratory annular flumes. Two 0.2-m-deep cylinders with diameters of 2 m and 2.3 m, respectively, form the inner and outer walls of the annular space, yielding a width of 0.3 m. During operation, the flume is lowered from a boat to penetrate the seabed at a predetermined elevation, giving a designed flume depth of 0.1 m. The flume has no bottom, and a ring at the top of the flume rotates at selected speeds to generate flow in the flume. The ring speed, which has a maximum at 14 rpm, is regulated by a shipboard personal computer and a 1-hp DC motor controller.

The flume is sealed between the rotating ring and side walls, which prevents sediment from escaping or entering the annulus. Therefore, measurement of an increase in suspended sediment within the flume determines the extent of bottom erosion. Instruments mounted over the seabed flume include an Optical Backscatter Sensor (OBS), two miniature Optical Transmissometers (OTS), a counter for ring speed, a water sampling system, and a data logger. On the ring, there is a plexiglass window to mount an underwater camera for photography of the seafloor around the channel to provide a view of the surface roughness.

Operation

The flume is lowered into place from a boat. After the flume has penetrated to the predetermined elevation, photographs of the bed condition are first taken and the ring rotation started. The ring speed is increased in a stepwise fashion. At each stage, there is a short period (first 2 minutes) of increasing speed followed by a longer period of constant speed. The OBS and the two OTS's then measure the suspended sediment concentration. The data logger serves as the analog-to-digital data converter and feeds the personal computer onboard for data recording.

Sample results

A typical result of an incipient erosion experiment conducted at Wolftrap shoal in the lower Chesapeake Bay is shown in Figure 27 in terms of the time

change of the measured suspended sediment concentration. The numbers shown above each step in the step-wise increase in ring speed are numerically computed bed shear stresses (dynes/cm^2). The mean water depth at this test site was 11.6 m, and the in situ sediments consisted of a mixture of fine sand (74 percent), silt (14 percent), and clay (12 percent) with a mean diameter of 0.03 mm. Biological activity at the site was judged to be quite significant.

Figure 27 indicates a critical erosion threshold of 1.28 dynes/cm^2, corresponding to the point of departure from the trend of constant concentration. The observed decreasing concentration level at constant ring speed is ascribed by the author to a combination of flume leakage, influence of suspended sediment on the bed shear stress, and redeposition of large sediment particles in low shear stress areas of the flume.

Other similar flumes

Two other similar flumes have been reported in the literature (Peirce et al. 1970, Amos et al. 1992). They differ largely in the driving system, size, and sealing device as summarized in Table 11.

Table 11
Field Rotating Annular Flumes

Investigators	Dimensions	Instrumentation[a]	Driving Mechanism
Peirce et al. (1970)	0.42 m outer diam x 0.05 m water depth	Pipette for sampling suspension	Battery-operated paddle wheel.
Maa (1991)	2.15 m mean diam x 0.20 m high x 0.30 m wide	One OBS, two OTS, data logger and underwater camera	Flow is generated by a rotating lid controlled by DC motor.
Amos et al. (1992)	2.00 m mean diam x 0.30 m high x 0.15 m wide	Three OBS, data logger	Flow is driven by a rotating lid equipped with paddles.

[a] OBS = optical backscatter sensor; OTS = optical transmissometer.

ISIS - Instrument for Shear Strength In Situ (Hydraulics Research Ltd., 1994)

The instrument, which was designed to measure the erosion shear strength of muddy sediments on inter-tidal mud flats, consists of a circular, inverted bell-shaped funnel 84 mm in diameter placed inside a cylindrical perspex column 90 mm in diameter. Other attachments include the pump and flow controller, batteries, reservoir, and flow meter. The whole assembly is mounted on a baseplate measuring 1 m x 0.35 m x 0.7 m. In operation, the

bell head is positioned at a typical distance of 4 - 8 mm above the mud bed. Water is drawn up through the center of the bell via pumping into a reservoir, which is then recirculated to replace the pumped water via the sides of the bell. The induced radial flow toward the bell center exerts an approximately even shear stress across the bed, the magnitude of which is controlled by the height between the bell head and the bed surface, and the pumped discharge through the system. In addition, turbidity is measured in the reservoir by an optical backscatter probe.

Sediment-Water Interface Probe (Nichols et al. 1978, Nichols 1989)

This is a dedicated bottom-mounted field instrument array designed for measuring fluid mud transport and behavior in the bottom boundary layer. As shown schematically in Figure 28, it consists of a central tripod support frame that houses the various measuring sensors and samplers. These include an optical turbidimeter, electromagnetic current meters, a nuclear transmission density probe, a pressure transducer, and suspended sediment pump samplers. These instruments are mounted independently and are connected by signal cables to shipboard signal processors and a data acquisition system.

The steel frame stands 3.7 m tall with a circular base 1.8 m in diam. It is fitted with lead ballast and steel pads to ensure stability when in position. A hydraulic cylinder, which is housed in a central shaft and has a vertical free play of 1.44 m, thrusts the sensors through the lower water column and drives the density probe through the sediment-water interface into the bed. The sensors provide simultaneous and continuous measurement of sediment density, turbidity, and current meter over the water depth. The suspended sediment sampler consists of a nozzle, which is connected to a submerged pump via flexible tubing. The pump delivers water to the deck overline and thence into sample bottles and filtration units.

The instrument system is designed to operate in two modes: 1) vertical profiling through the water column into the bed, and 2) temporal monitoring at one or several depth measurement points. Since the system is operated from a boat, its use is limited to normal weather conditions.

Figure 29 shows a portion of a typical analog time-series record during a deployment at the upper Chesapeake Bay at 30 cm above a fluid mud bed during ebb tidal current. The turbidity readings are in percent units. These high-frequency records display small-scale fluctuations, suggesting that the mud participates in intermittent bursts and sweeps associated with local accelerations and decelerations.

DAISY Tower Instrumentation Array (Bohlen 1982)

The system is designed to provide reasonably long-term in situ observations of near-bottom suspended material conditions as well as the prevailing hydrodynamic condition that induces it. As illustrated in Figure 30, it consists of an aluminum frame approximately 3 m in height with a circular base 2 m in diameter. The array consists of a control unit and four basic subsystems comprising a pump, an optical array, a current meter and camera setups, together with supplementary temperature and conductivity sensors.

The control unit consists of a digital data logger, which supplies power to the instrument array and records the output signals. Hence, it is self-contained with sufficient data storage capacity to permit sampling of all instruments four times an hour over 36 days. The individual instruments comprising the primary instrument package include transmissometers, a savonius rotor current meter, a super 8-mm movie camera with strobed light unit, and a variable-volume displacement pump and associated filtration units. Thermistors and flow-through cells for conductivity measurement make up the supplementary package.

Figure 31 shows the result of a field deployment in the vicinity of the New London dredged material disposal grounds, eastern Long Island Sound in approximately 20 m of water in January 1980 (13 days). The current was measured near the bottom. The suspended material concentrations display relatively low variability. The anomalously high spike near 100 hr has been attributed to aberrant fouling or proximity to disposal of dredged material.

OSU Instrumentation (Bedford et al. 1982, 1987)

This is an acoustics-based system that uses ultrasonic transducer technology to measure detailed vertical profiles of sediment concentration. Instrumentation is attached to a small mobile support system configured such that the instruments can either be deployed on a host tower or as a stand-alone unit. For example, it was part of the OSU C-DART Data Acquisition Tower deployed at the Old Woman Creek Estuarine Sanctuary, Lake Erie, to record the high-density multi-faceted data needed to couple wind wave conditions to lake bottom turbulent responses (Bedford et al. 1982). The array of instruments includes an acoustic sediment concentration profiler, two-axis electromagnetic current meters, transmissometer, pressure transducer, and thermistor.

Figure 32 shows a typical temporal variation pattern of the horizontal velocity and suspended load during a deployment in Central Long Island Sound in 20 m of water. In this particular deployment, the instrument array was attached to one leg of the DAISY Tower described above. The acoustic profiler was positioned 1 m off the bottom and measured the backscatter intensity in 1-cm intervals throughout the 1-m column. The 100-point

sediment concentration profile was sampled at 32 Hz and ensemble averaged into a stored 1-Hz signal. The signals from the current meter, positioned 68 cm above the bottom, were sampled at 4 Hz and smoothed to an effective temporal resolution of 1 Hz. An in situ computer operated the instruments.

The values shown in Figure 32 are 15-min averages. The data pertain to a continuous deployment (CC) whereby the instruments sampled data at the selected frequencies until data storage capacity was reached, a total duration of 3.5 hr. Another mode of deployment is the discrete or block-sampled deployment (CD) during which the devices sample at the same frequencies for 15 min every 3 hr. While the CD deployment is designed to sample through at least two tidal cycles, the CC deployment permits an estimate of the "sub-grid scale" activity. In this deployment, the effect of tower tilt, which can cause a misalignment between the current meter axis and the horizontal streamwise component leading to very large errors in Reynolds stress calculation, was corrected by an axis rotation of the data.

The velocity shows a gradual decline from a maximum flood velocity toward slack tide, which implies a corresponding decline in the total average kinetic energy. The suspended load also decreases, but starts to increase toward the end of the measurement period. It was found that time histories of suspended load do not correlate with the total energy distribution, but do correlate very closely with the time traces of the turbulent and wave energy. Measured data were then used to quantify the associated bottom sediment entrainment, deposition, and vertical net fluxes based on a turbulent control volume approach.

COE Field Tower (Mehta and Jiang 1990)

The field tower, shown schematically in Figure 33, consists of an aluminum frame 2.45 m high with a rectangular base 1.5 m x 1.0 m, which tapers to 0.25 m by 0.15 m at the top. Slanted bracing members provide adequate strength against buckling and torsion during installation and retrieval operations. The tips (pins) of the four legs are conical in shape and anchored into the ground to provide stability. A 0.8-m square wooden plank firmly fixed at the top of the tower functions as a base for the mounting of the data acquisition system. A central shaft 4.2 cm in diameter held within a concentric pipe with an outer diameter of 5.8 cm acts as a holder for an accelerometer mounted in a plexiglass "boat," which consists essentially of a horizontal oval disc with two vertical guide vanes. Other instruments include a pressure transducer and a current meter.

Figure 34 shows a typical horizontal mud acceleration spectrum computed from the accelerometer data collected during a deployment in Lake Okeechobee, Florida. The water depth was 1.43 m, the mud thickness was 0.54 m, and the accelerometer was embedded 20 cm into the mud. The spectrum shows a marked peak at a very low frequency corresponding to a long period oscillation distinct from direct wind forcing. A plausible explanation for the low frequency peak is a second-order effect resulting from

wind-induced wave forcing leading to surf-beat-like response of the fluid-like mud bottom to wave forcing.

HR Instrumented Bed Frame (Diserens et al. 1993, Teisson et al. 1993)

The bed frame is designed (by Hydraulics Research Ltd. of Wallingford, England) for continuous measurement of time-varying hydrodynamic and sediment-related parameters due to both tides and waves. It consists of a triangular frame with protruding legs that anchor it to the bottom. The instrument package includes current meters (Braystoke for tidal current and electromagnetic for wave-induced flow), turbidity sensors, and a pressure sensor. In addition, ultrasonic probes mounted on smaller frames 3 m away from the main frame enable the bed level change to be monitored. The sensors are connected to shore units (control and data logging) housed in a van by cable links.

Figure 35 shows some typical results of field measurement obtained during a deployment in an intertidal area at Eastham Dock, Mersey estuary, U.K. The bed frame was positioned approximately 1.5 m above mean low water. A vertical array of current meters and turbidity sensors sampled the data at 5 Hz to enable recording of high frequency wave and turbulence fluctuations. The data pertain to a spring-tide episode during which the water level rose to a maximum water depth of 5.5 m. The bed shear stress was calculated from the tidal mean velocities measured at three heights based on a logarithmic velocity distribution. The wave heights during the recorded deployments were very small and had no significant influence on bed shear stress.

The concentration and shear stress values shown are mean values averaged over 10-min intervals. The maximum suspended sediment at 0.1 m (0.9 kg/m^3) was higher than the corresponding maximum at 1.0 m above the bed (0.55 kg/m^3). Assuming that the sediment is generated locally and there is little spatial variation over the immediate area, the rise in near-bed suspension concentration was interpreted as suspended sediment descending through the water column. The measured deposition of mud was shown to correspond with periods of low bed shear stress, and more deposition occurred during periods of sustained high concentration levels.

3 Relationship Between Erosion Rate Constant and Bed Shear Strength

Introduction

A review of laboratory data on the erosion of cohesive sediment beds reveals that the resulting empirical relationship between the rate of erosion $\dot{\varepsilon}$ and the applied bed shear stress τ_b generally has one of the following two functional forms (Mehta 1988):

$$\dot{\varepsilon} = \alpha_1 \left(\frac{\tau_b - \tau_s}{\tau_s} \right) \tag{1}$$

$$\dot{\varepsilon} = \alpha_2 e^{\alpha_3 \left[\frac{\tau_b - \tau_s(z)}{\tau_s(z)} \right]^{1/2}} \tag{2}$$

where τ_s is the erosion bed shear strength for a placed bed, $\tau_s(z)$ is the bed shear strength as a function of depth z below the bed surface for a deposited bed, and α_1, α_2, and α_3 are empirical coefficients.

As discussed elsewhere (Hayter 1983), Equation 2 can be approximated by Equation 1 in certain cases. In any event, the focus here is on the linear functional form, Equation 1, with a view to establishing a possible link between the characteristic erosion rate constant s (= α_1/τ_s) and τ_s by reviewing the relevant laboratory data on placed bed erosion. It is clear from Equation 1 that s is the slope of the erosion line expressed as the rate of change of erosion rate with respect to shear stress, and is consistent with the definition used by Arulanandan et al. (1980). In this context, 152 data points have been gleaned from the literature. Further details on the data are given in Appendix A.

Data Analysis

An earlier effort in this direction has been made by Arulanandan et al. (1980) for natural soil samples using distilled water. Their efforts yielded the following expression for estimating the rate of change of erosion rate for a

natural undisturbed soil subjected to hydraulic shear stress from river (eroding) water:

$$s = 223\exp(-0.13\tau_c) \tag{3}$$

applicable over the range $3 \leq \tau_c \leq 20$ where s is in g/dynes-min and τ_s is the critical shear stress in dynes/cm^2. After examining the distribution of the 151 data points in a semi-log plot, it was noted that an equation of the form of Equation 3, which is a straight line on a semi-log plot, is unable to account for the observed flattening out tendency of the curve toward larger values of τ_s. Hence, the following functional form was selected to regress the data:

$$s = s_{max}\exp(-a\tau_s^b) \tag{4}$$

Based on an inspection of the data trend and spread, s_{max} was fixed at 200 g/N-s, and a family of seven curves could be distinguished, each surrounded by a separate cluster of data points. The resulting two-parameter fits to the data were obtained by the method of least squares, leading to the results given in Table 12. The respective curves are shown in Figures 36-38. The figures are separated into groups with different abscissa values in order to show the different extents of the accompanying data points and yet with enough clarity at the low τ_s region to distinguish them. Hence, for example, the Group 1 curve is shown alone in Figure 36 since the farthest data point is located close to 70 Pa. It is noted that the curves overlap in the small τ_s region. Also, the range of the reported values of erosion rate constant spreads over seven orders of magnitude.

Table 12
Sediment Data Groups

Group	Coefficients in Equation 4		Number of data points
	a	b	
1	1.345	0.368	7
2	2.892	0.372	16
3	3.905	0.356	34
4	4.938	0.355	20
5	6.594	0.382	26
6	9.011	0.386	23
7	10.582	0.252	26

For each group, the characteristics of the relevant data points were further examined under five important erosion resistance characterizing factors; namely, bulk density, clay content, total salt concentration in the pore fluid, clay cation exchange capacity, and state of the sediment bed (undisturbed or

remolded), in an attempt to establish a rational means of data division. The factors are summarized in Table 13. The grouping based on bulk density, clay content, and cation exchange capacity does not seem to indicate any distinct influence of these parameters. On the other hand, the grouping does correlate with state of sediment bed and total salt concentration in the pore fluid. In general, undisturbed sediment beds and those with higher total salt concentration exhibit higher bed shear strength (and correspondingly higher characteristic erosion rate constant) compared with their remolded counterparts and those with lower total salt concentration.

A nomograph shown in Figure 39 is then proposed for estimating the characteristic erosion rate constant, given the bed shear strength, based on the state of sediment bed and the total salt concentration in the pore fluid. However, it is cautioned that the grouping has been premised on the assumption that the results of erosion experiments used in this study are not dependent on the type of erosion apparatus employed. The soundness of this assumption has not been proven although it is inherent as a basis for reporting the results by the various investigators. Therefore, given the five-decadal range of the reported s values that were used in establishing the individual curves, the nomograph is to be used as a last resort for guidance purposes and should not in any way supplant the need for erosion experiments when the necessary facilities are available.

Table 13
General Characteristics of Data Groups

Group Number	Bulk Density (kg/m^3)			Clay Content (%)			Total Salt Concentration (meq/l)			Cation Exchange Capacity (meq/100 g)			State of Sediment Bed
	Range	Mean	SD	Range	Mean	SD	Range	Mean	SD	Range	Mean	SD	
1 (7)	1,440-2,750 (6)	1,910	460	5-53 (6)	24	16	1.1-205.0 (5)	54.1	87.3	9.2-19.8 (6)	12.5	3.9	Undisturbed (5)
2 (16)	1,420-2,080 (11)	1,730	170	12-46 (12)	27	12	2.2-145 (13)	26.9	41.7	7.3-27.5 (11)	17.5	6.4	Undisturbed (11)
3 (34)	1,480-1,860 (5)	1,670	160	6-50 (32)	28	10	3.7-39.5 (32)	19.0	6.7	8.5-22.9 (10)	15.1	5.5	Undisturbed (4)
4 (20)	1,270-1,990 (15)	1,820	210	12-42 (19)	23	10	1.3-205.0 (18)	30.5	64.1	7.9-30.1 (18)	15.0	5.4	Undisturbed (3) Remolded (11)
5 (26)	1,350-2,090 (16)	1,820	200	11-53 (22)	27	11	1.7-205.0 (22)	21.7	42.0	7.6-26.1 (15)	14.6	5.3	Undisturbed (2) Remolded (12)
6 (23)	1.070-2,240 (20)	1,740	310	6-80 (19)	33	26	2.2-32.5 (13)	6.9	9.0	7.6-25.0 (16)	16.1	6.4	Undisturbed (1) Remolded (11)
7 (26)	1,100-2,400 (20)	1,730	380	6-94 (22)	34	19	1.1-6.2 (6)	3.2	1.8	4.8-100.0 (16)	22.8	22.9	Remolded (6)

The numbers within parentheses refer to the number of data points.
SD = standard deviation; meq/l = milliequivalents per liter; meq/100 g = milliequivalents per 100 g.

References

Ali, K.H.M., and Georgiadis, K. (1991). "Laminar motion of fluid mud." *Proceedings of the Institution of Civil Engineers, Part 2*. London, 795-821.

Ali, K.H.M., O'Connor, B.A., and Nicholson, J. (1992). "Theoretical and experimental study of fluid mud." *Proceedings of the 5th international symposium on river sedimentation*. Karlsruhe, Germany, 277-86.

Alishahi, M.R., and Krone, R.B. (1964). "Suspension of cohesive sediments by wind-generated waves," Technical Report HEL-2-9, Hydraulic Engineering Laboratory, University of California, Berkeley.

Amos, C.L., Christian, H.A., Grant, J., and Paterson, D.M. (1992). "Sea-carousel - a benthic, annular flume," *Estuarine Coastal Shelf Science* 34(6), 557-77.

Arulanandan, K., Gillogley, E., and Tully, R. (1980). "Development of a quantitative method to predict critical shear stress and rate of erosion of natural undisturbed cohesive soils," Technical Report GL-80-5, U.S. Army Engineer Waterways Experiment Station, Vicksburg, MS.

Arulanandan, K., Loganathan, P., and Krone, R.B. (1975). "Pore and eroding fluid influences on surface erosion of soil," *Journal of Geotechnical Engineering Division*, ASCE 101(1), 51-66.

Arulanandan, K., Sargunam, A., Loganathan, P., and Krone, R.B. (1973). "Application of chemical and electrical parameters to prediction of erodibility." *Soil erosion: causes and mechanisms, prevention and control*, Special Report 135, Highway Research Board, Washington, DC, 42-51.

Bedford, K., Van Evra, R.E. III, and Valizadeh-Alavi, H. (1982). "Ultrasonic measurement of sediment resuspension." *Proceedings of the conference applying research to hydraulic practice*. P.E. Smith, ed., ASCE, New York, 575-83.

Bedford, K., Wai., O., Libicki, C., and Van Evra, R. (1987). "Sediment entrainment and deposition measurements in Long Island Sound," *Journal of Hydraulic Engineering* 113(10), 1325-42.

Berlamont, J., Ockenden, M., Toorman, E., and Winterwerp, J. (1993). "The characterization of cohesive sediment properties," *Coastal Engineering* 21, 105-28.

Bohlen, F. (1982). "In-situ monitoring of sediment resuspension in vicinity of active dredge spoils disposal area." *Proceedings of Oceans '82.* IEEE Press, New York, 1028-33.

Burt, T.N., and Game, A.C. (1985). "The carousel," Report No. SR33, Hydraulics Research, Wallingford, U.K.

Chapuis, R.P. (1986). "Quantitative measurement of the scour resistance of natural solid clays," *Canadian Geotechnical Journal* 23(2), 132-41.

Chapuis, R.P., and Gatien, T. (1986). "An improved rotating cylinder technique for quantitative measurement of the scour resistance of clays," *Canadian Geotechnical Journal* 23(1), 83-7.

Christensen, R.W., and Das, B.M. (1973). "Hydraulic erosion of remolded cohesive soils," Special Report No. 135, Highway Research Board, Washington, DC, 8-19.

Croad, R.N. (1981). "Physics of erosion of cohesive soils," Ph.D. diss., University of Auckland, New Zealand.

Dash, U. (1968). "Erosive behavior of cohesive soils," Ph.D. diss., Purdue University.

Diserens, A., Ockenden, M.C., and Delo, E.A. (1993). "Application of a mathematical model to investigate sedimentation at Eastham Dock, Mersey Estuary." *Nearshore and Estuarine Cohesive Sediment Transport.* A.J. Mehta, ed., American Geophysical Union, Washington, DC, 486-503.

Dunn, I.S. (1959). "Tractive resistance of cohesive channels," *Journal of Soil Mechanics and Foundation Engineering Division,* ASCE 85(3), 1-24.

Einsele, G., Overbeck, R., Schwarz, H.U., and Unsold, G. (1974). "Mass physical properties, sliding and erodibility of experimentally depositional and differently consolidated clayey muds," *Sedimentology* 21(3), 339-72.

Espey, W.H. (1963). "A new test to measure the scour of cohesive sediment," Technical Report UYD-01-6301, Hydraulic Engineering Laboratory, University of Texas, Austin.

Fukuda, M.K. (1978). "The entrainment of cohesive sediments in freshwater," Ph.D. diss., Case Western Reserve University, Cleveland, Ohio.

Gularte, R.C., Kelly, W.E., and Nacci, V.A. (1977). "The threshold erosional velocities and rates of erosion for redeposited estuarine dredged material." *Proceedings of the 2nd international symposium on dredging technology.* Paper H3, British Hydraulic Research Association, Cranfield, U.K.

Gust, G., and Morris, M.J. (1989). "Erosion thresholds and entrainment rates of undisturbed in situ sediments," *Journal of Coastal Research* SI5, 87-99.

Holland, A.F., Zingmark, R.G., and Dean, J.M. (1974). "Quantitative evidence concerning the stabilization of sediments by marine benthic diatoms," *Marine Biology* 27(3), 191-6.

Hwang, K.N., and Mehta, A.J. (1989). "Fine sediment erodibility in Lake Okeechobee, Florida," Report UFL/COEL-89/019, University of Florida, Gainesville.

Hydraulics Research Limited. (1994). "ISIS - Instrument for shear strength in-situ," Information Pamphlet, Wallingford, England.

Jonsson, I.G. (1966). "Wave boundary layers and friction factors." *Proceedings of the 10th coastal engineering conference.* Vol. 1, ASCE, New York, 127-48.

Kamphuis, J.W., and Hall, K.R. (1983). "Cohesive material erosion by unidirectional current," *Journal of Hydraulic Engineering* 109(1), 49-61.

Kandiah, A. (1974). "Fundamental aspects of surface erosion of cohesive soils," Ph.D. diss., University of California, Davis.

Kelly, W.E., and Gularte, R.C. (1981). "Erosion resistance of cohesive soils," *Journal of Hydraulics Division*, ASCE 107(10), 1211-24.

Krishnappan, B.G. (1991). "A rotating flume for cohesive sediment transport research," NWRI Contribution No. 91-, National Water Research Institute, Burlington, Ontario.

Kuijper, C., Cornelisse, J.M., and Winterwerp, J.C. (1989). "Research on erosive properties of cohesive sediments," *Journal of Geophysical Research* 94(C10), 14341-50.

Kusuda, T., Umita, T., Koga, K., Futawari, T., and Awaya, Y. (1985). "Erosional process of cohesive sediments," *Water Science Technology* 17(6/7), 891-901.

Lau, Y.L., and Krishnappan, B.G. (1991). "Size distribution and settling velocity of cohesive sediments during settling," *Journal of Hydraulic Research* 30(5), 673-84.

Li, Y. (1989). "Experiment and analysis on the transport and deposition of clay sediment," M.S. thesis, Hohai University, Nanjing, The People's Republic of China (in Chinese with English abstract).

Liou, Y.-D. (1970). "Hydraulic erodibility of two pure clay systems," Ph.D. diss., Colorado State University.

Lonsdale, P., and Southard, J.B. (1974). "Experimental erosion of North Pacific red clay," *Marine Geology* 17(4), M51-60.

Maa, J.P.-Y. (1991). "In-situ measurements of the critical bed shear stress for erosion." *Environmental hydraulics*. Lee and Cheung, ed., Balkema, Rotterdam, 627-32.

Maa, J.P.-Y. (1993). "VIMS sea carousel: its hydrodynamic characteristics." *Nearshore and estuarine cohesive sediment transport*. A.J. Mehta, ed., American Geophysical Union, Washington, DC, 265-80.

Maa, J.P.-Y., Wright, L.D., Lee, C.-H., and Shannon, T.W. (1993). "VIMS sea carousel: a field instrument for studying sediment transport," *Marine Geology* 115, 271-87.

Maa, P.-Y., and Mehta, A.J. (1987). "Mud erosion by waves: a laboratory study," *Continental Shelf Research* 7(11/12), 1269-84.

MAST-G6M. (1992). "On the methodology and accuracy of measuring physico-chemical properties to characterize cohesive sediment." *G6 coastal morphodynamics*, under preparation.

Mehta, A.J. (1973). "Deposition behavior of cohesive sediments," Ph.D. diss., University of Florida, Gainesville.

Mehta, A.J., and Partheniades, E. (1979). "Kaolinite resuspension properties," *Journal of Hydraulics Division*, ASCE 105(4), 411-16.

Mehta, A.J., Parchure, T.M., Dixit, J.G., and Ariathurai, R. (1982). "Resuspension potential of deposited cohesive sediment beds." *Estuarine comparison*. V.S. Kennedy, ed., Academic Press, New York, 591-609.

Mehta, A.J., and Jiang, F. (1990). "Some field observations on bottom mud motion due to waves," Report No. UFL/COEL-90/008, Coastal and Oceanographic Engineering Department, University of Florida, Gainesville.

Mehta, A.J., and Srinivas, R. (1993). "Observation on the environment of fluid mud by shear flow." *Nearshore and estuarine cohesive sediment transport*. A.J. Mehta, ed., American Geophysical Union, Washington, DC, 224-46.

Mimura, N. (1993). "Rates of erosion and deposition of cohesive sediments under waves." *Nearshore and estuarine cohesive sediment transport.* A.J. Mehta, ed., American Geophysical Union, Washington, DC, 247-64.

Moller-Jensen, P. (1993). "Wadden Sea mud; methods for estimation of transport, erosion and consolidation of marine cohesive sediments," Ph.D. diss., Department of Civil Engineering, Aalborg University, Denmark.

Moore, W.L., and Masch, F.D., Jr. (1962). "Experiments on the scour resistance of cohesive sediments," *Journal of Geophysical Research* 67(4), 1437-49.

Murakami, K., Suganuma, F., and Sasaki, H. (1989). "Experimental investigation on erosion and deposition of fine cohesive sediments in an annular rotating channel," *Report of the Port and Harbor Research Institute* 28(1), 43-76 (in Japanese with English abstract).

Narimousa, S., and Fernando, H.J.S. (1987). "On the sheared interface of an entraining stratified fluid," *Journal of Fluid Mechanics* 174, 1-22.

Nichols, M.M. (1989). "Field instrument system for fluid mud transport and behavior," *Journal of Coastal Research* SI5, 31-8.

Nichols, M.M., Thompson, G.S., and Faas, R.W. (1978). "A field study of fluid mud dredged material: its physical nature and dispersal," Technical Report D-78-40, U.S. Army Engineer Waterways Experiment Station.

Nowell, A.R.M., McCave, I.N., and Hollister, C.D. (1985). "Contributions of HEBBLE to understanding marine sedimentation," *Marine Geology* 66(1/4), 397-409.

Parchure, T.M. (1984). "Erosional behavior of deposited cohesive sediments," Ph.D. diss., University of Florida, Gainesville.

Parchure, T.M., and Mehta, A.J. (1985). "Erosion of soft cohesive sediment deposits," *Journal of Hydraulic Engineering* 111(10), 1308-26.

Partheniades, E. (1965). "Erosion and deposition of cohesive soils," *Journal of Hydraulics Division,* ASCE 91(1), 105-38.

Partheniades, E., and Paaswell, R.E. (1970). "Erodibility of channels with cohesive boundary," *Journal of Hydraulics Division*, ASCE 96(3), 755-71.

Partheniades, E., Kennedy, J.F., Etter, R.J., and Hoyer, R.P. (1966). "Investigations of the depositional behavior of fine cohesive sediments in an annular rotating channel," Report No. 96, Hydrodynamics Laboratory, Massachusetts Institute of Technology, Cambridge.

Paulic, M., Montague, C.L., and Mehta, A.J. (1986). "Influence of light on sediment erodibility." *Proceedings of the 3rd international symposium on river sedimentation.* S.Y. Wang, et al., ed., Jackson, MS, 1759-64.

Peirce, T.J., Jarman, R.T., and de Turville, C.M. (1970). "An experimental study of silt scouring." *Proceedings of the Institution of Civil Engineers.* London, 231-43.

Raudkivi, A.J., and Hutchison, D.L. (1974). "Erosion of kaolinite clay by flowing water." *Proceedings of the Royal Society of London.* A337, 537-54.

Rohan, K., Lefebvre, G., Douville, S., and Milette, J.-P. (1986). "A new technique to evaluate erodibility of cohesive material," *Geotechnical Testing Journal* 9(2), 87-92.

Rohan, K., and Lefebvre, G. (1991). "Hydrodynamic aspects in the rotating cylinder erosivity test," *Geotechnical Testing Journal* 14(2), 166-70.

Schunemann, S., and Kuhl, H. (1993). "Experimental investigations of the erosional behavior of naturally formed mud from the Elbe Estuary and adjacent Wadden Sea, Germany." *Nearshore and Estuarine Cohesive Sediment Transport.* A.J. Mehta, ed., American Geophysical Union, Washington, DC, 314-30.

Shaikh, A., Ruff, J.F., and Abt, S.R. (1988). "Erosion rate of composite NA-montmorillonite soils," *Journal of Hydraulic Engineering* 114(3), 296-305.

Sheng, Y.P. (1989). "Consideration of flow in rotating annuli for sediment erosion and deposition studies," *Journal of Coastal Research* SI5, 207-16.

Talebbeydokhti, N., and Klingeman, P.C. (1992). "Suspension of fine-grained sediment," *Iranian Journal of Science and Technology* 16(1), 29-42.

Task Committee on Erosion of Cohesive Materials. (1968). "Erosion of cohesive sediments," *Journal of Hydraulics Division,* ASCE 94(4), 1017-49.

Teeter, A.M. (1994). "A particle entrainment simulator to gage cohesive sediment erodibility," Dredging Research Technical Note DRP 01-xx, U.S. Army Engineer Waterways Experiment Station, Vicksburg, MS (under review).

Teeter, A.M., and Pankow, W. (1989). "Deposition and erosion testing on the composite dredged material sediment sample from New Bedford Harbor, Massachusetts," Technical Report HL-89-11, U.S. Army Engineer Waterways Experiment Station, Vicksburg, MS.

Teisson, C., Ockenden, M., Le Hir, P., Kranenburg, C., and Hamm, L. (1993). "Cohesive sediment transport processes," *Coastal Engineering* 21(1-3), 129-62.

Thorn, M.F.C., and Parsons, J.G. (1980). "Erosion of cohesive sediments in estuaries: an engineering guide." *Proceedings of the 3rd international symposium on dredging technology*. Bedford, England, 349-58.

Tofts, H. (1993). "Erosional behavior of partly cohesive, partly non-cohesive sediments in uniform flow." *Proceedings of the 6th International Conference on Urban Storm Drainage*. Niagara Falls, Ontario.

Tsai, C.-H., and Lick, W. (1986). "A portable device for measuring sediment resuspension," *Journal of Great Lakes Research* 12(4), 314-21.

Tsai, C.H., and Lick, W. (1988). "Resuspension of sediments from Long Island Sound," *Water Science Technology* 20(6/7), 155-64.

van Leussen, W., and Winterwerp, J.C. (1990). "Laboratory experiments on sedimentation of fine-grained sediments: A state-of-the-art review in the light of experiments with the Delta Tidal Flume." *Residual currents and long-term transport*. R.T. Cheng, ed., American Geophysical Union, Washington, DC, 241-59.

Villaret, C., and Paulic, M. (1986). "Experiments on the erosion of deposited and placed cohesive sediments in an annular flume and a rocking flume," Report No. UFL/COEL-86/007, Coastal and Oceanographic Engineering Department, University of Florida, Gainesville.

Watanabe, A., Thimakorn, P., and Das Gupta, A. (1978). "Concentration of suspended clay in periodic flow." *Proceedings of the 16th Coastal Engineering Conference*. Vol. 2, ASCE, New York, 1918-31.

Wolanski, E., Asaeda, T., and Imberger, J. (1989). "Mixing across a lutocline," *Limnology and Oceanography* 34(5), 931-8.

Young, R.A. (1977). "SEAFLUME: a device for in-situ studies of threshold erosion velocity and erosional behavior of undisturbed marine muds," *Marine Geology* 23, M11-8.

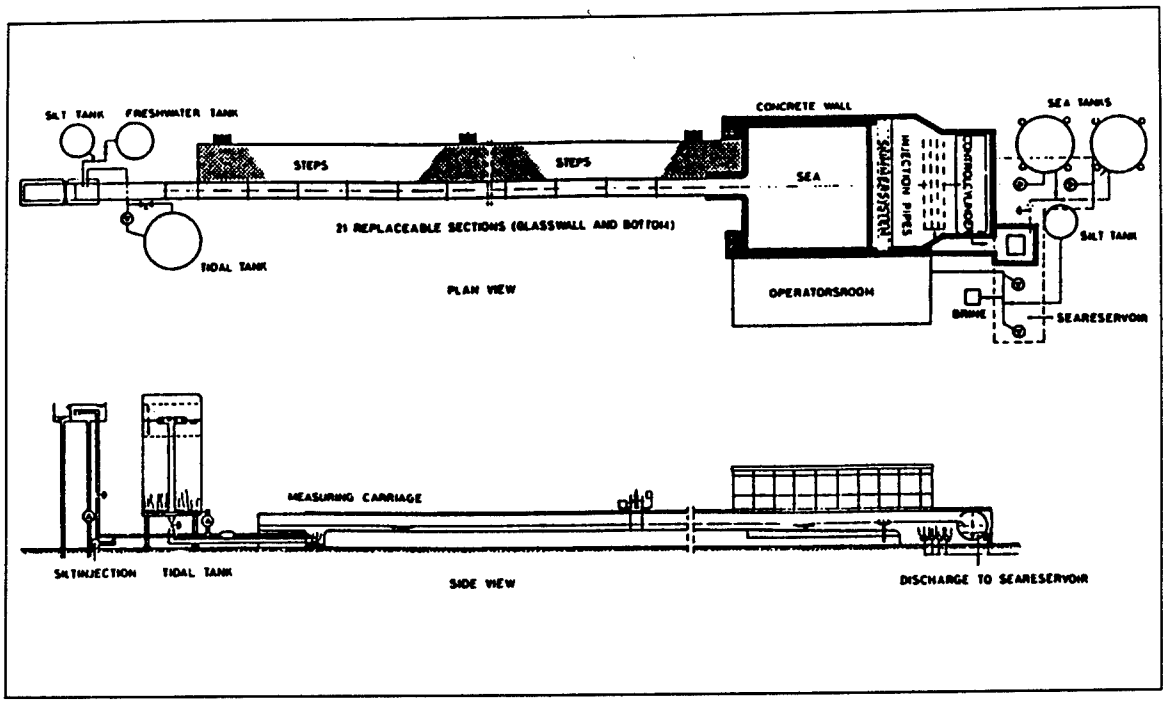

Figure 1. Schematic of the Delft Tidal Flume (from Kuijper et al. (1989))

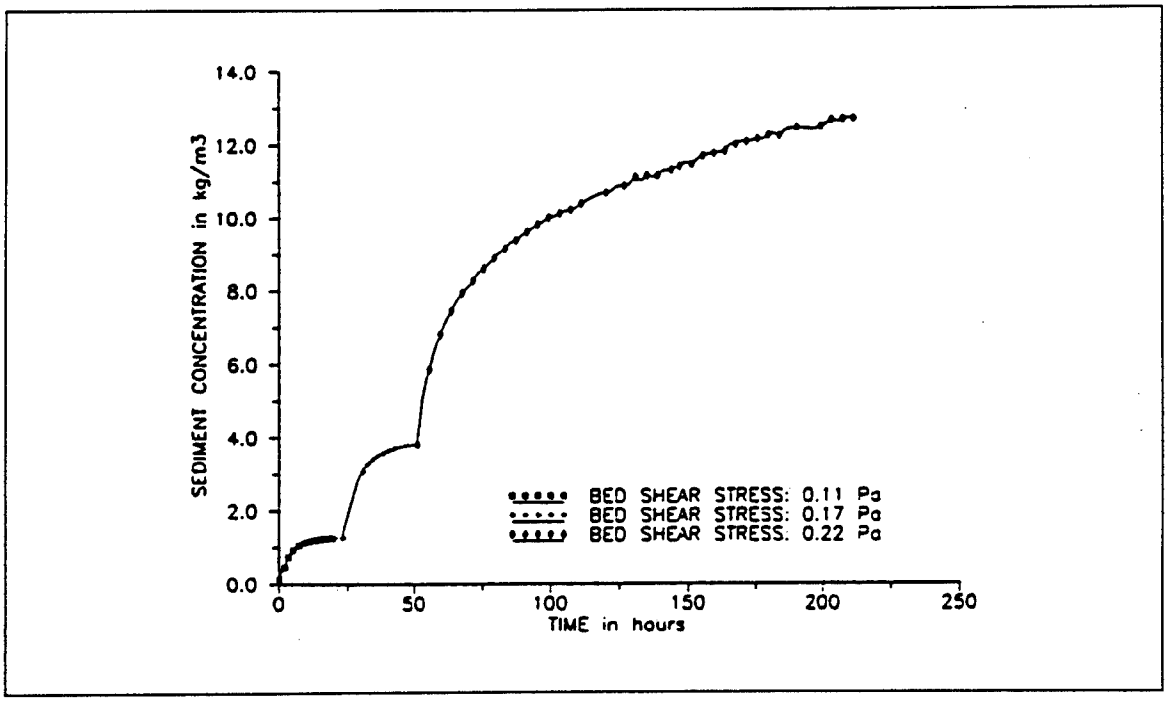

Figure 2. A typical suspended sediment-time curve for an erosion experiment in the tidal flume (from Kuijper et al. (1989))

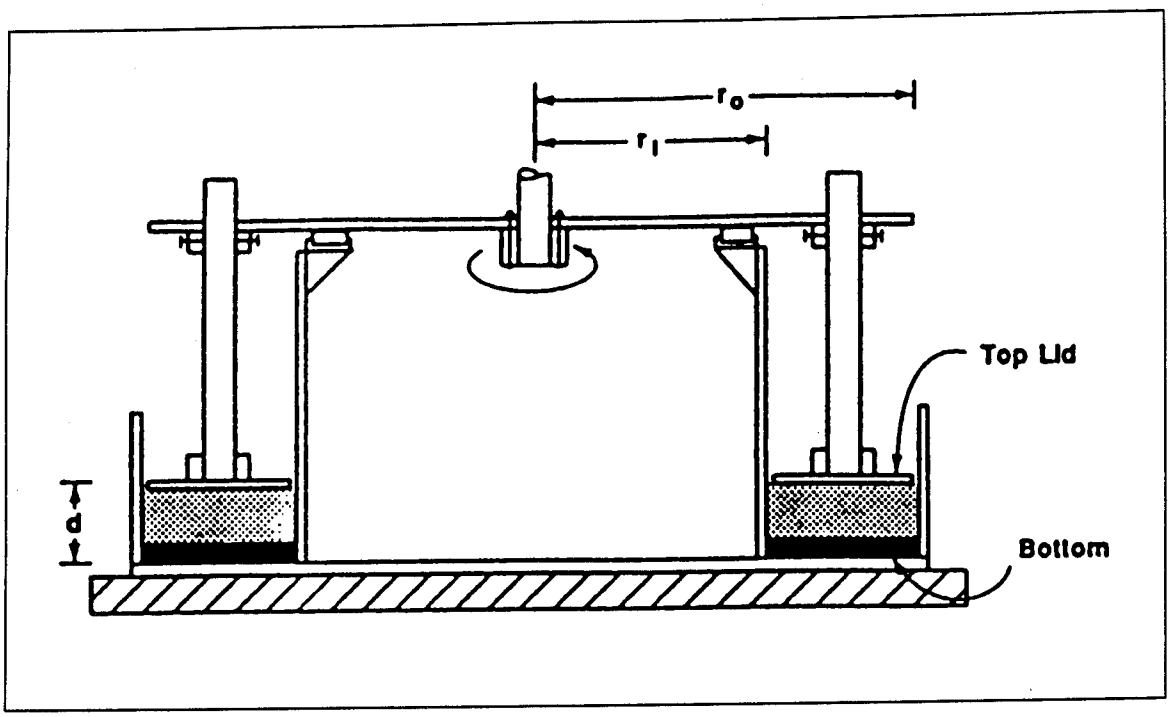

Figure 3. Schematic of a laboratory rotating annular flume (from Sheng (1989))

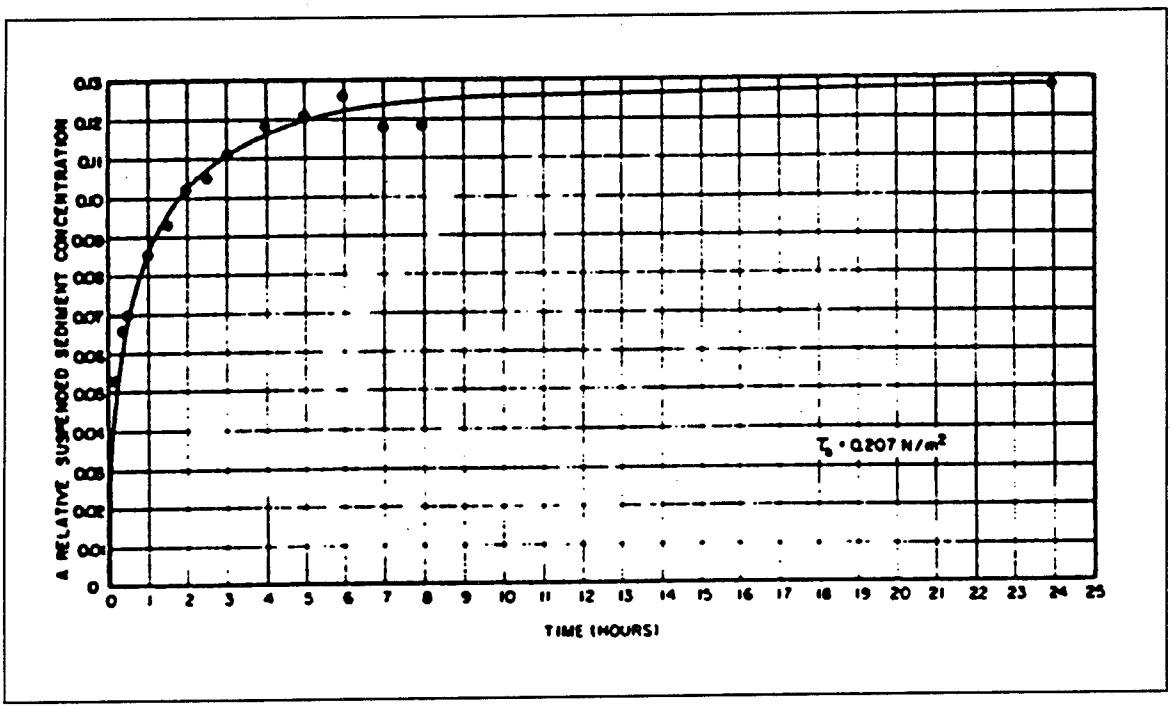

Figure 4. A typical result of resuspension experiment using the annular flume for a stratified bed at a bed shear stress (τ_b) of 0.21 Pa (from Mehta and Partheniades (1979))

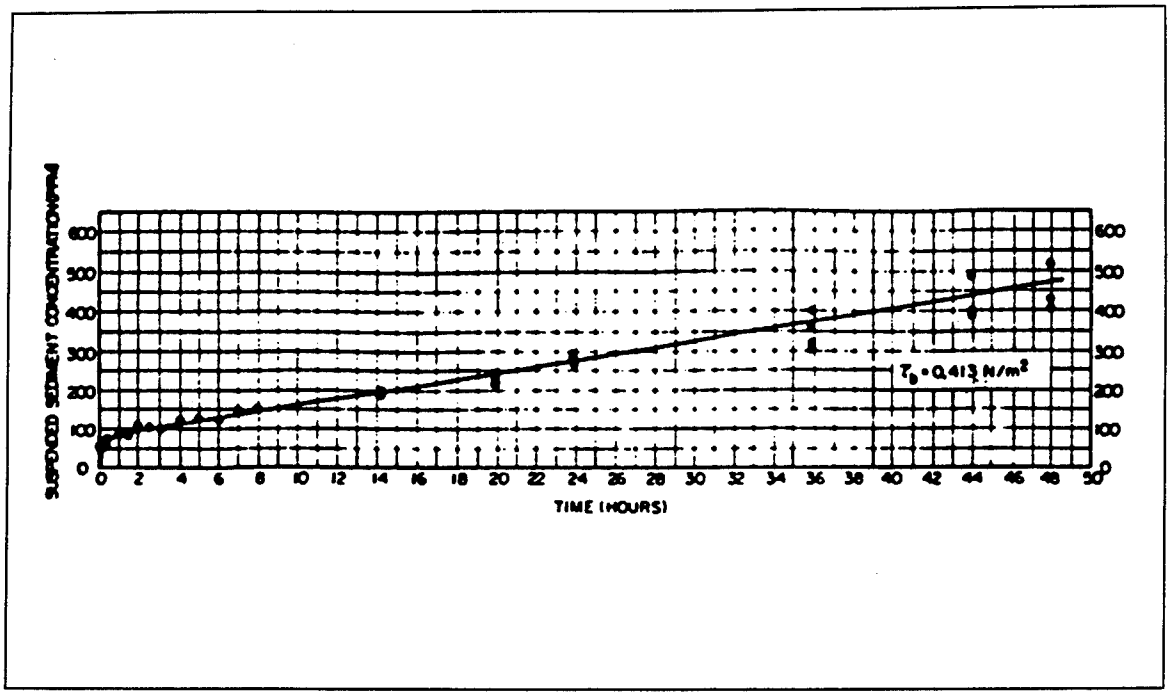

Figure 5. Typical results of resuspension experiment using the annular flume for a uniform bed at a bed shear stress (τ_b) of 0.41 Pa (from Mehta and Partheniades (1979))

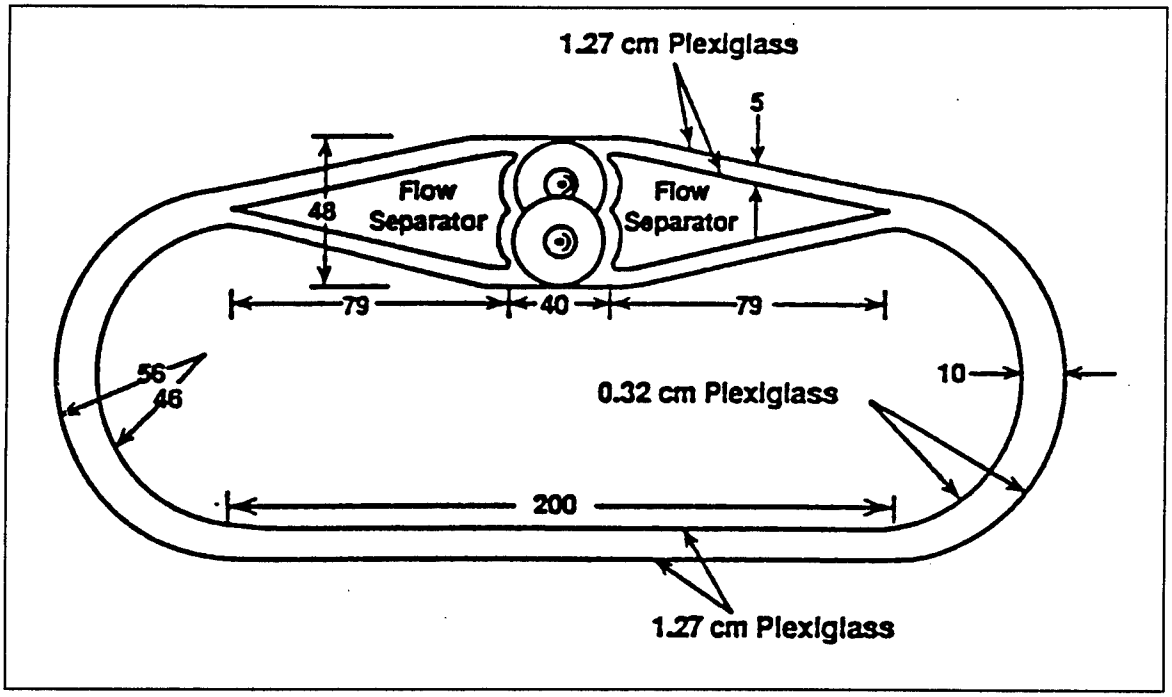

Figure 6. Schematic of a race-track flume (from Mehta and Srinivas (1993))

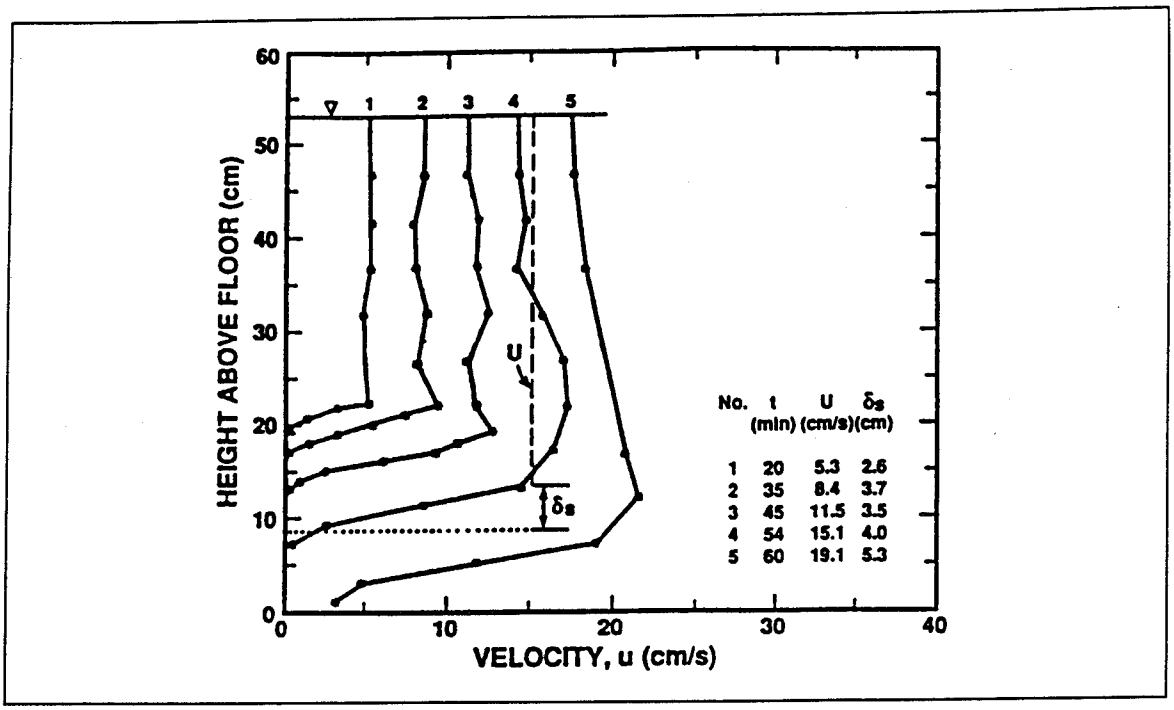

Figure 7. Typical velocity profiles from a test run using a race-track flume with bottom mud composed of kaolinite (from Mehta and Srinivas (1993)). t is the elapsed time following test initiation, U is the characteristic mixed-layer velocity, and δ_s is the shear layer thickness. As an example, the dashed line indicates the location of the bottom elevation of δ_s for profile No. 4 (t = 54 min)

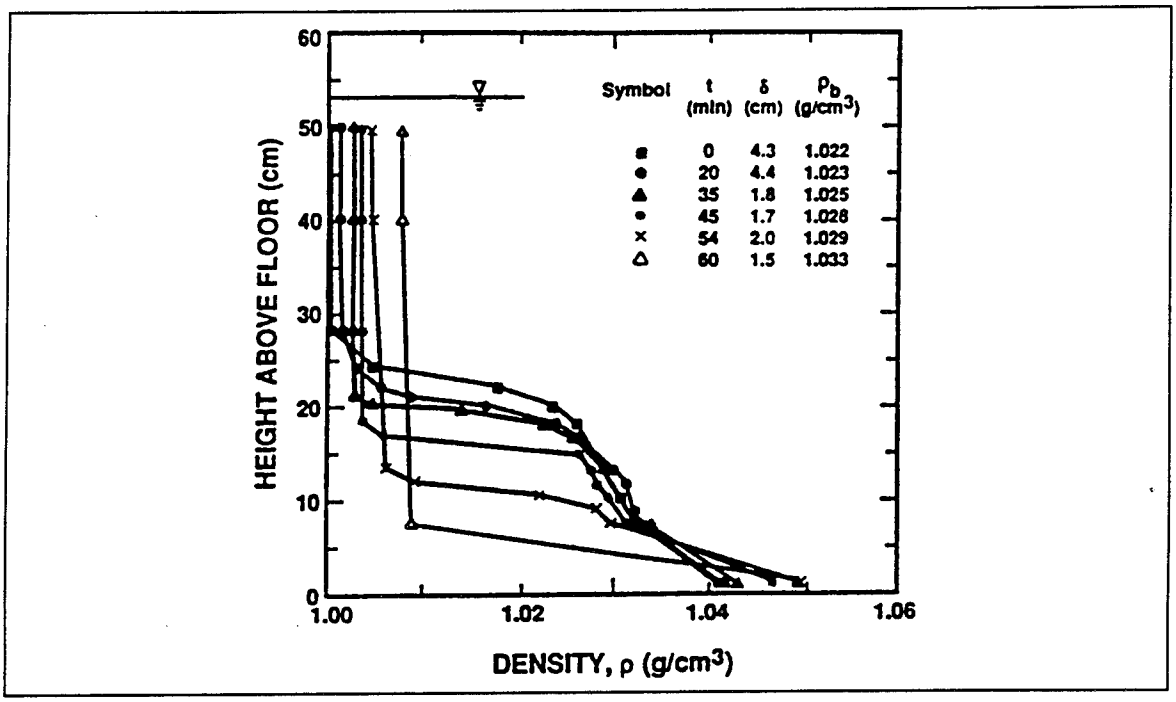

Figure 8. Density profiles corresponding to the velocity profiles shown in Figure 11 (from Mehta and Srinivas (1993)). δ is the density interfacial layer thickness and ρ_b is the density value at the base of the corresponding δ. The initial fluid-bed interface is indicated by the density profile at t = 0

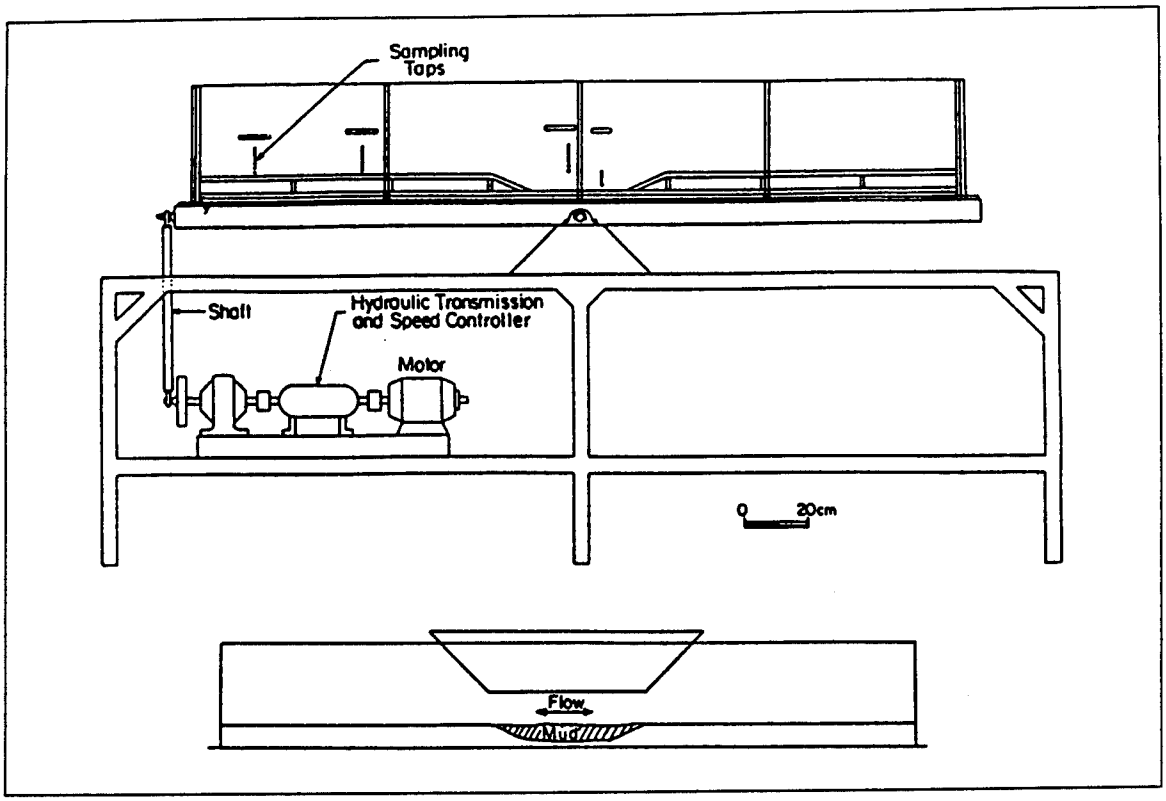

Figure 9. a) Schematic of a rocking flume; b) Top constriction placed in the rocking flume (from Villaret and Paulic (1986))

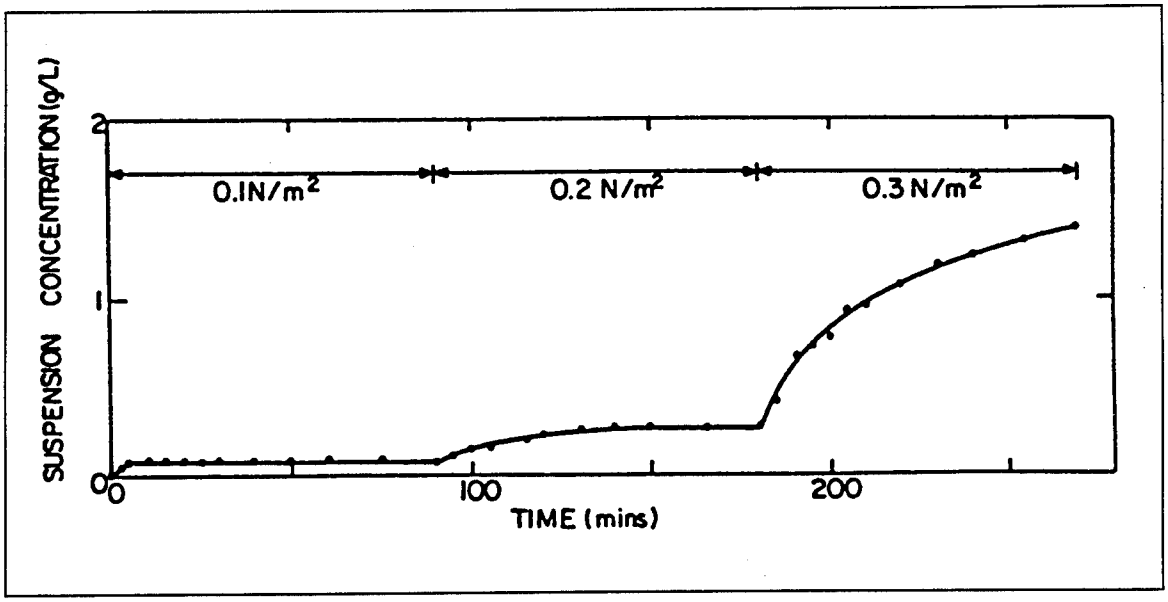

Figure 10. A typical concentration-time curve for a deposited kaolinite bed using the rocking flume (from Villaret and Paulic (1986))

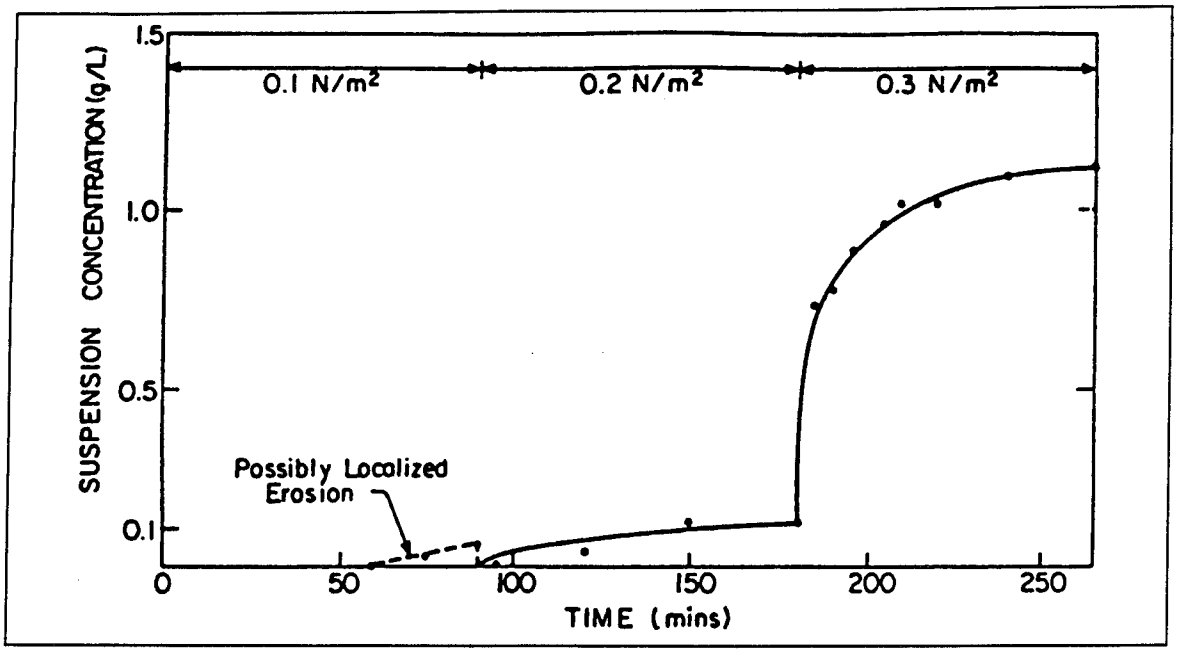

Figure 11. A typical concentration-time curve for deposited Cedar Key (Florida) mud bed using the rocking flume (from Villaret and Paulic (1986))

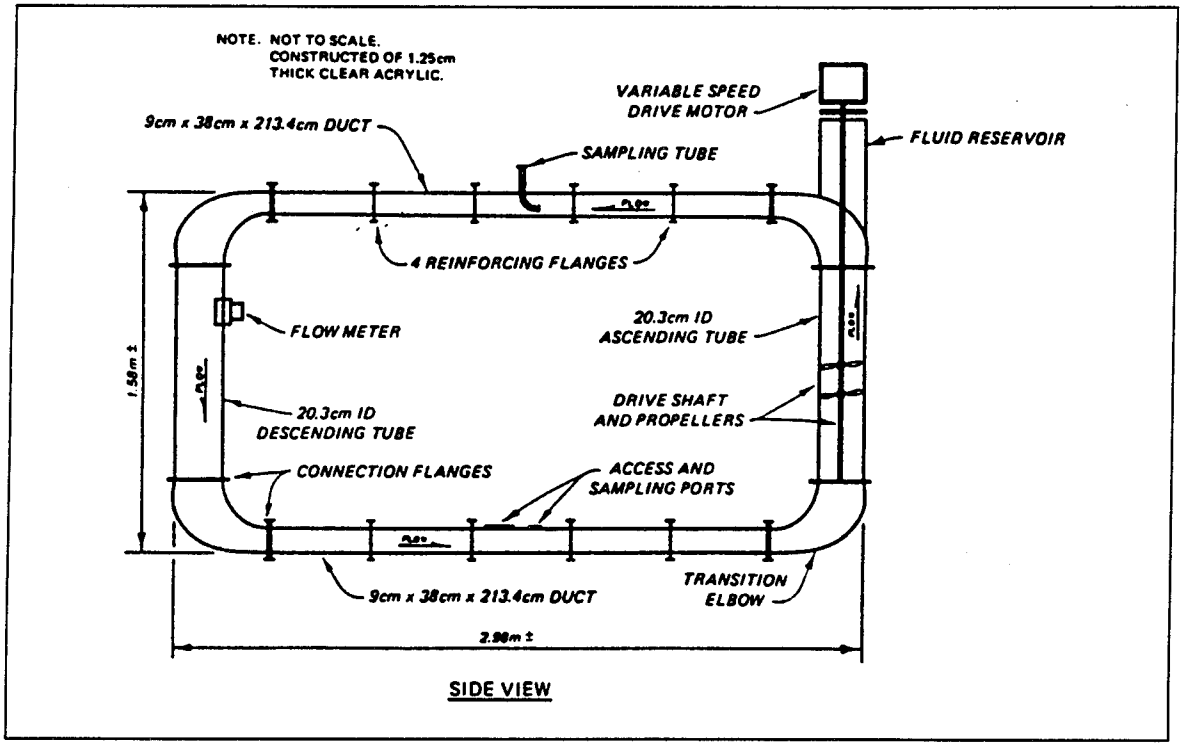

Figure 12. Schematic of a closed-conduit sediment water tunnel (from Teeter and Pankow (1989))

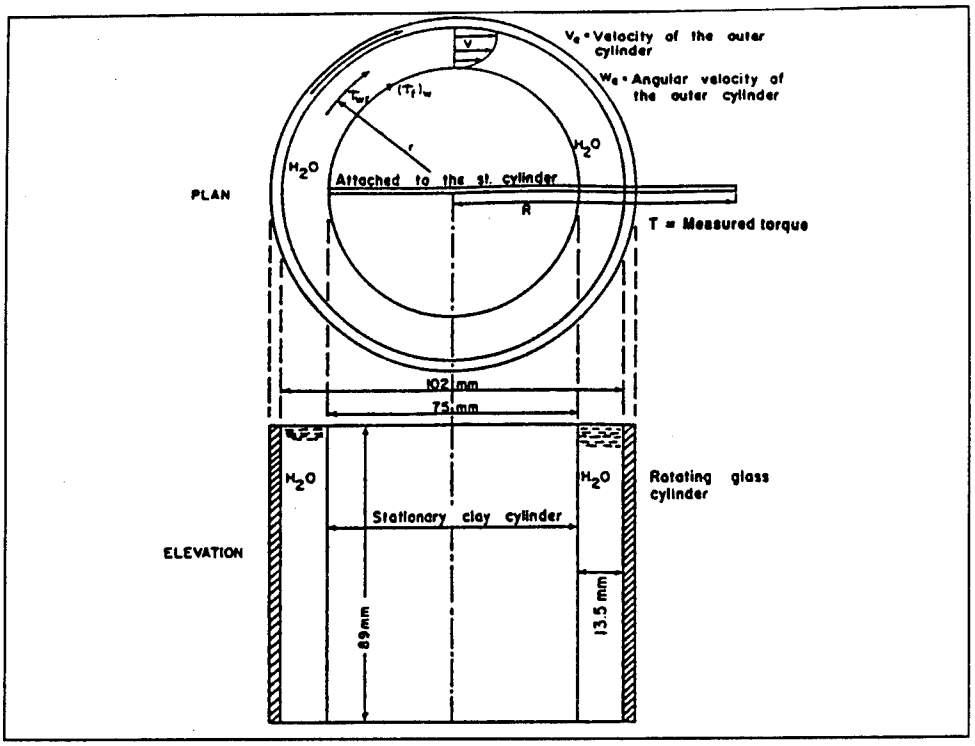

Figure 13. Schematic of a rotating cylinder apparatus (from Rohan and Lefebvre (1991))

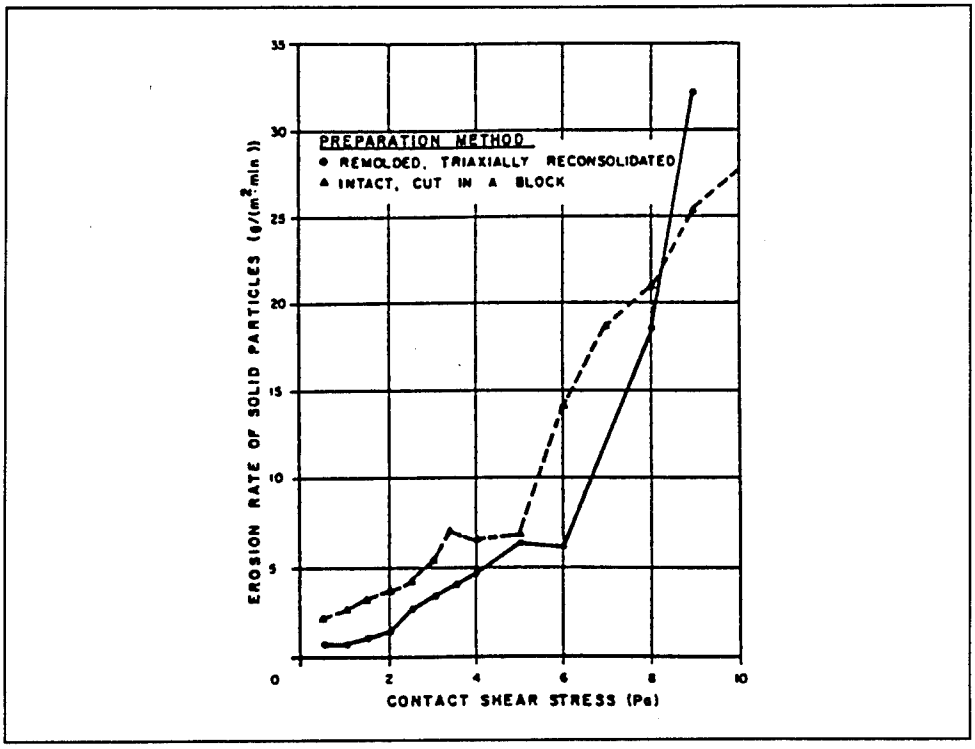

Figure 14. A typical erosion rate versus shear stress curve using a rotating cylinder apparatus for intact clay samples and triaxially prepared samples (from Chapius (1986))

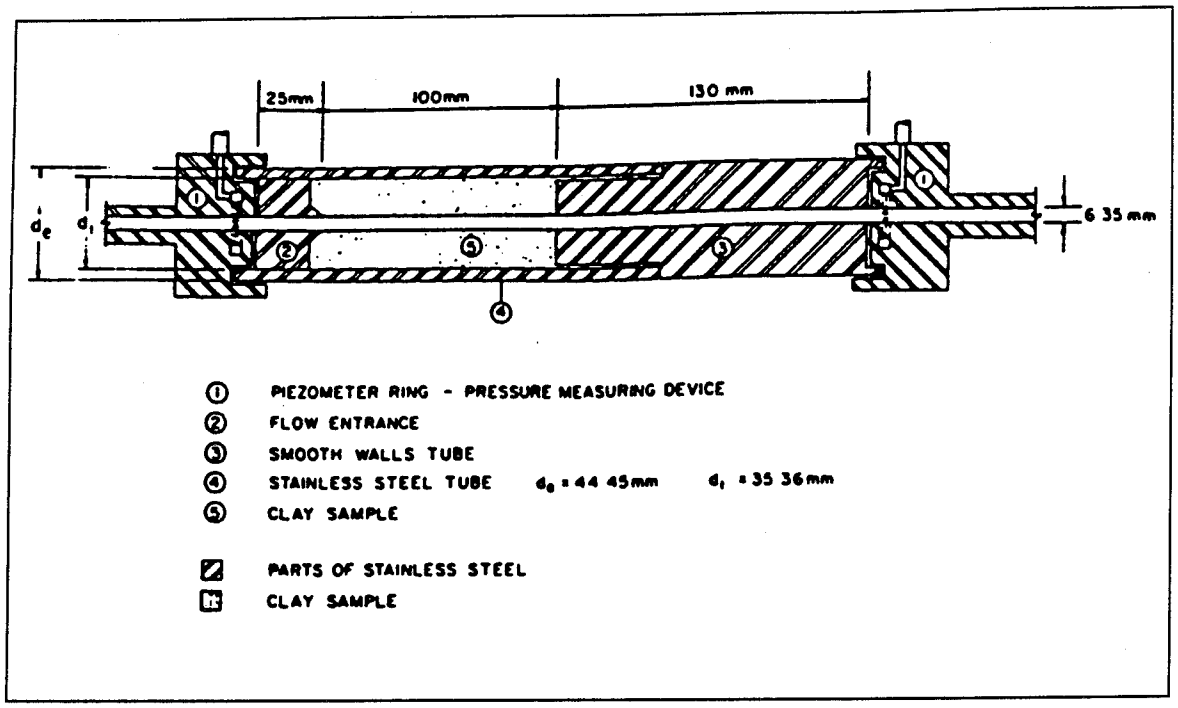

Figure 15. Schematic of a drill-hole test apparatus (from Rohan et al. (1986))

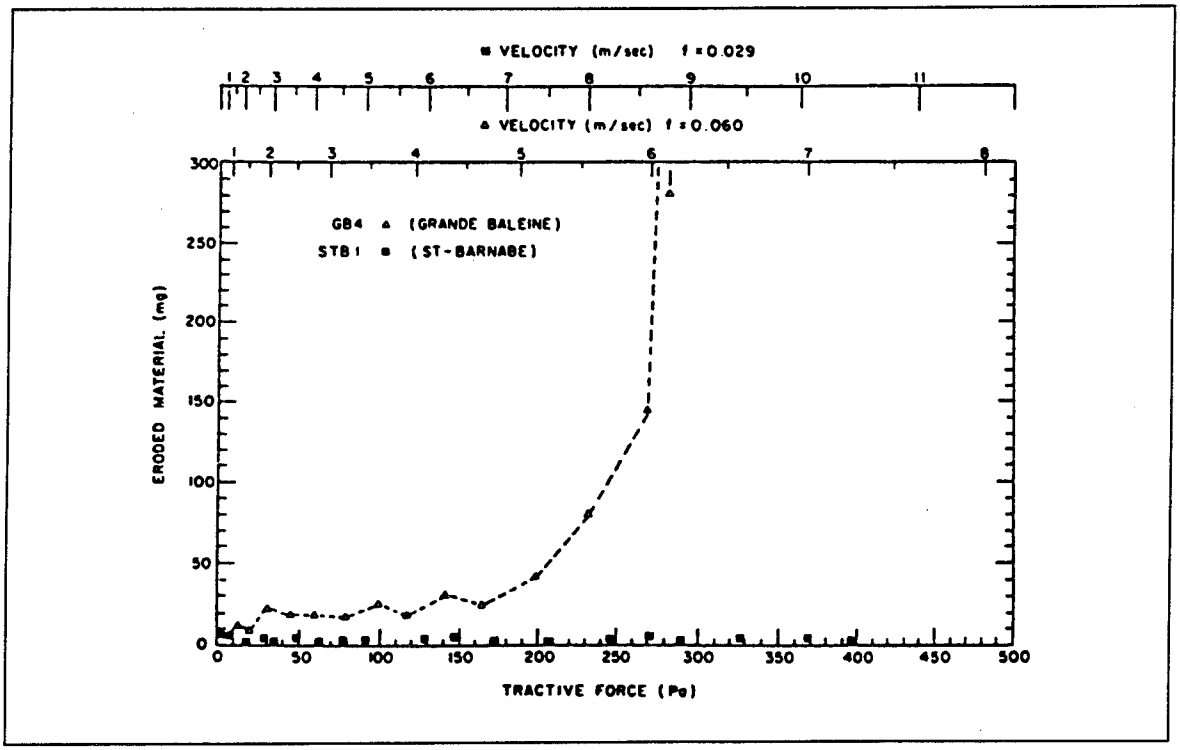

Figure 16. A typical eroded sediment mass versus tractive force curve from a drill-hole test apparatus (from Rohan et al. (1986))

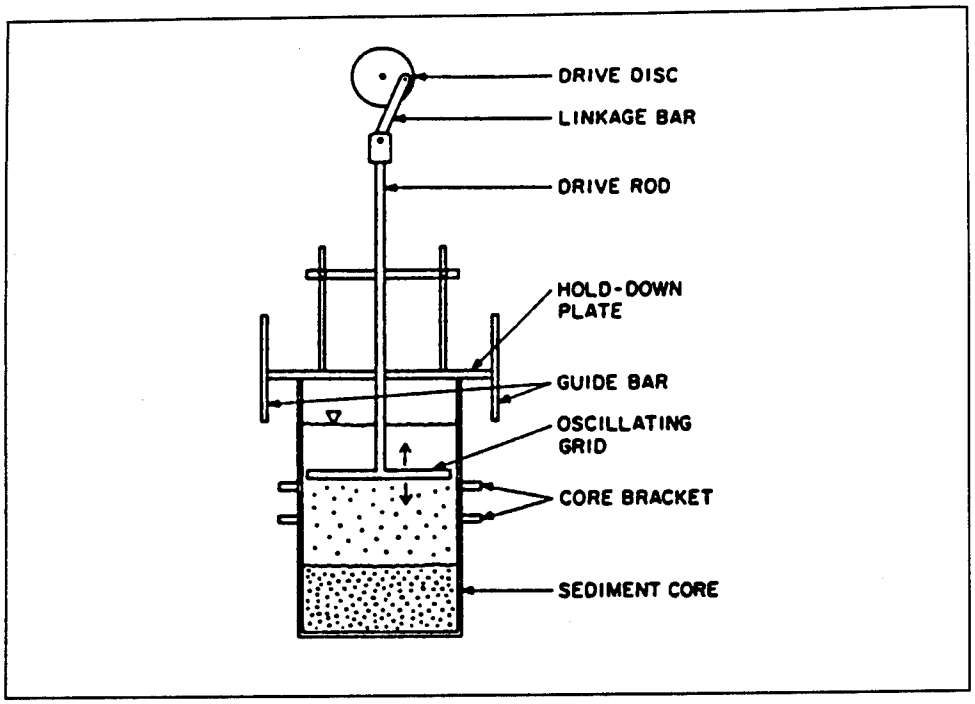

Figure 17. Schematic of a vertical grid oscillator (from Tsai and Lick (1986))

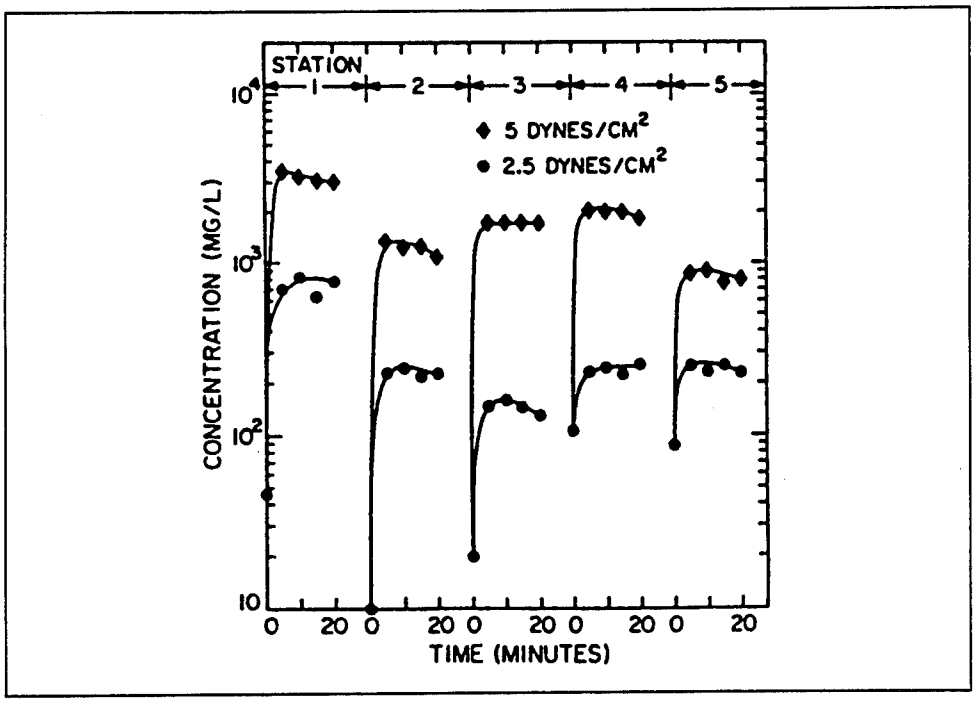

Figure 18. Time histories of the shaker concentration at five stations (from Tsai and Lick (1986))

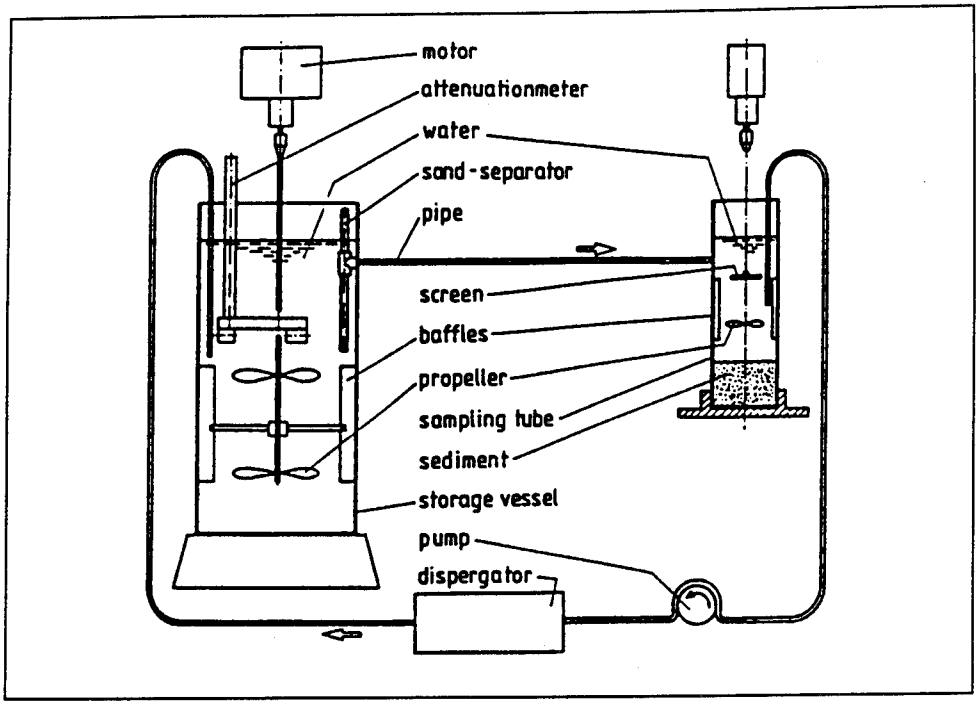

Figure 19. Schematic of the EROMES System (from Schunemann and Kuhl (1993))

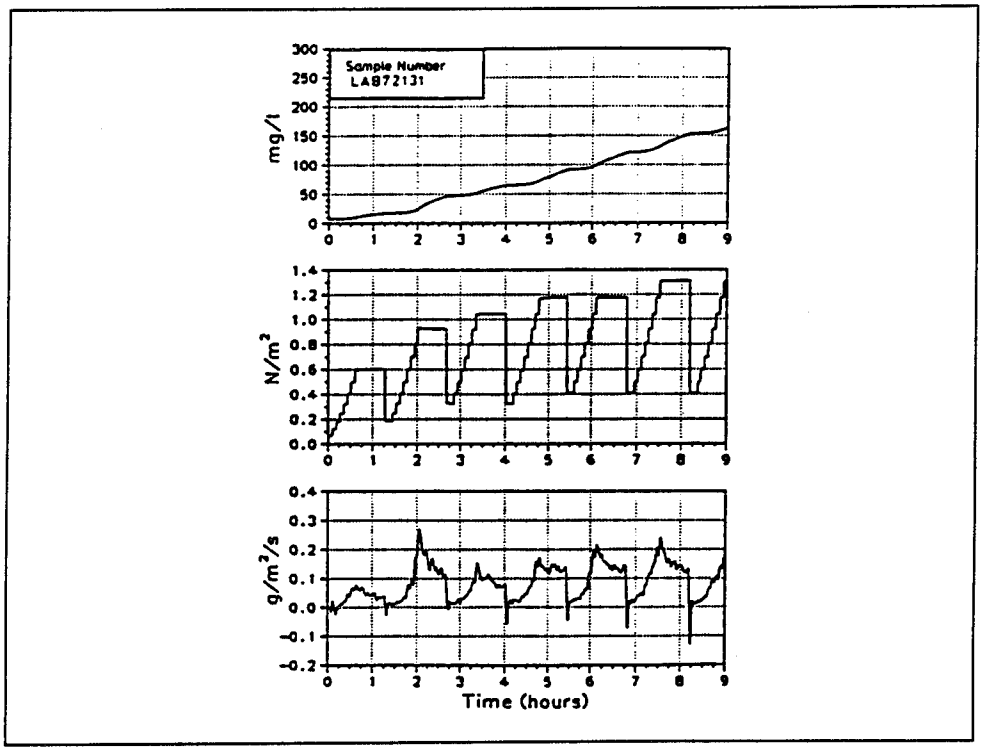

Figure 20. Typical results from an erosion experiment using the EROMES System (from Schunemann and Kuhl (1993)). Upper: suspended concentration; middle: bottom shear stress; lower: erosion rate

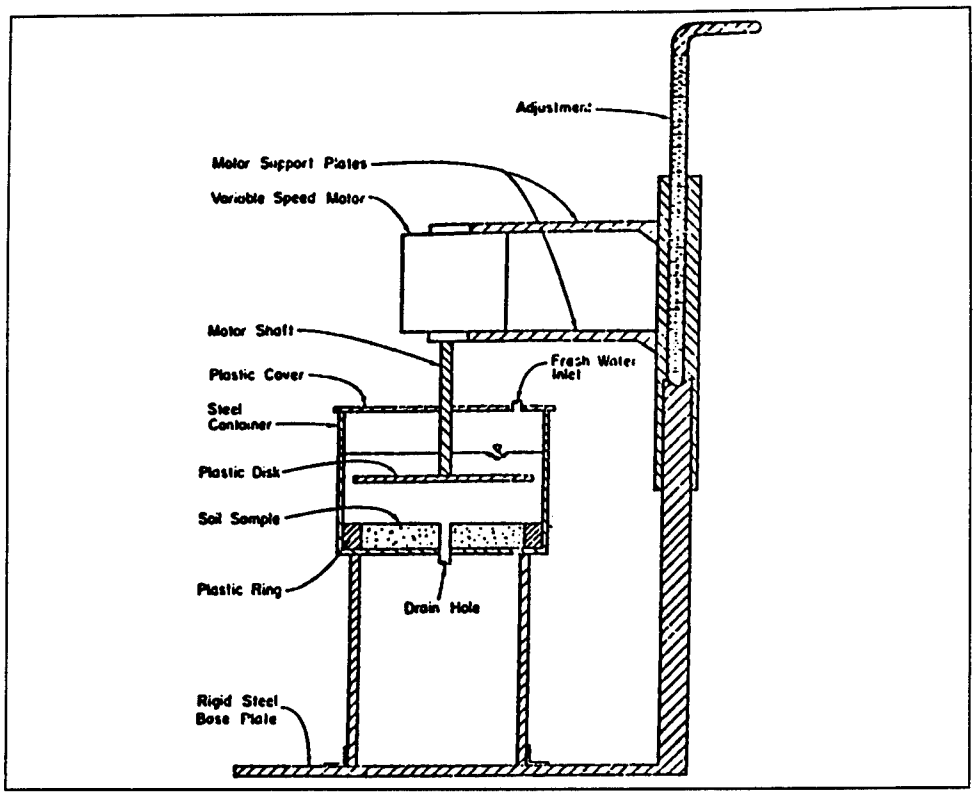

Figure 21. Schematic of a rotating disk device (from Liou (1970))

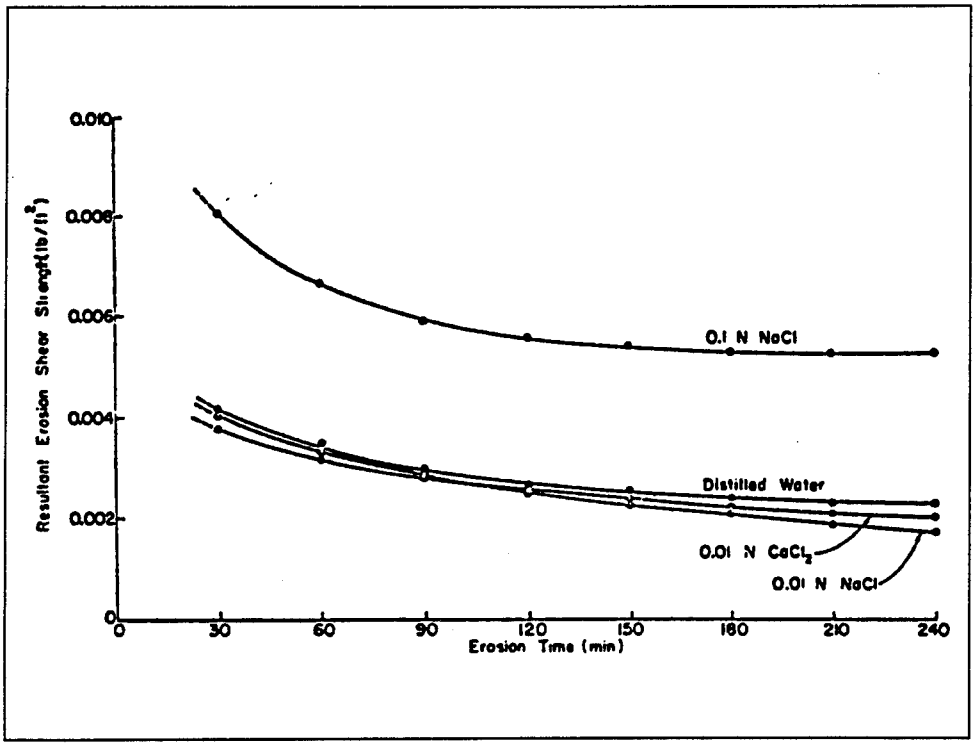

Figure 22. Typical time variations of erosion shear strength using a rotating disk device for high-water-content bentonite samples without chemical additives, and with 0.1 N, 0.01 N NaCl, and 0.01 N $CaCl_2$ additives (from Liou (1970))

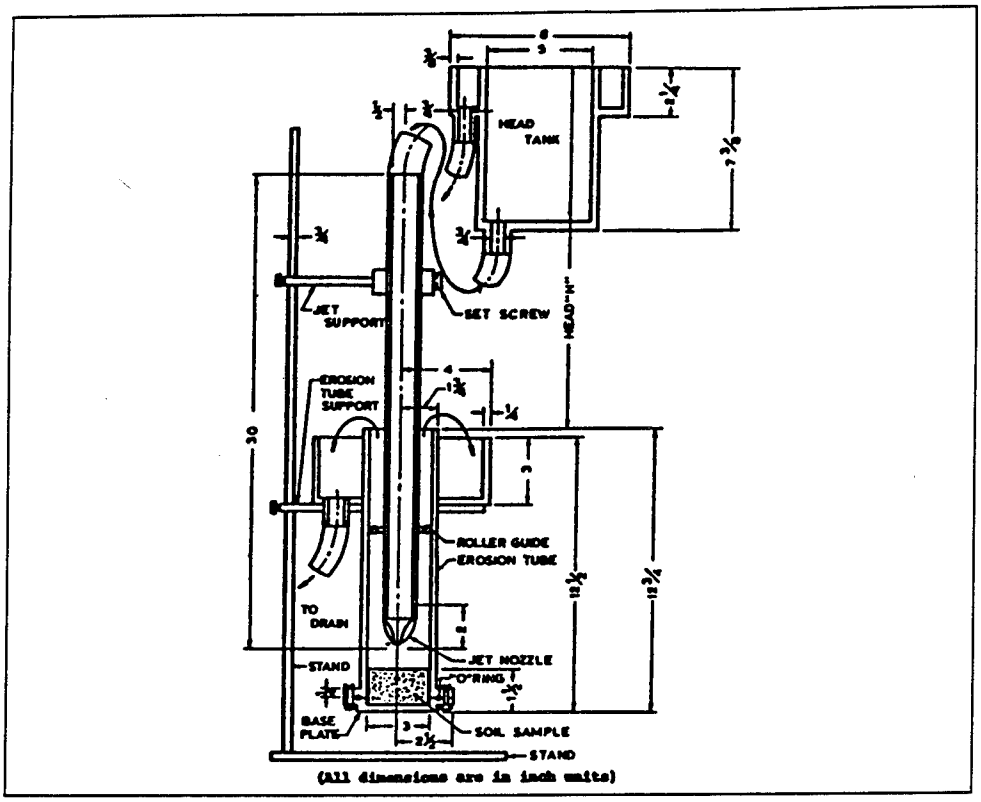

Figure 23. Schematic of a submerged jet apparatus (from Dash (1970))

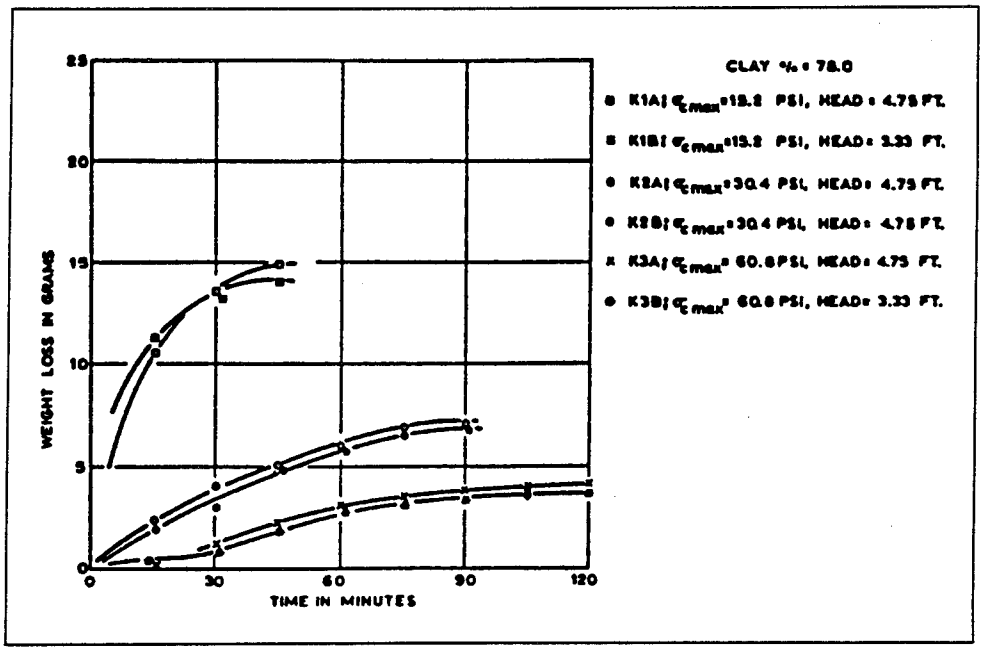

Figure 24. Typical time variations of weight loss using a submerged jet apparatus for consolidated samples with no sand (from Dash (1970)). σ_{cmax} denotes maximum consolidation pressure.

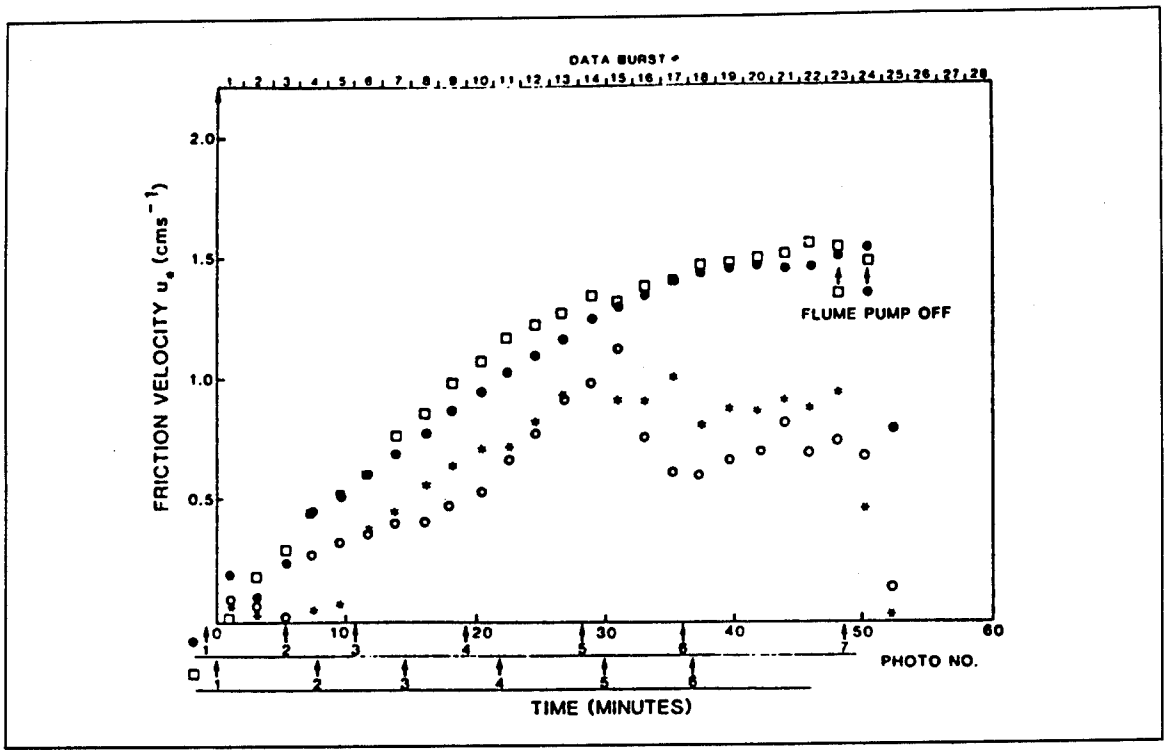

Figure 25. Typical time variation of optical transmissometer outputs during a SEAFLUME deployment (from Gust and Morris (1989)). Open and solid circles refer to the front and back optical transmissometers, respectively

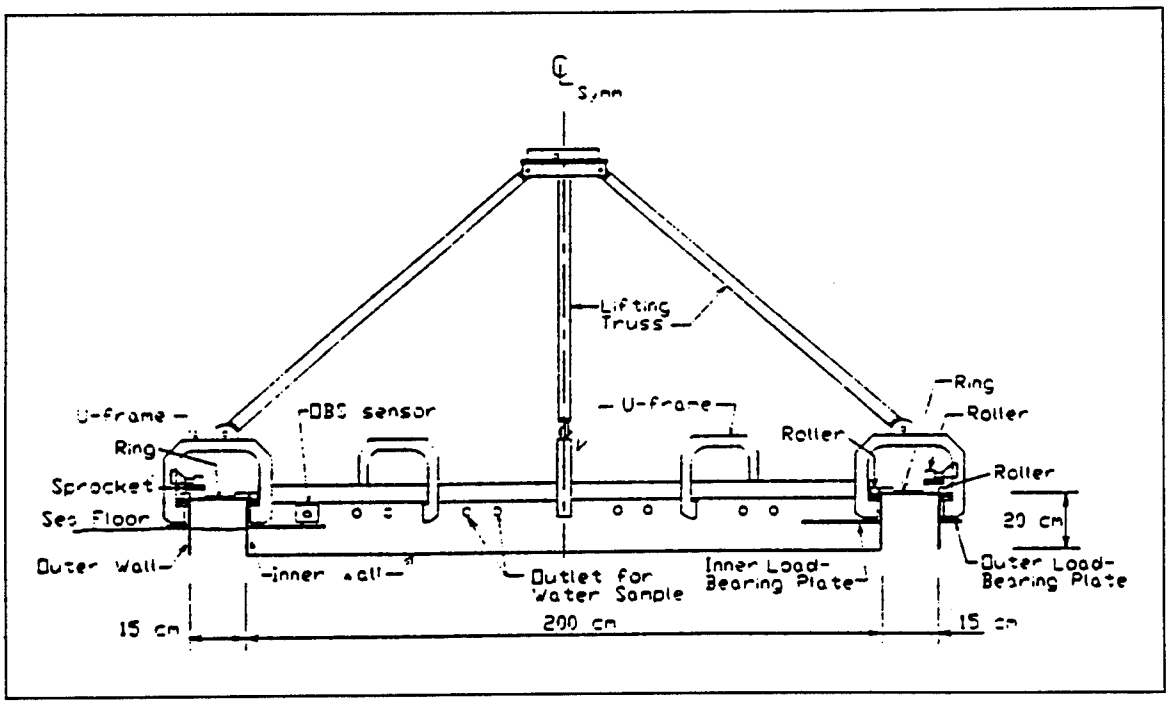

Figure 26. Schematic of a field rotating annular flume (from Maa et al. (1993))

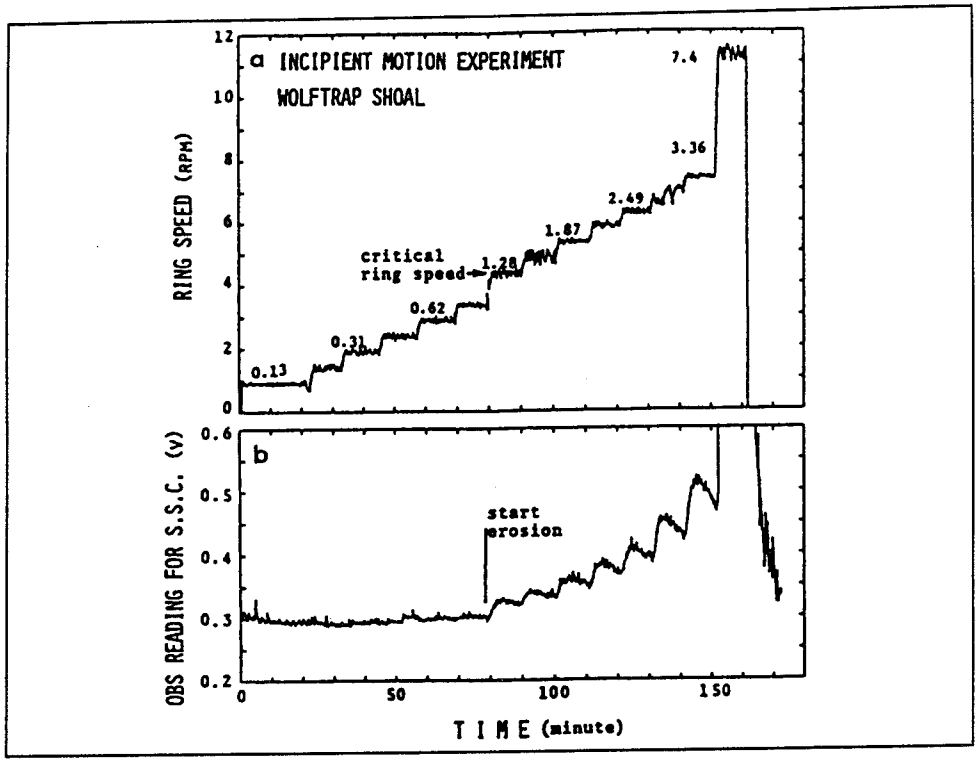

Figure 27. Typical results of an incipient erosion motion experiment during the Sea Carousel deployment (from Maa (1991)): a) ring speed versus time; b) OBS reading for suspended sediment concentration (SSC). Numbers are shear stresses in dynes/cm^2

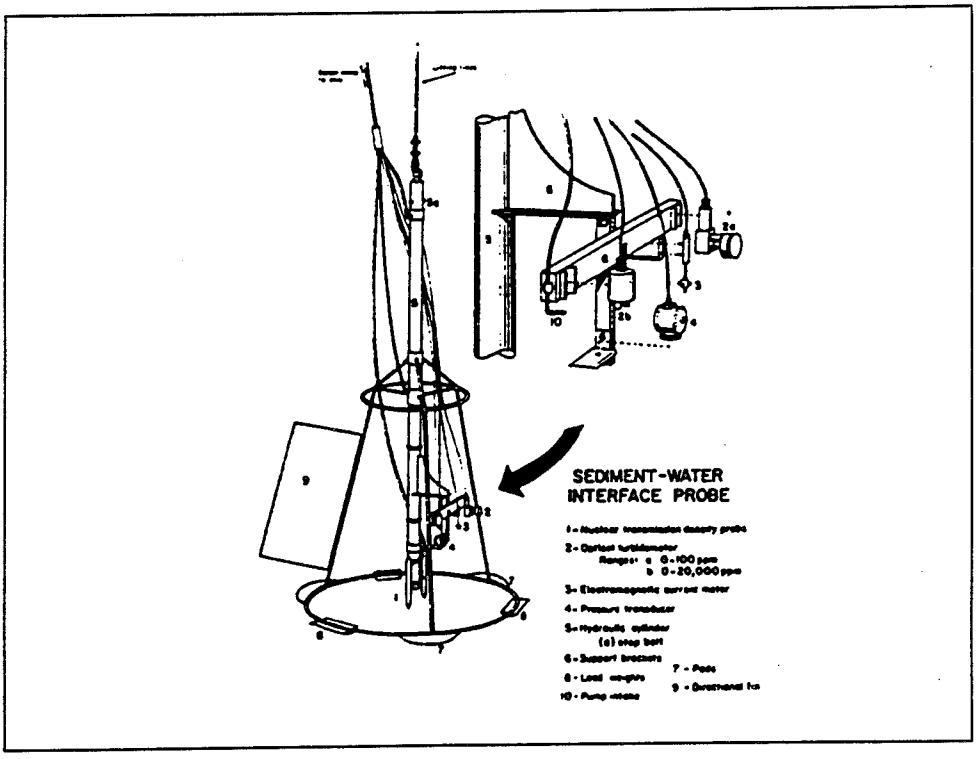

Figure 28. Schematic of the Sediment-water Interface Probe (from Nichols et al. (1978))

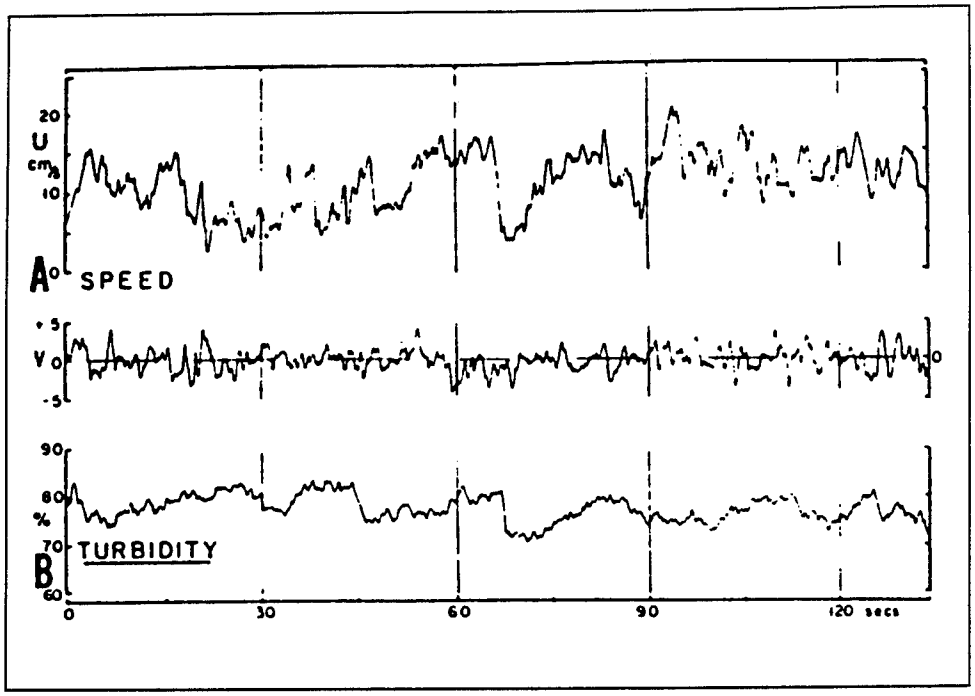

Figure 29. A typical analogue time-series record (from Nichols (1989)): a) current-speed, *u* and *v*, components at 0.2 time constant, showing intermittent nature of contributions at 30 cm above a fluid mud during ebb-tidal current, b) turbidity showing small-scale fluctuations, station 19, upper Chesapeake Bay. Turbidity units are in percent meter reading

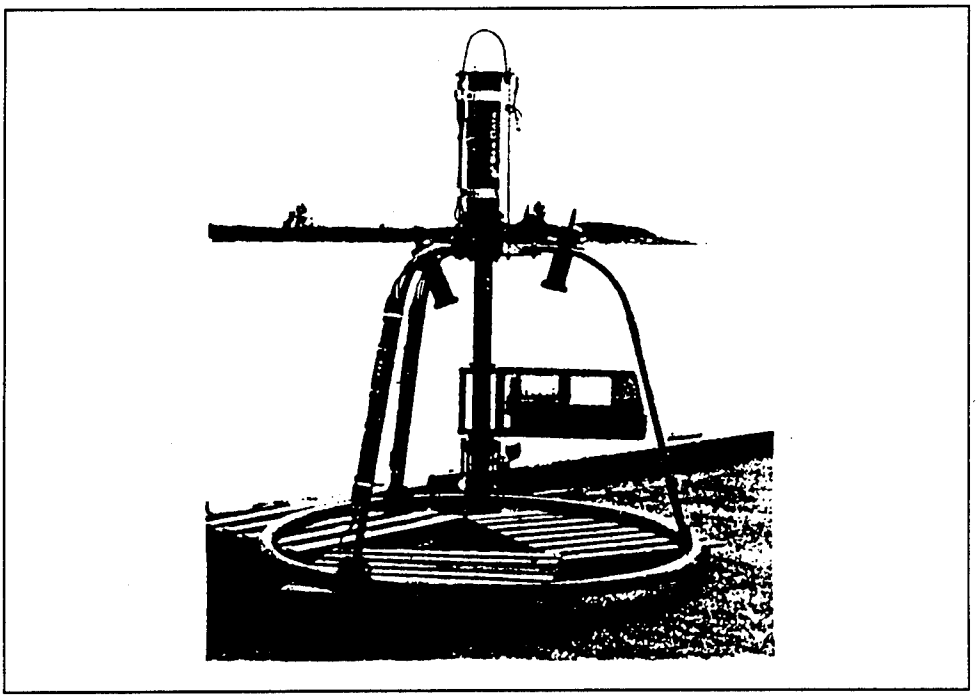

Figure 30. DAISY Tower Instrumentation Array (from Bohlen (1982))

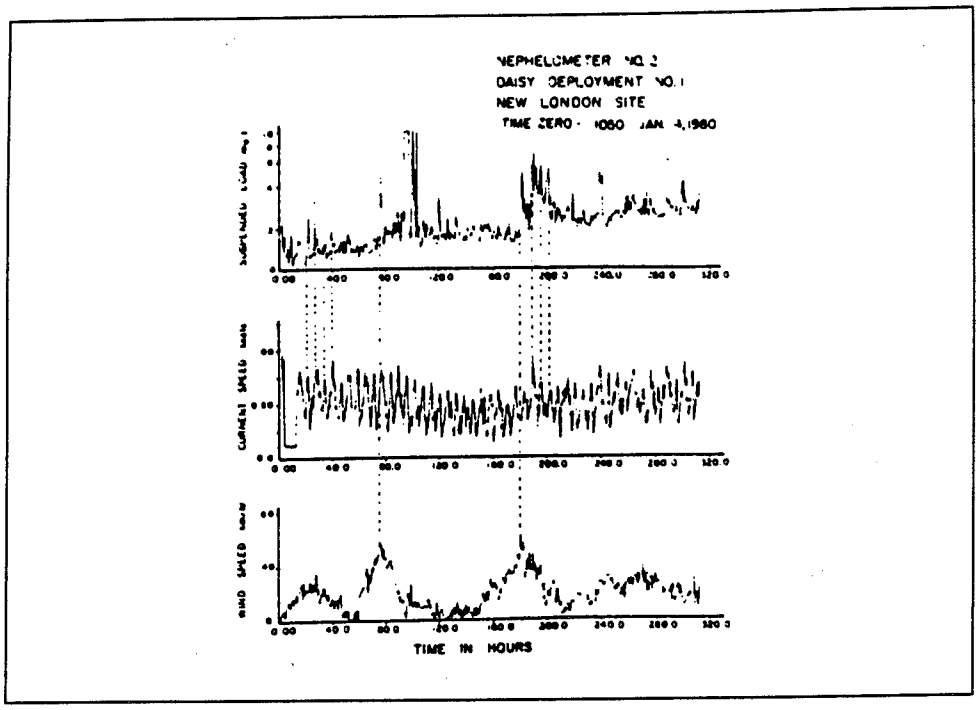

Figure 31. Typical results from a field deployment of DAISY Tower (from Bohlen (1982)). Upper: suspended sediment concentration; middle: near bottom current speed; lower: wind speed at 10-m elevation, Millstone Point, Long Island Sound

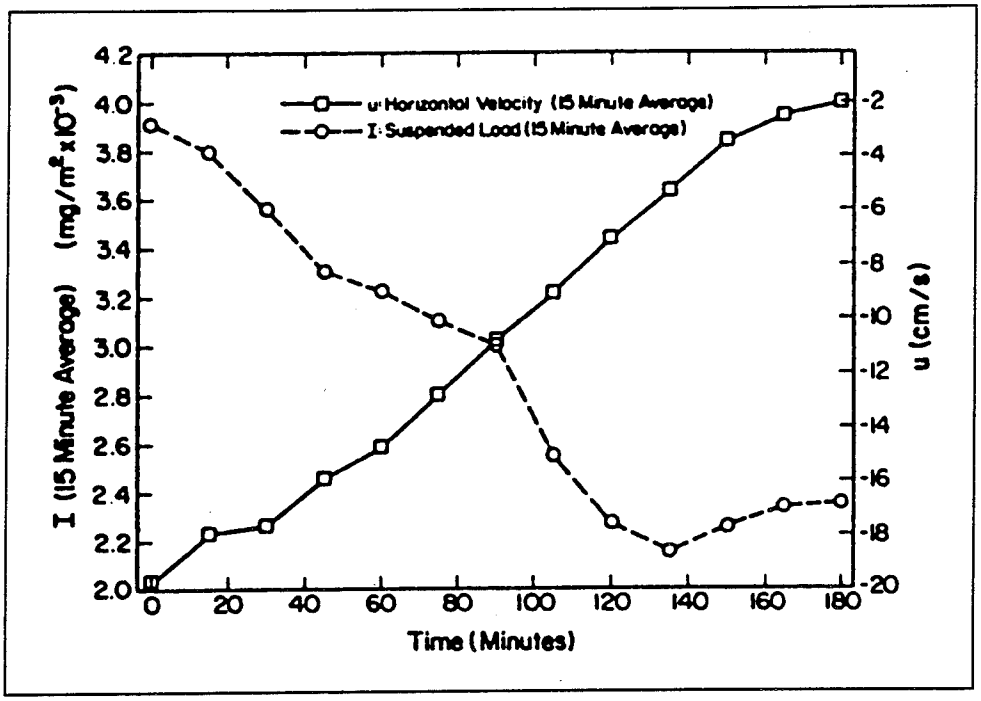

Figure 32. A typical time-trace of 15-min average horizontal velocity and suspended load for continuous deployment of the OSU instrumentation (from Bedford et al. (1987))

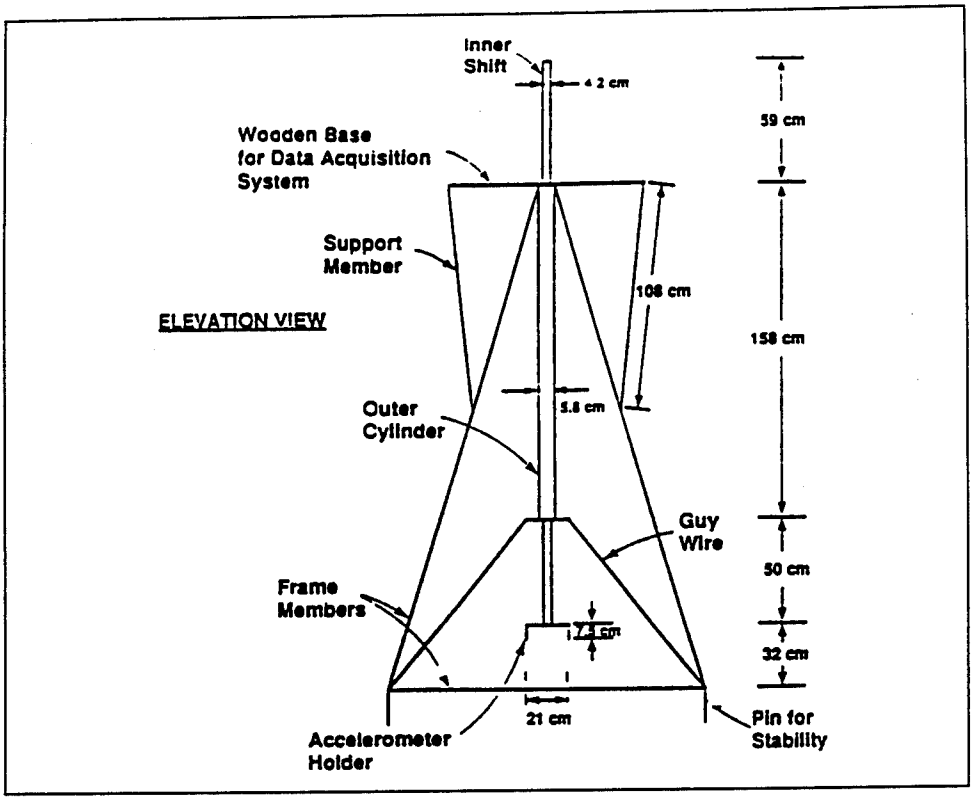

Figure 33. Schematic of the COE Field Tower (from Mehta and Jiang (1990))

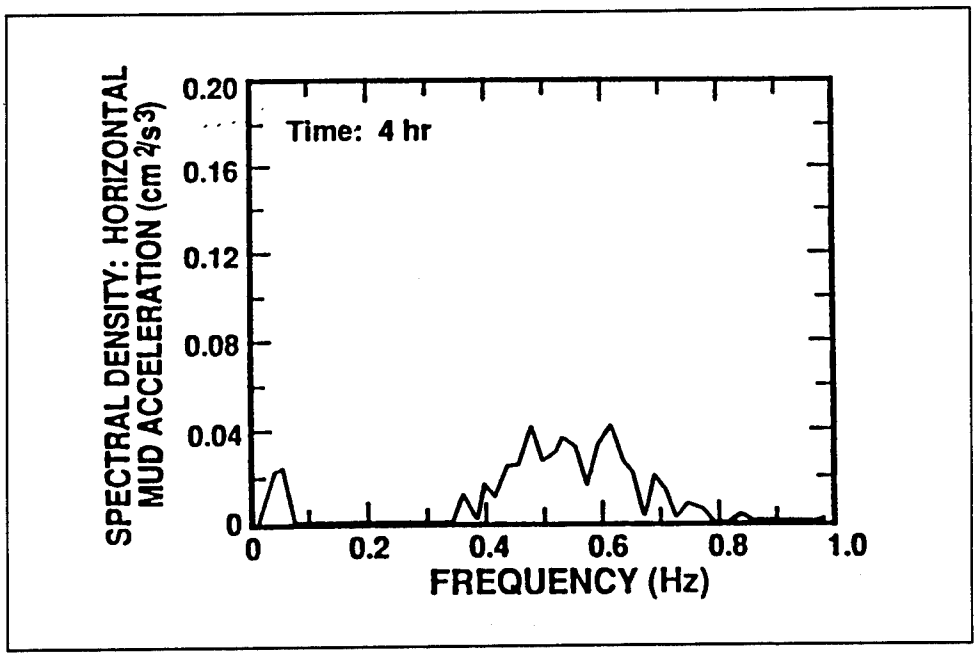

Figure 34. A typical computed horizontal mud acceleration spectrum from accelerometer data collected during a deployment of the COE Field Tower (from Mehta and Jiang (1990))

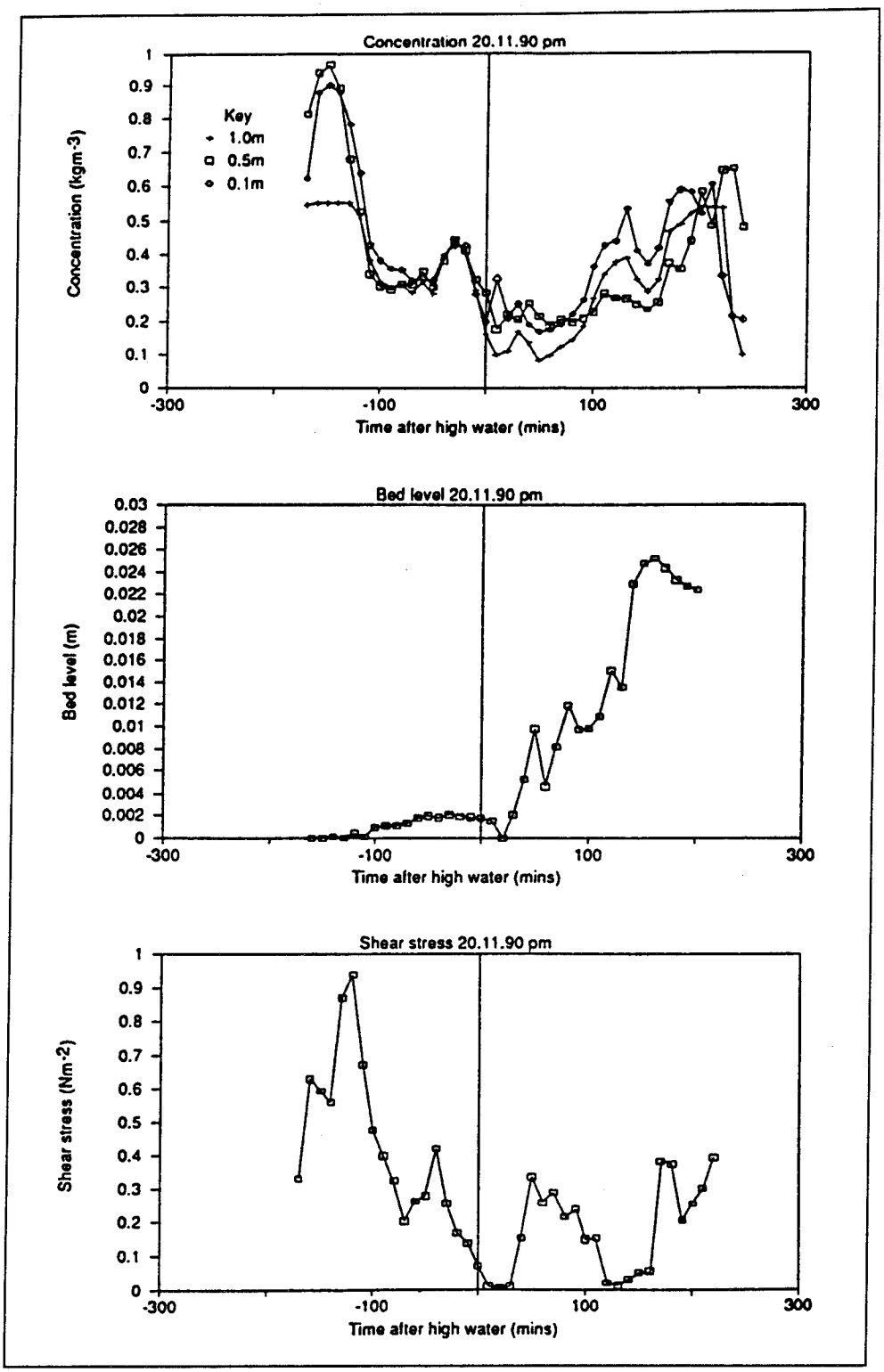

Figure 35. Typical results of field measurement at Mersey Site spring tide, 11/20/90: a) concentration, b) bed level, c) shear stress (from Teisson et al. (1993))

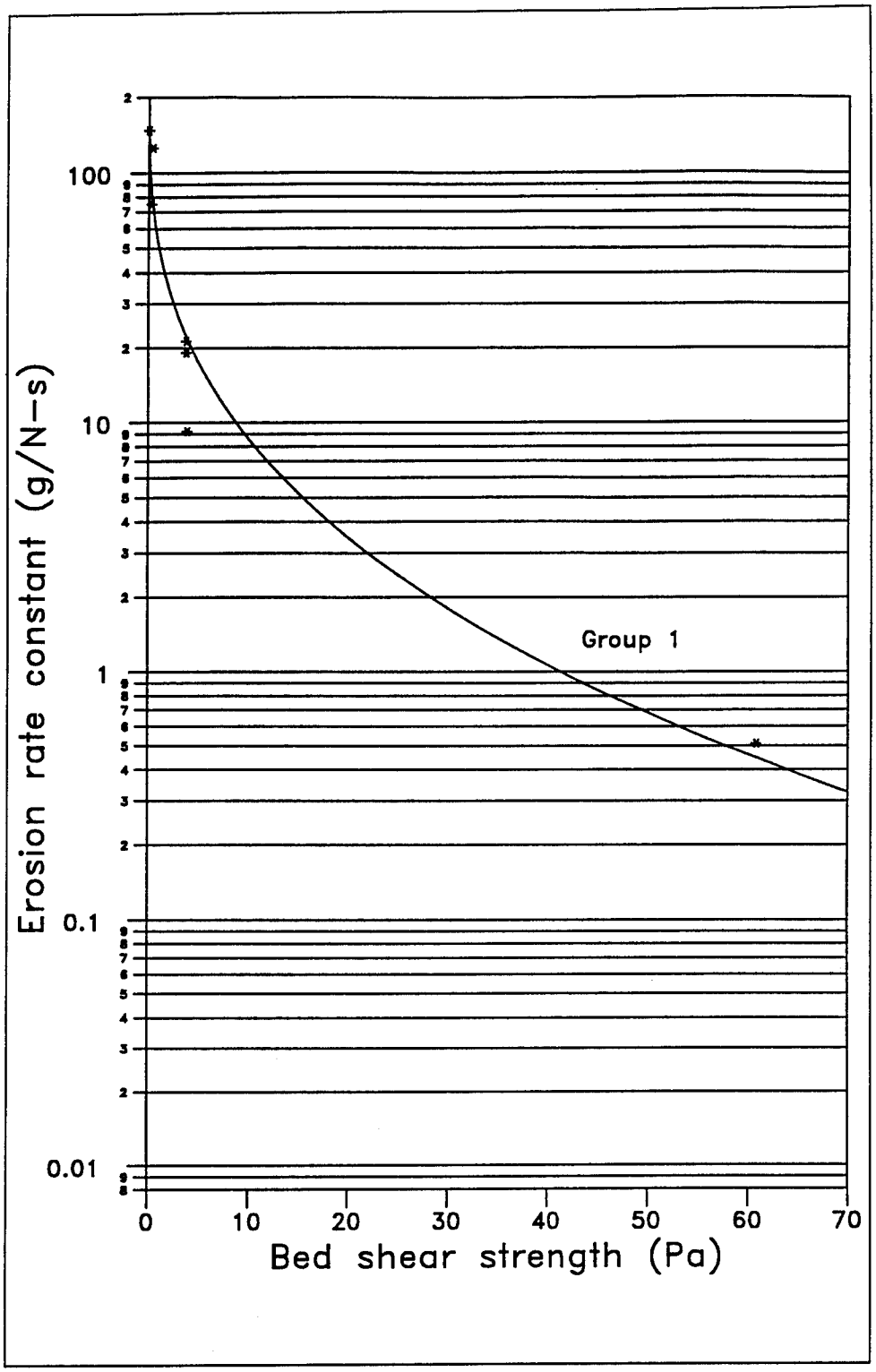

Figure 36. s - τ_s curve for Group 1

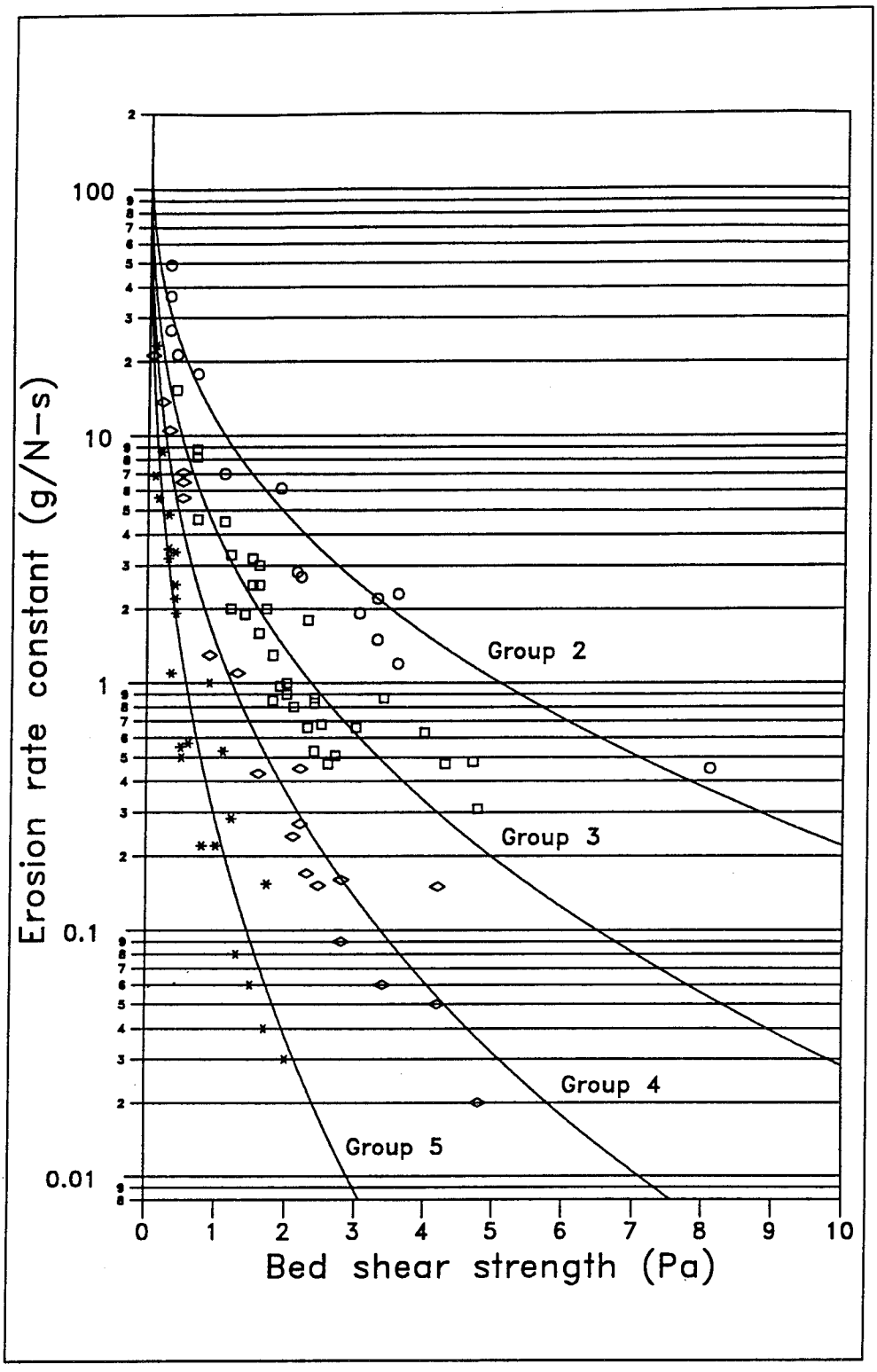

Figure 37. s - τ_s curve for Groups 2, 3, 4, and 5

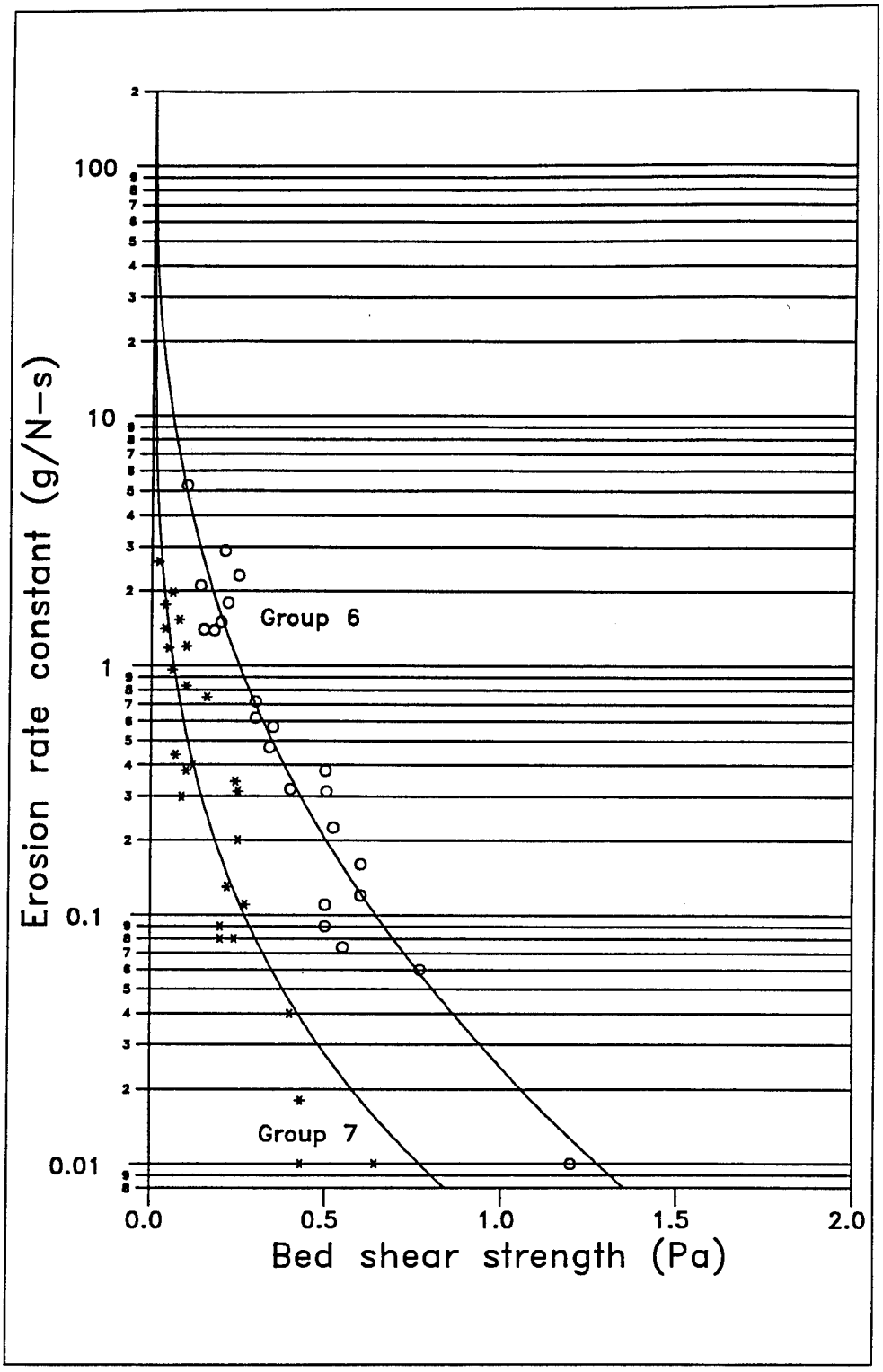

Figure 38. s - τ_s curve for Groups 6 and 7

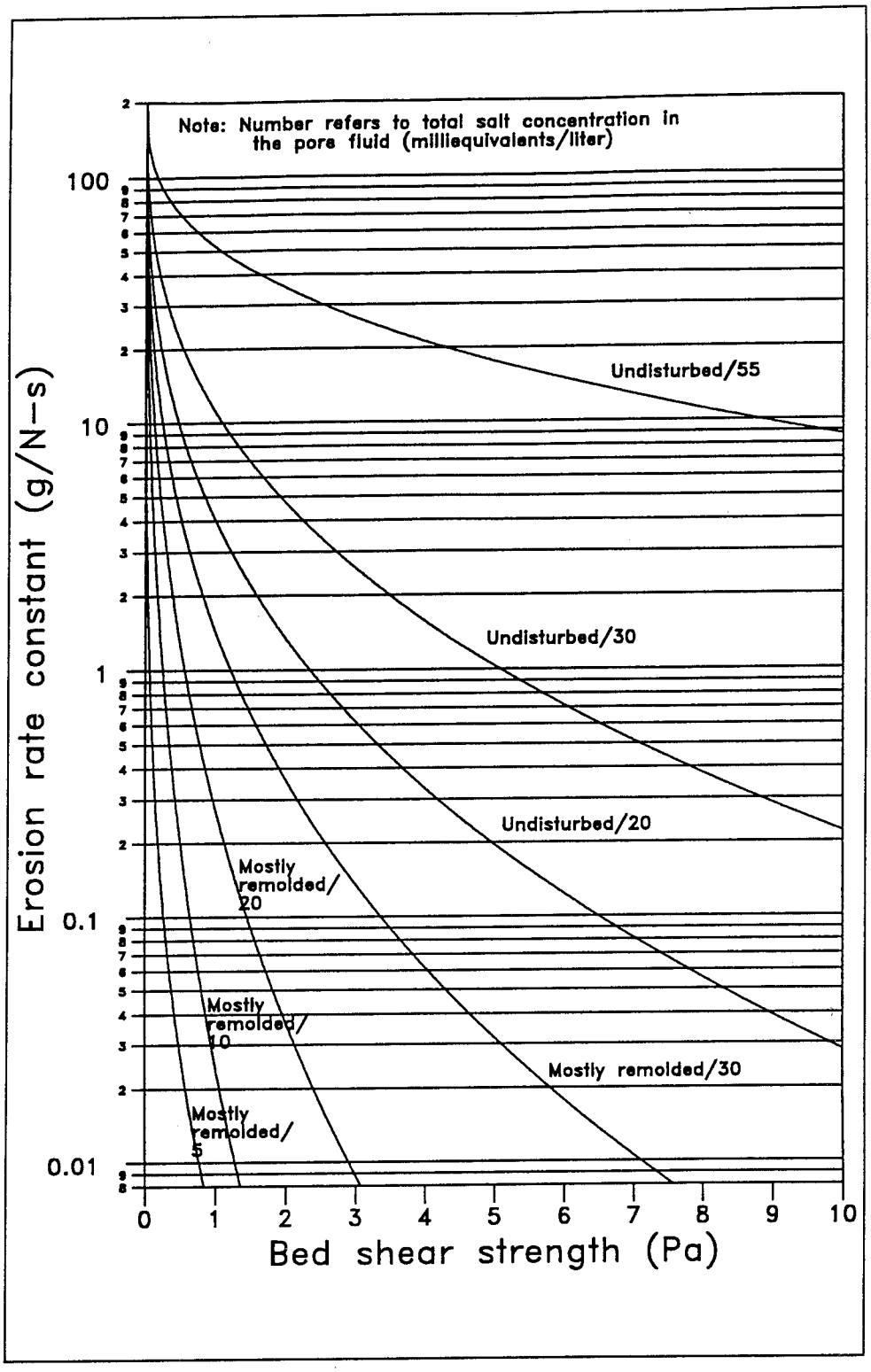

Figure 39. Nomograph for characteristic erosion rate constant

Appendix A
Tabulation of Test and Soil Conditions, Bed Shear Strength (τ_s) and Characteristic Erosion Rate Constant (s)

Table A1
Tabulation of Test and Soil Conditions, Bed Shear Strength (τ_s), and Characteristic Erosion Rate Constant (s)

Investigator(s)	Test Condition[a]	Soil Condition[b]	τ_s (Pa)[c]	s (g/N-s)
Espey (1963)	Rotating Cylinder 0/0.47/-/2,750	Taylor marl 50% < 5 μm	60.9[1]	0.51
Partheniades (1965)	Straight Flume (Series I) dense, uniform bed 33/1.1/-/2,240	Mare Island Strait, San Franscisco Bay: principally M 60% < 2 μm	0.43[7]	0.01
	Straight Flume (Series II) stratfied bed 33/1.2/-/2,240	Same as above	1.20[6]	0.01
Christensen and Das (1973)	Drill-hole Apparatus 0/0.35/13/-	K 53% < 2 μm	0.49[5]	0.55
	0/0.33/13/-	K 62% < 2 μm	0.77[6]	0.06
Raudkivi and Hutchison (1974)	Closed Conduit 0.01M $NaNO_3$/0.51/21/-	K (CEC= 4.8) 2 - 5 μm	0.22[7]	0.13
	0.01M $NaNO_3$/0.51/32/-	Same as above	0.24[7]	0.08
Kandiah (1974)	Rotating Cylinder Homoionic ($MgCl_2$ pore fluid) TS = 20.0 meq/l	I(30%)+SF(70%)	3.4[3]	0.87
	Homoionic ($CaCl_2$ pore fluid) TS = 9.8 meq/l	Same as above	1.3[4]	1.1
	TS = 21.0 meq/l	Same as above	3.0[3]	0.66
	TS = 39.5 meq/l	Same as above	4.7[3]	0.48
	TS = 80:0 meq/l	Same as above	8.1[2]	0.45
	TS = 20.0 meq/l	Yolo Loam Silt + K(50%) SAR = 48	0.7[3]	8.8
		K(40%)	0.7[3]	8.2
		K(30%)	0.72[3]	4.6

Notations: TS = total salt concentration in pore fluid (milliequivalents/liter); K = kaolinite; M = montmorillonite; I = illite; SF = silica flour; SAR = sodium adsorption ratio; CEC = cation exchange capacity (milliequivalents/100 g); CH = chlorite; S = sepiolite; OM = organic matter in percent; CC = clay content in percent.

[a] The four values in 1/2/3/4 refer to 1 = salinity of pore fluid in ppt except for Arulandandan et al. (1980) where it refers to total salt concentration in soil pore space (milliequivalents/liter) (the value in parentheses, where it appears, refers to total salt concentration (meq/l) in the eroding fluid); 2 = percent water content by weight; 3 = temperature in °C; 4 = bulk density, ρ (kg/m^3). A dash denotes that the information is not available.

[b] The five values in 1/2/3/4/5 refer to 1 = plasticity index, 2 = percent organic content by weight, 3 = SAR, 4 = CEC as defined above, and 5 = clay content in percent. A dash denotes that the information is not available.

[c] Superscripts on the values listed under τ_s refer to the data group number.

(Sheet 1 of 7)

Table A1 (Continued)

Investigator(s)	Test Condition[a]	Soil Condition[b]	τ_s (Pa)[c]	s (g/N-s)
Kandiah (1974) continued	TS = 20.0 meq/l	Yolo Loam Silt + K(30%) SAR = 2.5	1.2[3]	2.0
		K(40%)	1.4[3]	1.9
		K(50%)	1.6[3]	1.6
	TS = 20.0 meq/l	Yolo Loam Silt + I(40%) SAR = 48	0.3[5]	4.8
		I(30%)	0.4[5]	2.5
		I(20%)	0.4[5]	2.2
	TS = 20.0 meq/l	Yolo Loam Silt + I(20%) SAR = 2.5	1.9[3]	0.97
		I(30%)	2.0[3]	0.90
		I(40%)	2.1[3]	0.80
	TS = 20.0 meq/l	Yolo Loam Silt + M(30%) SAR = 48	0.1[5]	6.9
		M(20%)	0.15[5]	5.6
		M(10%)	0.25[6]	2.3
	TS = 20.0 meq/l	Yolo Loam Silt + M(10%) SAR = 2.5	2.0[3]	1.0
		M(20%)	2.4[3]	0.83
		M(30%)	2.7[3]	0.51
	TS = 20.0 meq/l	Remolded bay mud: CC=11% SAR = 46.5 CEC = 15.0 meq/100g	0.2[5]	8.6
		Remolded natural soil (S&W#1): CC=17% SAR = 46.5 CEC = 12.0	0.3[4]	10.5
		Remolded Yolo Loam: CC=12% SAR = 46.5 CEC = 10.4	0.5[4]	5.6
	TS = 20.0 meq/l	Remolded bay mud: CC=11% SAR = 4 CEC = 15.0 meq/100g	1.5[3]	3.2

(Sheet 2 of 7)

Table A1 (Continued)

Investigator(s)	Test Condition[a]	Soil Condition[b]	τ_s (Pa)[c]	s (g/N-s)
Kandiah (1974) (continued)	TS = 20.0 meq/l	Remolded Yolo Loam: CC=12% SAR = 4 CEC = 10.4 meq/100g	1.6[3]	2.5
		Remolded natural soil (S&W#1): CC=17% SAR = 4 CEC = 12.0 meq/100g	1.7[3]	2.0
	TS = 20.0 meq/l	Remolded natural soil (S&W#2): CC=33% SAR = 4 CEC = 21.2 meq/100g	2.3[3]	1.8
	TS = 20.0 meq/l	Remolded natural soil (Meyers Clay): CC=28% SAR = 4 CEC = 22.5 meq/100g	2.4[3]	0.53
		Remolded natural soil (S&W#3): CC=42% SAR = 4 CEC = 30.1 meq/100g	2.8[4]	0.16
	TS = 20.0 meq/l	I(30%) + SF(70%) OM = 2.8%	0.30[5]	3.2
		OM = 5.7%	0.40[5]	3.4
		SAR = 3.0 OM = 0%	1.80[3]	1.3
		OM = 0.85%	2.40[3]	0.87
		OM = 2.7%	4.30[3]	0.47
		OM = 5.6%	3.60[2]	1.2
	TS = 20.0 meq/l -/-/42/-	I(30%) + SF(70%) SAR = 3.0	1.2[3]	3.30
	-/-/23/-		1.8[3]	0.85
	-/-/18/-		2.3[3]	0.66
	-/-/9.5/-		2.6[3]	0.47
Arulanandan et al. (1973)	Rotating Cylinder -/0.28/-/-	Yolo loam SAR = 23.2	0.41[5]	1.92

(Sheet 3 of 7)

Table A1 (Continued)

Investigator(s)	Test Condition[a]	Soil Condition[b]	τ_s (Pa)[c]	s (g/N-s)
Arulanandan et al. (1973) (continued)	Rotating Cylinder -/0.28/-/-	SAR = 12.4	3.04[2]	1.92
		SAR = 9.4	4.77[3]	0.31
		SAR = 1.1	19.4[2]	0.15
	-/0.40/-/-	0.001N NaCl pore fluid SAR = 35	2.14[2]	2.82
		0.005 N NaCl pore fluid	4.0[3]	0.63
Arulanandan et al. (1975)	Rotating Cylinder 0/0.28/-/-	Yolo Loam: 0.005N NaCl CEC = 19.8; 19% < 2 µm pore fluid with SAR = 1.1	0.10[6]	5.25
	0/0.28/-/-	Pore fluid SAR = 1.6	0.06[4]	21.20
	0/0.30/-/-	Pore fluid SAR = 10.7	0.01[1]	147.3
Gularte et al. (1977)	Closed Conduit 31/1.13-2.22/-/2,400	Thames River spoil: OM = 6.1 - 12.6 10% < 2 µm	0.27[7]	0.11
Fukuda (1978)	Annular Flume: Type I 0/0.76/-/-	Western Basin sediment, Lake Erie d_{50} = 3 µm	0.16[7]	0.75
	0/0.79/-/-		0.07[7]	0.44
Thorn and Parsons (1980)	Straight Flume 10 min erosion test 28/-/-/-	Grangemouth Mud K(17%)+I(17%)+CH(17%) CEC = 20 OM = 10%	0.02[7]	2.62
	20 min erosion test (ρ = 2,080)		0.06[7]	1.97
	30 min erosion test (ρ = 2,080)		0.08[7]	1.53
	10 min erosion test (ρ = 1,510)	Brisbane mud M(30%)+K(15%)+I(5%) CEC = 35	0.04[7]	1.76
	20 min erosion test (ρ_B = 1.510)		0.04[7]	1.41
	30 min erosion test (ρ_B = 1.510)		0.05[7]	1.18
	10 min erosion test (ρ_B = 1,720)	Belawan Mud M(20%)+K(30%)+I(30%) CEC = 25	0.21[6]	2.89
	20 min erosion test (ρ_B = 1,720)		0.22[6]	1.79
	30 min erosion test (ρ_B = 1,720)		0.18[6]	1.39

(Sheet 4 of 7)

Table A1 (Continued)

Investigator(s)	Test Condition[a]	Soil Condition[b]	τ_s (Pa)[c]	s (g/N-s)
Arulanandan et al. (1980) (Undisturbed bed)	Straight Flume 32.5/0.29/-/1,720	8.0/5.1/6.1/13.6/13%	3.6[2]	2.3
	205/0.36/-/1,680	9.0/7.0/21.7/11.3/22%	3.8[1]	19.2
	145/0.42/0/1,550	0./7.8/23.1/7.3/13%	0.7[2]	17.8
	2.7/0.29/-/1,810	26.6/11.0/0.1/20.4/40%	0.3[2]	26.7
	34.0/0.24/-/1,420	14.3/10.4/0.4/11.6/25%	2.2[2]	2.7
	55.0/0.26/-/1,980	49.7/7.1/14.8/9.8/53%	3.8[1]	21.3
	2.5/0.36/-/1,740	16.5/5.0/0.1/14.5/30%	0.2[4]	13.7
	5.6/0.29/-/1,810	1.9/4.0/0.2/9.0/17%	0.4[3]	15.3
	29.0/0.38/-1,810	23.7/5.2/4.7/20/30%	0.1[5]	23.3
	9.6/0.23/-/2,090	11.0/4.2/1.9/12.1/25%	0.3[5]	3.5
	10.8/0.30/-/2,080	36.1/7.5/9.2/27.5/42%	0.4[2]	21.3
	2.95/0.41/0/1,850	31.3/5.5/0.5/26.1/46%	1.9[2]	6.1
	4.7/-/-/1,820	34.1/4/0.9/18.8/25%	3.3[2]	2.2
	6.0/0.46/-/1,610	25.3/8.6/1.3/24.1/42%	1.1[2]	7.0
	28.0/0.5/-/1,610	29.0/11.6/0.6/22.9/40%	1.5[3]	2.5
	2.4/0.39/-/1,630	0./5.1/0.2/7.6/12%	0.2[6]	1.5
	2.2/0.43/-/1,270	8.8/5.5/0.3/20/14%	0.5[4]	7.1
	3.8/0.44/-1,690	8.6/5.7/0.4/13.3/12%	0.3[2]	49.2
	8.0/0.35/-/1,950	6.8/3/0.7/9.2/18%	0.4[1]	125.8
	6.1/0.38/-/1,760	21.3/9.1/0.3/17.5/34%	0.5[4]	6.5
	1.5/0.34/-/1,440	0./4.9/0.1/11.3/5%	0.3[1]	75.0
	3.7/0.31/-/1,480	3./5./0.4/8.5/6%	1.1[3]	4.5
	1.1/0.30/-/1,670	10.5/5.1/0.2/13.5/29%	3.9[1]	9.2
	4.8/0.43/-/1,730	15.3/6.4/0.6/16/28%	0.3[2]	36.7
	4.0/0.3/-/1,610	14.3/5.7/0.5/13.9/29%	1.6[3]	3.0
	2.2/0.32/-1,700	15.5/6.2/0.6/14.2/30%	3.3[2]	1.5

(Sheet 5 of 7)

Table A1 (Continued)

Investigator(s)	Test Condition[a]	Soil Condition[b]	τ_s (Pa)[c]	s (g/N-s)
Arulanandan et al. (1980) (Remolded bed)	Rotating Cylinder 32.5(0.)/0.30/-1,900	8.1/5.1//6.1/13.6/13%	0.14[6]	2.1
	32.5(2.05)/0.30/-/1,930		1.1[5]	0.53
	32.5(4.1)/0.30/-/1,930		2.2[4]	0.45
	205(0.)/0.29/-/1,950	9.0/7.0/21.7/11.3/22%	1.0[5]	0.22
	205(13.25)/0.30/-/1,930		4.2[4]	0.15
	205(26.5)/0.29/-/1,930		3.4[4]	0.06
	2.7(0.)/0.34/-/1,850	26.6/11/0.1/20.4/40%	2.0[5]	0.03
	2.9(0)/0.32/-/1,860	11.1/4.7/0.1/15.5/33%	0.6[6]	0.16
	2.9(1.45)/0.33/-1,850	11.1/4.7/0.1/15.5/33%	4.2[4]	0.05
	2.5(0.9)/0.32/-/1,890	16.5/5/0.1/14.5/30%	0.4[7]	0.04
	5.6(1.25)/0.28/-/1,950	1.9/4/0.2/9/17%	0.9[5]	1.0
	5.6(2.5)/0.28/-/1,930	1.9/4/0.2/9/17%	0.8[5]	0.22
	1.3(0.)/0.24/-/1,960	3.2/3.3/0.1/7.9/17%	2.2[4]	0.27
	1.3(0.65)/0.24/-/1,990	3.2/3.3/0.1/7.9/17%	2.8[4]	0.09
	1.7(0.33)/0.38/-/1,740	18.8/5.8/0.1/20.3/37%	0.2[7]	0.09
	1.7(0.66)/0.38/-/1,820	18.8/5.8/0.1/20.3/37%	1.3[5]	0.08
	2.95(0.)/0.54/-/1,630	31.3/5.5/0.5/26.146%	0.6[5]	0.57
	4.7(0.)/0.31/-/1,830	34.1/4/0.9/18.8/25%	0.3[6]	0.72
	2.8(0.)/0.44/-/1,740	29/11.6/0.6/22.9/40%	0.5[6]	0.09
	2.4(0.)/0.34/-/1,930	0./5.1/0.2/7.6/12%	0.35[5]	1.1
	2.4(0.235)/0.31/-/1,950	0./5.1/0.2/7.6/12%	0.3[6]	0.62
	2.4(0.705)/0.31/-/1,930	0./5.1/0.2/7.6/12%	0.35[6]	0.57
	2.2(0.69)/0.30/-/1,940	8.8/5.5/0.3/20/14%	0.5[6]	0.38
	2.2(1.38)/0.30/-/1,940	8.8/5.5/0.3/20/14%	1.6[4]	0.43
	3.8(0.69)/0.31/-/1,960	8.6/5.7/0.4/13.3/12%	0.1[7]	0.38
	3.8(1.38)/0.27/-/1,950	8.6/5.7/0.4/13.3/12%	0.5[6]	0.11
	8.0(0.565)/0.31/-1,900	6.8/3/0.7/9.2/18%	1.5[5]	0.06
	6.1(0.)/0.32/-/1,890	21.3/9.1/0.3/17.5/34%	2.1[4]	0.24
	6.1(0.572)/0.36/-/1,820	21.3/9.1/0.3/17.5/34%	1.7[5]	0.04
	1.5(3.81)/0.27/-/1,910	0./4.9/0.1/11.3/5%	0.9[4]	1.3
	3.7(1.3)/0.27/-/1,990	3/5/0.4/8.5/6%	0.15[6]	1.4

(Sheet 6 of 7)

Table A1 (Concluded)

Investigator(s)	Test Condition[a]	Soil Condition[b]	τ_s (Pa)[c]	s (g/N-s)
Arulanandan et al. (1980) (remolded bed) (continued)	3.7(2.6)/0.27-/1,970	3/5/0.4/8.5/6%	0.12[7]	0.4
	1.1(0.2)/0.38/-/1,810	10.5/5.1/0.2/13.5/29%	0.10[7]	1.2
	1.1(0.4)/0.39/-/1,800	10.5/5.1/0.2/13.5/29%	0.50[5]	0.5
	4.8(0.2)/0.35/-/1,860	15.3/6.4/0.6/16/28%	2.50[3]	0.68
	4.8(0.4)/0.35/-/1,850	15.3/6.4/0.6/16/28%	2.30[4]	0.17
	4.0(0.952)/0.31/-/1,900	14.3/5.7/0.5/13.9/29%	0.60[6]	0.12
	6.2(0.)/0.28/-/1,970	15.5/6.2/0.6/14.2/30%	0.10[7]	0.83
	6.2(0.537)/0.28/-/1,950	15.5/6.2/0.6/14.2/30%	0.40[6]	0.32
	6.2(1.61)/0.28/-/1,930	15.5/6.2/0.6/14.2/30%	2.00[5]	0.03
	6.2(3.22)/0.29/-/1,910	15.5/6.2/0.6/14.2/30%	4.80[4]	0.02
Gularte et al. (1981)	Closed Conduit 2.5/0.60/-/-	Grundite: I(50%)+Silt(50%)	0.06[7]	0.965
	10/0.6/-/-	Same as above	0.25[7]	0.314
Villaret and Paulic (1986)	Annular Flume 10/-/24-27/1,630	Placed K: CEC = 6	0.25[7]	0.20
	Same as above	Placed Cedar Key mud: M(73%)+K(21%) CEC = 100; OM = 11%	0.20[7]	0.08
Hwang (1989)	Annular Flume: Type I placed bed, lake water bulk density = 1,100 kg/m^3	Lake Okeechobee mud principally K + M + S OM = 40%	0.43[7]	0.018
	bulk density = 1,190 kg/m^3		0.64[7]	0.01
	bulk density = 1,070 kg/m^3		0.34[6]	0.47
	bulk density = 1,090 kg/m^3		0.55[6]	0.074
MAST G6M (1992)	bulk density = 1,140 kg/m^3	-	0.09[7]	0.30
	bulk density = 1,210 kg/m^3	-	0.24[7]	0.34
	bulk density = 1,270 kg/m^3	-	0.50[6]	0.31
	bulk density = 1,310 kg/m^3	-	0.52[6]	0.23
	bulk density = 1,350 kg/m^3	-	1.22[5]	0.28
	bulk density = 1,380 kg/m^3	-	1.73[5]	0.15
	bulk density = 1,410 kg/m^3	-	2.47[4]	0.15

(Sheet 7 of 7)

REPORT DOCUMENTATION PAGE

Form Approved
OMB No. 0704-0188

1. AGENCY USE ONLY *(Leave blank)*	2. REPORT DATE	3. REPORT TYPE AND DATES COVERED
	November 1994	Final report

4. TITLE AND SUBTITLE

Cohesive Sediment Erosion

5. FUNDING NUMBERS

Work Unit 32590

6. AUTHOR(S)

S.-C. Lee, A. J. Mehta

7. PERFORMING ORGANIZATION NAME(S) AND ADDRESS(ES)

Coastal and Oceanographic Engineering Department
University of Florida, Gainesville, FL 32611

8. PERFORMING ORGANIZATION REPORT NUMBER

9. SPONSORING/MONITORING AGENCY NAME(S) AND ADDRESS(ES)

U.S. Army Corps of Engineers
Washington, DC 20314-1000
U.S. Army Engineer Waterways Experiment Station
3909 Halls Ferry Road, Vicksburg, MS 39180-6199

10. SPONSORING/MONITORING AGENCY REPORT NUMBER

Contract Report
DRP-94-6

11. SUPPLEMENTARY NOTES

Available from the National Technical Information Service, 5285 Port Royal Road, Springfield, VA 22161.

12a. DISTRIBUTION/AVAILABILITY STATEMENT

Approved for public release; distribution is unlimited.

12b. DISTRIBUTION CODE

13. ABSTRACT *(Maximum 200 words)*

This report consists of three chapters: Chapters 1 and 2 deal with erosion test devices and field instrument assemblies, while Chapter 3 is an analysis of published erosion rate ($\dot{\varepsilon}$)-bed shear strength (τ_s) data in an attempt to establish a functional link between the characteristic erosion rate constant (defined as the slope of the erosion rate-bed shear stress plot), s, and τ_s. A wide range of erosion test devices has been used both in the laboratory and in the field in the effort to further elucidate the phenomena of cohesive sediment erosion. They differ in configuration and flow geometry, size, mechanisms of generating flow, operation protocol, and measurement methodology. These devices are further complemented by various custom-designed field instrument assemblies, which provide valuable prototype data for model calibration and validation. The report reviews six categories of laboratory erosion test devices and eight categories of field devices/measuring assemblies. For each category, a representative device from the literature is described with a view to illustrating its salient features and typical test results. Similarly, the field instrument assemblies are individually described, including a brief discussion on typical field results. The description is confined to a documentation of the suite of equipment with incidental comments on their merits without an effort to compare them on a relative basis.

(Continued).

14. SUBJECT TERMS	15. NUMBER OF PAGES
See reverse.	83
	16. PRICE CODE

17. SECURITY CLASSIFICATION OF REPORT	18. SECURITY CLASSIFICATION OF THIS PAGE	19. SECURITY CLASSIFICATION OF ABSTRACT	20. LIMITATION OF ABSTRACT
UNCLASSIFIED	UNCLASSIFIED		

13. (Concluded).

In Chapters 1 and 2, 152 pairs of measured erosion rate constant-bed shear strength values have been gleaned from the literature for analysis. The data are limited to those that exhibit a linear relationship linking the rate of erosion to the bed shear strength. A family of curves of the functional form $s = 200 \exp(-a \tau_s^b)$ where a and b are empirical constants and the relevant units are g/N-s and Pa for s and τ_s, respectively, is apparent from the data spread. Further examination of the trend of several important erosion resistance characterizing factors reveals that the succession of curves behaves consistently with respect to the variation in the state of sediment bed (undisturbed or remolded) and the total salt concentration in the pore fluid. Based on these observations, a nomograph has been suggested for estimating the erosion rate constant, given the bed shear strength, subject to the caveat that the nomograph be used only as a last resort to provide general guidance, and is not intended to supplant erosion experiments, which should always remain the first choice. It may be noted that the nomograph is applicable only for placed beds/undisturbed beds/remolded beds which have a uniform shear strength with depth.

14. (Concluded).

Cohesive sediment erosion	Field instrument assemblies
Erosion rate constant	Laboratory erosion testing
Erosion test devices	Sediment shear strength